Su-AM-SymI-1

STRETCH CHANNELS WHETHER THEY MEANT TO BE OR NOT TO BE.
C.E.Morris, Loeb Institute, Ottawa Civic Hospital, Ottawa Canada K1Y 4E9.

In some neurons, mechanosensitive ion channels (MSCs) are physiological transducers; in others MSCs are protected from mechanical stimuli and act instead to control excitability via neurotransmitters. In snail neurons, we can reproducibly alter the mechanosensitivity of the latter type of MSCs, suggesting that physiological "toggling" of their mechanosensitivity may also occur. If membrane is patched with minimal mechanical disruption, large mechanical step-stimuli yield MSC activity, but only after a 0.5-3 s delay. As the stimulus is repeated, delay progressively shortens and post-delay channel activation increases. Evidently, progressive disorganization of the cortical cytoskeleton renders it less capable of absorbing mechanical loads which instead are conveyed (via membrane skeleton?) to MSCs. Many treatments that disrupt cortical organization lessen delay and increase activity: cytochalasins in DMSO (but not DMSO alone), elevated intracellular Ca^{2+}, N-ethylmaleimide (sulfhydryl reagent), osmotic shocks. Confocal monitoring of DiI-labelled plasma membrane during osmotic shocks reveals substantial membrane rearrangements which inevitably perturb the mechanical environment of all integral membrane proteins.

What mediates cytoskeleton-dependent variations in MSC mechanosensitivity? Direct MSC/cortical cytoskeleton coupling? Or is the spectrin membrane skeleton an intermediary? Since it remains unknown how/whether MSCs couple to membrane skeleton, we cannot say. In hopes of determining whether direct links to the membrane skeleton can couple mechanical loads to channel gating, we are constructing and testing fusion proteins constituted of Shaker (a voltage-gated channel bearing a moving voltage sensor) and a spectrin-binding domain from ankyrin.
Supported by NSERC and MRC, Canada and the HSF of Ontario.

Su-AM-SymI-2

MOLECULAR GENETICS OF TOUCH SENSATION IN *C. ELEGANS*: MECHANOTRANSDUCTION AND MECHANO-DESTRUCTION.
((M. Driscoll)) Dept. of Molecular Biology and Biochemistry, Rutgers University, Center for Advanced Biotechnology and Medicine, 679 Hoes Lane, Piscataway, NJ 08855.

Little is known about the molecular identities of proteins that transduce mechanical stimuli into cellular responses. Our interest is in molecules that mediate mechanotransduction in the nematode *Caenorhabditis elegans*. In this animal, sensitivity to gentle touch is mediated by six mechanosensory neurons called touch receptor cells. M. Chalfie and colleagues have identified over 400 mutations that disrupt the function of the touch receptors. Some of the genes identified in this study encode proteins with specialized functions in mechanotransduction. Molecular characterization of these genes has identified subunits of a candidate mechanosensory ion channel, specialized tubulins, and extracellular matrix proteins needed for mechanotransduction.

mec-4, *mec-10* (and possibly *mec-6*) are genes required for touch sensitivity that encode members of a *C. elegans* gene family related to the vertebrate epithelial Na^+ channel. The *mec-4* and *mec-10* expression patterns, the prop-erties of mutant alleles and the similarities to ENaC underlie our working hypothesis that MEC-4 and MEC-10 may be subunits of a mechanically-gated channel. *mec-4* and other family members have a second interesting property--specific amino acid changes in the encoded proteins induce degenerative cell death. Toxic substitutions appear to increase ion influx through the channel.

Mechanically gated channels are thought to be tethered inside and outside the cell in order to establish gating tension. A model for mechanotransduction focusing on interactions of channel subunits with intracellular and extracellular proteins will be discussed.

Su-AM-SymI-3

INTERACTIONS OF THE EPITHELIAL NA CHANNEL WITH SIGNAL TRANSDUCTION DOMAINS AND WITH THE CYTOSKELETON
((O.Staub and D. Rotin)) The Hospital for Sick Children, Toronto, Canada

The apically located amiloride-sensitive epithelial sodium channel(s) constitutes the rate-limiting step for sodium transport in kidney, colon and lung epithelia. Proper regulation of this channel is essential for maintenance of Na+ balance, blood volume, and blood pressure. The rat epithelial Na+ channel (rENaC) was recently cloned and shown to be composed of 3 homologous subunits ($\alpha\beta\gamma$), each containing two proline rich sequences (P1 and P2) at its C terminus. We have previously shown that the proline rich C terminus of αrENaC localizes the protein to the apical membrane of alveolar epithelial cells, likely by binding to the SH3 domain of α-spectrin. The other two subunits of the channel (β and γ rENaC) do not bind α-spectrin, nor SH3 domains. Their proline-rich regions were recently shown to be effectively deleted in patients with Liddle syndrome (a hereditary form of systemic hypertension), a deletion that leads to hyperactivation of the channel. To identify putative regulatory protein(s) which interact with the proline rich regions of β or γrENaC, we used the yeast two hybrid method to screen a rat lung library using the P2 region of βrENaC as a bait. Using this approach, we have identified the rat homologue of NEDD4 (rNEDD4) as the binding partner for the proline-rich regions of β and γrENaC. rNEDD4 contains a calcium lipid binding (CaLB) domain, three WW domains and a ubiquitin ligase domain. Our subsequent two hybrid assays, and *in vitro* binding and peptide competition experiments revealed that the WW domains of rNEDD4 mediate this binding. Moreover, mutations of key amino acids in the WW binding sequence (P2 region) of βrENaC, recently described in Liddle patients, led to abrogation of rNedd4-WW binding. Our work demonstrates that the WW domains of rNEDD4 bind to the proline rich sequences deleted from β or γENaC in Liddle patients, and suggest that NEDD4 may be a regulator of the epithelial Na+ channel.

Su-AM-SymI-4

MECHANOSENSITIVITY OF LIGAND-GATED CHANNELS.
((P. Ascher, P. Paoletti, and M. Casado)) Laboratoire de Neurobiologie, Ecole Normale Superieure, 75005 Paris, France.

Mechanosensitive channels include channels which can only be opened or closed by the application of mechanical forces, and channels in which mechanical stimuli only modulate the openings and closings produced by "physiological" stimuli. We have reported (Paoletti and Ascher, Neuron, 1994) that, in neurons in culture, membrane stretch can modulate the opening of the glutamate activated channels associated with the NMDA receptor, without affecting other ligand-gated channels. Is the tension transmitted to the NMDA channels through the lipid bilayer or through the cytoskeleton? A role of the lipid bilayer is supported by the fact that the alterations of the NMDA responses induced by stretch closely resemble those induced by the addition of compounds like arachidonic acid or docosahexaenoic acid, which are generally assumed to interact with the lipid bilayer. On the other hand, a role of the cytoskeleton is supported by the observation that pharmacological compounds which alter the cytoskeleton modify the NMDA responses (Rosenmund and Westbrook, Neuron, 1995) and by the demonstration of a link between NMDA receptors and the cytoskeletal protein PSD 95 (Kornau et al., Science, 1995).

Experiments will be presented in which we have tried to test both hypotheses by taking advantage of the observation that the stretch sensitivity can be also observed on recombinant NMDA receptors expressed in HEK 293 cells, and therefore can be analyzed on mutated receptors.

MITOCHONDRIAL CHANNELS I

Su-AM-A1

TRANSPORT MECHANISMS FOR DICARBOXYLATES IN MITOCHONDRIA.
((G. Liu, B. Hinch, and A.D. Beavis)) Medical College of Ohio, Toledo, OH 43699.

Dicarboxylates such as malonate (DC_3) and succinate (DC_4) can be transported by the dicarboxylate carrier and also by the inner membrane anion channel (IMAC), longer chain dicarboxylates such as azelate (DC_9) and sebacate (DC_{10}) also appear to be able to enter mitochondria and undergo β-oxidation. We have now examined the transport mechanisms of dicarboxylates ranging from oxalate to sebacate. All of these anions can be transported electrophoretically via IMAC; however, the rate decreases as the chain length increases from C_2 to C_5 and all exhibit the same temperature and pH dependence previously described for malonate, i.e., the rate increases with pH. Dicarboxylates can also be transported electroneutrally. Unlike the flux through IMAC, the flux through this pathway increases as the pH is lowered with a Hill coefficient = 2, suggesting that the anions are transported with two protons. The rate also increases exponentially as the chain length increases in a manner suggesting that rate of transport is proportional to the partition coefficient. Fluxes of DC_2 - DC_5 through this pathway are too slow to measure. The Arrhenius plots for this pathway, unlike those for IMAC, are linear from 5°C - 45°C. No inhibitors of this pathway have been identified. From these results, we conclude that this neutral transport is mediated by the lipid bilayer. We also show that only DC_2 - DC_4, are transported at significant rates through the dicarboxylate carrier. (This study was supported by NIH grant HL/GM47735 and the Ohio Affiliate of the AHA).

Su-AM-A2

FLUX OF ATP THROUGH VDAC CHANNELS IN THE OPEN AND CLOSED STATE.
((Tatiana Rostovtseva and Marco Colombini)) Dept. Zoology, University Maryland, College Park, MD 20742

VDAC channels form the major permeability pathway through the mitochondrial outer membrane. Previous observations on mitochondria and VDAC reconstituted into liposomes indicated that adenine nucleotides should cross this membrane through VDAC channels. Here we report the direct measurement of ATP flux through VDAC channels reconstituted into planar phospholipid membranes. The unidirectional flux through the open state is 3.2 x 10^6 ATP molecules per sec per channel for 100 mM ATP. That translates into a permeability of 2.3 cm/sec assuming a 1.5 nm pore radius (reduced to 0.9 nm after correcting for the radius of ATP). The flux through the closed state is essentially zero (within the error of the measurement). Therefore the gating of VDAC can be an effective way of controlling the flux of adenine nucleotides through the outer membrane. (supported by ONR grant # N00014-90-J-1024)

Su-AM-A3

SUBCELLULAR FRACTIONATION OF VOLTAGE-DEPENDENT ANION CHANNEL IN DEVELOPMENT. ((D. J. Suciu, L. Zimmerman, M. W. McEnery,)) Department of Physiology & Biophysics, Case Western Reserve University, Cleveland, OH 44106.

In mature neurons, the voltage-dependent anion channel (VDAC) is localized to mitochondria. This channel is a binding protein for hexokinase (R. A. Nakashima, P. S. Mangan, M. Colombini, P. L. Pedersen 1986. *Biochemistry.* 25:1015-1021.) but also probably has a role regulation of mitochondrial metabolism. In rat brain, the first two weeks postnatal is a time characterized by the growth of axons and the establishment of synaptic connections processes requiring extensive amounts of energy . Understanding the profile of mitochondria proteins in the growth of neurons will guide elucidation of the complex changes which occur at growing nerve terminals. We have explored the distribution of a VDAC antigen using density gradient sedimentation. Using standard subcellular fractionation, and purified antibodies to detect protein, we have determined the migration of various proteins through the gradient. The antibodies include the VDAC (mitochondria), syntaxin (synapse), GAP43 (growth cone), and the α_1-subunit of the N-type calcium channel (pre-synaptic membrane). VDAC is fractionated within a component whose heterogeneous distribution in immature neurons differs from adult, in contrast with other synaptic proteins.

Su-AM-A4

DERIVATION OF A STRUCTURAL MODEL FOR THE VDAC POLYPEPTIDE. ((C.A. Mannella, S. Stanley, C. Lawrence)) The Wadsworth Center, Empire State Plaza, Albany, NY 12201-0509; Department of Biomedical Sciences, The University at Albany, SUNY.

A structural model is being derived for the mitochondrial outer membrane channel VDAC. The proposed structure is a porin-like β-barrel, based on comparisons of the low-resolution outline of the lumen of the fungal channel (obtained by electron crystallography) with the atomic structure of R. capsulata porin, using the positions of the N-termini (determined for VDAC by antibody binding) as a reference. The C-terminal two-thirds of the polypeptide contains at least 11 11-residue-long β-strands tilted 30° with respect to the long axis of the pore. (Strand positions were determined by scanning VDAC sequences with a residue-frequency motif found in bacterial porins using the Gibbs sampler.) The N-terminal third of VDAC contains an amphiphilic α-helix (residues 5-19, found by the Gibbs sampler), and several additional β-strands (unlike the others in tilt and/or length). Between the N- and C-domains, there is a flap that may correspond to loop 3 in porin. Sidedness of various segments is given by their accessibility to sequence-specific antibodies. It is proposed that conformational changes in VDAC may involve the movement of the helix and/or flap in and out of the lumen. (Supported by NSF grant MCB 9506113.)

Su-AM-A5

CHARACTERIZATION OF A BACTERIALLY EXPRESSED YEAST VDAC PROTEIN MISSING THE FIRST EIGHT RESIDUES. ((D.A. Koppel, K.W. Kinnally, C.A. Mannella)) The Wadsworth Center, Empire State Plaza, Albany, NY 12201-0509; Department of Biomedical Sciences, The University at Albany, SUNY.

We have overexpressed VDAC genes from *S. cerevisiae* and *N. crassa* (gift of M. Forte, Oregon Health Sciences Univ.) in *E. coli* as fusion proteins with maltose binding protein, using the pMAL expression system. The fusion protein can be solubilized from inclusion bodies in 5 M guanidine·HCl, and transferred to nonionic detergents by dialysis. A yeast VDAC protein missing the first 8 residues, yVDAC Δ(1-8), has been purified by two-step hydroxylapatite chromatography, before and after cleavage of the fusion protein with factor Xa. When inserted in phospholipid bilayers from LDAO suspension, yVDAC Δ(1-8) exhibits voltage-independent current transitions that flicker rapidly and have smaller amplitudes (1.8 vs. 2.5 nS in 1 M KCl) than wild-type fungal VDAC isolated from mitochondria in LDAO. Experiments are underway to determine if this abnormal behavior is associated with the truncation in the N-terminal region (which may form an amphipathic α-helix involved in gating), or with other conditions peculiar to bacterial expression, such as renaturation from inclusion bodies or the absence of sterols (which are retained by the protein when isolated from mitochondria). (Supported by NSF grant MCB 9506113.)

Su-AM-A6

PROBING THE GATING PROCESS OF VDAC BY USING THE BIOTIN-STREPTAVIDIN SYSTEM. ((J. Song*, M. Forte+, E. Blachly-Dyson+ and M. Colombini*)) *Dept of Zool, Univ of Maryland, College Park, MD 20742. +Vollum Institute, Oregon Health Sciences Univ, Portland, OR 97201-3098.

The mitochondrial channel, VDAC, has two gating processes one at positive and one at negative potentials. The working model is that the channel is a β barrel and closure involves the translocation of portions of the wall of the barrel out of the membrane to the surface. The C-terminal β strand is proposed to be part of this mobile voltage sensor for one gating process only. It is located within the membrane in the open state and in one closed conformation and on the surface in the other closed state. To test this hypothesis, a cys was introduced at one end of this strand in *N.crassa* VDAC, E282C. After biotinylation these channels were reconstituted into planar phospholipid membranes. Addition of streptavidin could trap the channel in a closed state (by binding to the biotinylated cys) when added to one side of the membrane and not the other, indicating that this site reached the surface in only one closed conformation. QED (supported by NIH grant GM 35759)

Su-AM-A7

ANTI-HUMAN TYPE-1 ANTIBODIES RECOGNIZE CORRESPONDING PROTEINS IN ALL VERTEBRATE CLASSES. IN *XENOPUS LAEVIS* THE CHANNEL IS EXPRESSED IN THE PLASMALEMMA OF OOCYTES.
((S. Reymann, P. Steinacker, H.D. Kratzin and F.P. Thinnes)) Max-Planck-Institut für Experimentelle Medizin, Hermann-Rein-Str.3, D-37075 Göttingen, Germany (Spon. by C.A. Mannella).

Four highly specific monoclonal antibodies against human Type-1 porin (Winkelbach et al., Biochem. Med. Metab. Biol. 52, 120, 1994) were applied in Western blots of membrane fractions of 600 x g supernatants from different vertebrate muscles. The monoclonals recognize a single band of 30-31 kDa in shark, osseous fish, frog, tortoise, chicken, cattle and man, whereas no labelling is observed in lancelet. We proposed plasmalemma-integrated VDAC to form part of a ubiquitous chloride channel complex (for review see Reymann et al., Biochem. Mol. Med. 54, 75, 1995). Thus, we further investigated *Xenopus laevis*, the oocytes of which are of physiological interest. Here, the anti-Type-1 VDAC antibodies label the surface of oocytes in indirect immunofluorescence experiments. The proteins labelled in *Xenopus* muscle or oocytes were isolated. By sequencing some tryptic peptides it was verified to be VDAC which was labelled in Western blots.

Su-AM-A8

PATCH-CLAMP STUDIES OF TWO CHANNELS FROM HUMAN MITOCHONDRIA ((R. C. Murphy[1,2], M. King[3], J. J. Diwan[2] and K. W. Kinnally[1])) [1]Molecular Medicine, Wadsworth Center, Empire State Plaza P.O. Box 509, Albany, N.Y. 12201-0509, Dept. of Biomed. Sci. Univ. at Albany, State University of New York, Albany, NY, [2]Biology, Rensselaer Polytechnic Inst., Troy, NY, [3]College of Physicians and Surgeons of Columbia Univ., New York, NY

Patch-clamp techniques were used to characterize the channel activity of mitoplasts (mitochondria with their inner membrane exposed) from two human osteosarcoma cell lines, a mitochondrial genome-deficient cell line (ρ^0) and the wild-type cell line (ρ^+) from which the ρ^0 cells were derived. The channel activities most often recorded from murine tissue are mCS (mitochondrial Centum picoSiemen activity) and MCC (multiple conductance channel activity). mCS is a ~100 pS channel activity that is voltage-dependent and slightly anion-selective. MCC is a high-conductance voltage-dependent channel. This channel activity may have a role in protein import as it is transiently blocked by peptides that target precursor proteins to the mitochondria. We have found mCS and MCC activities in wild-type and mitochondrial-genome deficient mitoplasts. The comparison of these activities from murine, ρ^+ and ρ^0 mitoplasts indicate a strong conservation of electrophysiological characteristics. The mtDNA does not seem to play a role in regulation of expression or activty of mCS and MCC. [This research was supported by NSF grant MCB917658.]

Su-AM-B1

CONFORMATIONS OF MYOSIN SUBFRAGMENT-ONE ATPase INTERMEDIATES FROM SMALL-ANGLE SCATTERING. ((R. A. Mendelson[1], D. K. Schneider[2] and D. B. Stone[1])) [1]C.V.R.I. and Dept. Biochem. & Biophys., Univ. Calif. San Francisco, CA 94143; [2]Biology Dept., Brookhaven National Laboratory, Upton, NY 11973.

In order to elucidate the structural changes that occur during the hydrolysis of ATP by myosin, low-angle neutron and X-ray scattering have been used to investigate the shape of the myosin head (S1) with various bound nucleotides and analogs. It was found that the radii-of-gyration (R_g's) of S1·MgADP·AlF_4 and S1·MgADP·V_i were similar and significantly smaller (≈3%) than the similar R_g's of nucleotide-free S1, S1·MgADP and S1·MgADP·BeF_x. In addition, S1 in the presence of MgATP, which is predominantly in the S1·MgADP·P_i state under the experimental conditions employed, showed a change in R_g comparable to that of S1·MgADP·AlF_4 and S1·MgADP·V_i. The results obtained here are in close harmony with crystallographic results on truncated S1 bearing MgADP·BeF_x and MgADP·AlF_4 (Fisher *et al.*, Biochem. 34:8960, 1995). These two systems are postulated to represent the pre-hydrolysis state and the transition state of ATP hydrolysis, respectively, and the structural difference between them might alter the orientation of the light-chain-binding domain (tail) of intact S1 relative to the remainder of the molecule. Since this orientation is the major determinant of the R_g of S1, the current data support the hypothesis that a unitary large-scale conformational cocking of S1 for subsequent force production occurs just before or during ATP hydrolysis. Modeling changes in R_g by rigid-body rotations indicates that the longitudinal component of the force-producing throw is likely to be less than 6 nm. (Supported by NIH AR39710 & AR42895)

Su-AM-B2

INCREASED SPEED OF ACTIN MOVEMENT BY MUTANT CARDIAC MYOSIN FROM PATIENTS WITH FAMILIAL HYPERTROPHIC CARDIOMYOPATHY IN AN *IN VITRO* MOTILITY ASSAY. ((**H. Jiang** *, **A. Chang**§, **K. Poetter** §, **N.D. Epstein** §, **L. Fananapazir**§, & **J.R. Sellers** *)) *Lab. of Molecular Cardiology & §Cardiology Branch, NHLBI, NIH, Bethesda, MD 20892.

We and others have shown that a number of point mutations of ß-myosin heavy chain are associated with familial hypertrophic cardiomyopathy (HCM). Functional studies using an *in vitro* motility assay had revealed decreased speed of actin filaments translocation by some of these mutant myosins. Here we report an increased velocity of actin movement over ß-myosin from HCM patients with a missense mutation at residue 719 (Arg-->Gln) of ß-cardiac myosin heavy chain. Ventricular myosin was purified from cardiac biopsies of patients with the mutation and from normal subjects. Gel-electrophoresis analysis of control and mutant myosin revealed no differences in the molecular migration of the heavy or light chains. The velocity of actin filament sliding over myosin was measured at different ionic strengths (10 to 80 mM KCl) and comparison was made between the paired mutant and normal control. The rate of actin movement by mutant myosin was 0.78 ± 0.04 µm/s whereas the myosin from control was 0.67 ± 0.02 µm/s ($P<0.01$) at 40 mM KCl. In both cases the quality of actin filament movement was the same. In order to understand the mechanism(s) underlying such an increase in actin motility, the mutation was mapped onto the chicken skeletal muscle S1 crystal structure. It lies near the interface of the essential light chain and head region. This area has recently been proposed to act as a hinge for intermolecular movements that are hypothesized to occur during energy transduction. It is possible that removal of a charged amino acid affects these movements. (HJ is supported by a MRC Canada Fellowship)

Su-AM-B3

THE NONMUSCLE MYOSIN HEAVY CHAIN II ISOFORMS, MHC-A AND MHC-B, HAVE DIFFERENT ENZYMATIC ACTIVITIES AND SUBCELLULAR LOCALIZATIONS. ((C.A. Kelley, J.R. Sellers, D. Bui, R.S. Adelstein and I.C. Baines)) NHLBI, NIH, Bethesda, MD 20892-1762. (Spon. by E. Eisenberg)

We are studying the functions of isoforms of the heavy chain of nonmuscle myosin II. There are at least two isoforms of the heavy chain that are products of two separate genes, MHC-A and MHC-B. We used unique peptide sequences in these isoforms to generate antibodies specific for each isoform. These antibodies were used to purify MHC-A and MHC-B for *in vitro* enzymatic studies and subcellular localization. MHC-A and MHC-B were purified from cultured Xenopus kidney epithelial cells by immunoprecipitation with isoform-specific peptide antibodies followed by elution with their cognate peptides. Using an *in vitro* motility assay, we found that the velocity of movement of actin filaments by MHC-A was four-fold faster than that by MHC-B. Likewise, the V_{max} of the actin-activated ATPase activity of MHC-A was approximately three-fold higher than that of MHC-B. Immunofluorescence microscopy using isoform-specific antibodies demonstrated that MHC-B was concentrated in the cell cortex with some diffuse cytoplasmic staining. In contrast, MHC-A was absent from the cell periphery and was arranged in a fibrillar staining pattern in the cytoplasm. Both myosins co-localized with F-actin as shown by double staining with rhodamine-phalloidin. The distinct localizations of MHC-A and MHC-B, together with data demonstrating their markedly different enzyme activities, should help discern the functions of these nonmuscle myosin isoforms in a variety of cellular motile events.

Su-AM-B4

CHIMERIC SUBSTITUTIONS OF THE ACTIN-BINDING LOOP ACTIVATE DEPHOSPHORYLATED BUT NOT PHOSPHORYLATED SMOOTH MUSCLE HEAVY MEROMYOSIN. ((A.S. Rovner[1], Y. Freyzon[2], and K.M. Trybus[2])) Dept. of Molecular Physiology and Biophys., Univ. of Vermont, Burlington, VT 05405[1], and Rosenstiel Basic Medical Sciences Research Ctr, Brandeis University, Waltham, MA 02254[2]

Regulatory light chain (RLC) phosphorylation is necessary to activate smooth muscle myosin, unlike the constitutively active striated muscle myosins. Here we show that a surface loop located at the 50/20-kDa junction, which is part of the actomyosin interface, contributes to this fundamental difference between myosins. Substitution of the native actin-binding loop (ABL) of smooth muscle heavy meromyosin (HMM) with that from either chicken skeletal or rat β-cardiac myosin caused the chimeric HMMs to become unregulated like the myosin from which the loop was derived. Dephosphorylated chimeric HMMs gained the ability to move actin in a motility assay and had 50-70% of the actin-activated ATPase activity of phosphorylated wild-type (WT) HMM. Vmax for the phosphorylated chimeras did not exceed the level of phosphorylated WT-HMM. Direct binding measurements showed that dephosphorylated WT and chimeric HMMs bound to actin with equal affinity in the presence of MgATP. This result implies that a foreign ABL activates dephosphorylated HMM by increasing the rate of a kinetic step other than actin binding, similar to the mechanism by which RLC phosphorylation activates the native molecule. In contrast, a foreign actin binding loop had no effect on trapping of nucleotide at the active site in the absence of actin, suggesting that interaction with actin is needed for a functional role. Native regulated molecules have thus evolved a loop sequence which is unable to trigger rapid product release when actin is present and the RLC is dephosphorylated, thereby allowing regulated release of phosphate under the control of RLC phosphorylation.

Su-AM-B5

REGIONS OF THE ROD IMPORTANT FOR MYOSIN AND PARAMYOSIN ASSEMBLY IN *C. ELEGANS* BODY WALL MUSCLE. ((P.E. Hoppe and R.H. Waterston)) Dept. of Genetics, Washington University School of Medicine, St. Louis, MO 63110

C. elegans body wall muscle contains two isoforms of myosin heavy chain, MHC A and MHC B, that differ in their ability to initiate thick filament assembly. Mutant animals that lack the major isoform, MHC B, show a commensurate reduction in thick filament number and move very poorly. In contrast, mutant animals that lack the minor isoform, MHC A, contain no normal thick filaments, are completely paralyzed, and die as larvae. Only MHC A is present at the center of the bipolar thick filament where myosin dimers must associate in an antiparallel fashion, and where initiation of filament assembly is thought to occur (Miller *et al.*, 1983, Cell 34, 477). To elucidate the nature of MHC A-specific function, we mapped the regions that confer A-specific function by constructing chimeric myosins and testing these constructs *in vivo*. In this manner we have identified 2 distinct regions of the MHC A rod that are sufficient in chimeric myosins for filament inititiation function. Comparison of the protein sequences of A and B in these regions revealed that MHC A has an increased number of hydrophobic residues and decreased number of charges displayed on the rod surface, making it more similar to paramyosin which forms the thick filament core. We propose that these regions of increased surface hydrophobicity mediate close contacts between MHC A and paramyosin in an antiparallel arrangement at the filament center. In addition, MHC A shows unique genetic interaction with paramyosin: overexpresson of MHC A but not MHC B improves the structural defects and motility in animals homozygous for *e73*, a missense allele of paramyosin. Using our chimeric myosins, we found the C-terminus of MHC A to be essential for *e73* suppression. This location of the suppressing activity suggests that parallel myosin-paramyosin assembly occurs by the same molecular stagger as that proposed for paramyosin-paramyosin association (Gengyo-Ando and Kagawa 1991, J Mol. Biol 219, 429).

Su-AM-B6

THE PHOSPHORYLATION EFFECT ON THE CONFORMATION OF THE REGULATORY LIGHT CHAIN MUTANTS OF CHICKEN GIZZARD MYOSIN. ((F. Qian, S. Sukduang, A. Wong, & R.C. Lu)) Muscle Research Group, Boston Biomed. Res. Inst., Boston, MA 02114

In order to study the effects of light chain phosphorylation on the conformation of the smooth muscle myosin, four regulatory light chain mutants, RLC5, RLC18, RLC28, and RLC165, that contain single Cys at 5, 18, 28, and 165, respectively, and the wild type (RLC108) were expressed in E.coli using vector pAED4. Each RLC was labeled with benzophenone-4-iodoacetamide (BPIA) and photolysis was carried out in the free state or in the bound state under various conditions. SDS-PAGE showed that intrachain crosslinks were formed in all five cases in the free state, although the efficiency varies. Each RLC formed more than one kind of crosslinked products, exhibiting different mobilities on SDS-PAGE. Phosphoryation of the RLCs had no effect on the crosslinking patterns in the free state. In the bound state, the yield of the crosslinked products decreased in all cases except RLC5. Further, only one instead of multiple species of crosslinked products formed when phosphorylated RLCs were used. Our results clearly showed that the effects of phosphorylation on the conformation of light chains were manifested when light chains were associated with heavy chains; the conformation of RLCs in the bound state became less flexible after phosphorylation. Supported by NIH AR41637, AR28401.

Su-AM-B7

THE HEAD TO HEAD INTERACTIONS VIA THE N-TERMINAL REGION OF THE REGULATORY LIGHT CHAIN MUTANTS OF CHICKEN GIZZARD MYOSIN. ((F. Qian, A. Wong, & R.C. Lu)) Muscle Research Group, Boston Biomed. Res. Inst., Boston, MA 02114

Four regulatory light chain mutants, RLC5, RLC18, RLC28, and RLC165 that contain single Cys at 5, 18, 28, and 165, respectively, and the wild type (RLC108) were expressed in E.coli using vector pAED4. Each RLC was labeled with benzophenone-4-iodoacetamide (BPIA) and photolysis was carried out in the free state or in the bound state under various conditions. After photolysis, myosin containing RLC28 exhibited three types of crosslinked products on SDS-PAGE. In addition to the intrachain crosslinked RLC, bands with mobilities corresponding to the dimer of RLC and RLC crosslinked to the heavy chains appeared. The formation of RLC dimers were more prominant for myosin containing RLC18. Further, if photolysis was carried out on phosphorylated myosin, the RLC18 dimers appeared as a doublet on SDS-PAGE Similar results were obtained for RLC5 whereas no dimer was visible for myosin containing RLC108 or RLC165. The fact that no dimers formed if photolysis was carried out on RLCs in the free state whether or not it was phosphorylated suggests that the dimers were derived from the RLCs from two heads of myosin. Thus our results show that the N-terminal region of RLC from two heads can come within 11Å to each other and the interaction between two heads of myosin is affected by phosphorylation. Supported by NIH AR41637, AR28401.

Su-AM-B8

PHOSPHORYLATION-DEPENDENT DISTANCE CHANGE BETWEEN RESIDUES 5 AND 165 IN THE REGULATORY LIGHT CHAIN OF SMOOTH MUSCLE MYOSIN ((L.J. Ruan, F. Qian, T. Tao, & R.C. Lu)) Muscle Research Group, Boston Biomedical Res. Inst. 20 Staniford St., Boston, MA 02114.

We have used the technique of resonance energy transfer to study the effects of phosphorylation on the conformation of chicken gizzard smooth muscle myosin regulatory light chain (RLC). Five double Cys RLC mutants, RLC5/165, RLC18/165, RLC28/165, RLC108/165 and RLC28/108 (the numbers refer to the positions of the Cys's) were produced. Each mutant was labeled with 1,5-IAEDANS as the fluorescent donor, and DDP-Mal as the non-fluorescent acceptor. Distance measurements were then carried out on the unphosphorylated and phosphorylated RLC's when bound to myosin heavy chain under various conditions. We obtained distances of 34, 27, 28, 29 and 35 Å for the unphosphorylated RLC's (in the order of the list above). Upon phosphorylation RLC5/165 showed a measurable decrease in the efficiency of energy transfer, corresponding to a ~3 Å increase in distance. Small decreases in transfer efficiency was also apparent for RLC18/165, and no phosphorylation dependent changes were detectable for RLC108/165 and RLC28/108. These results indicate that phosphorylation of RLC causes no large scale inter- or intra-domain reorganization in the molecule, but induces a small displacement of the N-terminal phosphorylation region (residues 1-20) away from the C-terminal domain. (Supported by NIH P01-AR41637)

FOLDING AND SELF-ASSEMBLY: STRUCTURES AND FOLDING PATHWAYS

Su-AM-C1

STRUCTURE AND FLEXIBILITY OF LAMBDA CRO VARIANTS . M. C. Mossing and A. K. M. M. Mollah. Department of Biological Sciences, University of Notre Dame, Notre Dame, IN 46556.

The solution structure of an engineered monomer of the λ Cro Repressor has been determined. It is compared to a recently determined crystal structure (Albright, R.A. Mossing M.C. and Matthews, B.W. Biochemistry in press). Both structures confirm the success of the original design while at the same time pointing to the importance of subtle rearrangements of the core of the protein which accompany DNA binding. The flexibility of the structure has been probed by NMR measurements of amide Hydrogen exchange and ^{15}N relaxation. Combinatorial mutagenesis of hydrophobic core residues has revealed combinations of amino acids which result in substantial stabilization of the structures of both Cro monomers and dimers. The effects of these altered core residues on DNA recognition are under investigation.

Su-AM-C2

THE SOLUTION STRUCTURE OF APOCYTOCHROME b_5. ((C.J. Falzone, C.D. Moore, M.R. Mayer, and J.T.J. Lecomte)) Chemistry Department, The Pennsylvania State University, University Park, PA 16802.

The water-soluble fragment of rat liver cytochrome b_5 is a 98-residue polypeptide folded around a single heme group. The X-ray structure of this fragment shows that it contains a 5 stranded β-sheet and that the heme is inserted within an irregular 4-α helical bundle. There are two additional helices (h1 and h6), contacting sheet but not the heme, which provide side chains to the main hydrophobic core of the protein. A drastic destabilization of cytochrome b_5 occurs when the heme is removed from its site. By using proton-detected ^{15}N NMR spectroscopy to provide over 700 experimental restraints for structure calculation, we show that the destabilization is accompanied by local unfolding at the prosthetic group site. Intact secondary structure is observed in half the molecule, and forms the hydrophobic core. This structure comprises 4 of the 5 strands and the helices h1 and h6. The empty binding site contains only two well-defined turns of helices, whereas the remainder is capable of adopting several conformations. Amide backbone dynamics indicate enhanced internal motion in these regions of the apoprotein. This study presents the apoprotein as a partially folded structure, with a half-formed prosthetic group site ready to accept the heme.

Su-AM-C3

IONIZATION CRITICAL TO CATALYSIS IN CARBOXYPEPTIDASE AND CARBONIC ANHYDRASE AS DETERMINED BY XAFS

K. Zhang[1] and D. S. Auld[2], 1 Biostructures Institute 3401 Market st 345, Philadelphia PA 19104. 2 CBBSM Harvard Medical School, Boston MA 02115.

Carboxypeptidase and carbonic anhydrase are zinc enzymes catalyzing peptide hydrolysis and CO_2 hydration, respectively. Both enzymes have a water molecule bound at their metal sites which is essential for catalysis. In carboxypeptidase, the ionization of the water ligand of zinc is thought to be responsible for either promoting the formation of hydrogen bond with Glu-270 at pH 6 to stabilize the active site structure or disrupting the same hydrogen bond at pH 9, while the ionization of the water ligand of zinc is generally believed to be responsible for the pKa near 7 in carbonic anhydrase. This ionization permits a direct nucleophilic attack of zinc-bound OH^- on the substrate (CO_2). The examination of the XAFS spectrum of carboxypeptidase A over the pH range 7-11 reveals a near edge feature that titrates with pH to give a pK_a identical to the kinetic pK_{EH}. XAFS structural analysis indicates the average first shell ligand distance decreases as the pH increases. Outer shell analyses further indicate that the conformation of the histidine ligands remain unchanged over this pH region. Thus it is reasonable to assign the ionization of the metal-ligand water as the group responsible for pK_{EH}. We also examined the XAFS spectrum of carbonic anhydrase from pH 5.3 to 9. A near edge spectral change is also observed in this pH region. This change, however, is not as dramatic as that observed for carboxypeptidase A. The average first coordination distance for the four ligands is decreased slightly as the pH increases, consistent with the notion that the water ligand is ionized. The analysis also indicates that the zinc is at a more penta-coordinated site at higher pHs rather than a tetrahedral coordination geometry at lower pHs. (This work is supported by NIH GM47534.)

Su-AM-C4

COOPERATIVITY OF CALCIUM BINDING: A MOLECULAR DYNAMICS STUDY OF CALBINDIN D_{9k} IN THE APO, SINGLY AND DOUBLY LOADED STATES.

((Sylvie Marchand and Benoît Roux)), Groupe de recherche en transport membranaire, Département de physique, Université de Montréal, Montréal, Québec, Canada H3C 3J7

Molecular dynamics simulations were used to study the structure and dynamics of calbindin D_{9k}, a protein that binds two calcium ions in a cooperative fashion. Each of the apo, singly and doubly loaded structures was solvated in a sphere of 2285 water molecules and the systems were simulated during 200ps using a modified version of the CHARMM program. Long range electrostatics were taken into account by special methods: electrostatic interactions were not truncated and the solvent reaction field was incorporated through a stochastic boundary potential. The changes in structure and dynamics were evaluated in order to gain insights into the cooperative interactions between the two binding sites. Results indicate that the doubly loaded state is closer, both from structural and dynamical points of view, to the singly loaded state than either of these is to the apo state. Morover, the differences in dynamics are more significant than the differences in structure, suggesting that flexibility is the prime factor affected by calcium binding. General conclusions agree with experimental observations of NMR backbone relaxation order parameters. The influence of amino acid substitutions on the cooperativity of binding will be examined using free energy simulations.

Su-AM-C5

ALTERATION OF THE CFTR FOLDING PATHWAY BY A COMMON CYSTIC FIBROSIS CAUSING MUTATION. ((B.-H. Qu and P. J. Thomas)) Department of Physiology, University of Texas Southwestern Medical Center at Dallas, Dallas, TX 75235-9040.

Most cases of cystic fibrosis arise from the inability of the mutant cystic fibrosis transmembrane conductance regulator, CFTR, to mature and transit to the apical membrane of affected epithelial cells. To study the molecular basis of this defect, the amino terminal nucleotide binding domain, NBD1 (G404 to S589), of CFTR and the major disease-causing mutant form, deletion of phenylalanine 508, ΔF508, were overexpressed at high yield in *Escherichia coli*. The wild type and ΔF508 mutant NBD1 were purified and refolded into functional monomers as revealed by TNP-ATP binding and HPLC gel filtration chromatography. Notably, the thermal stabilities of the two NBD1s are similar. Moreover, the ΔF508 mutation does not significantly alter the thermodynamic stability of the domain as determined by guanidinium hydrochloride denaturation. These results demonstrate that F508 makes no significant contributions to native state stability. In contrast, the stability of a smaller peptide fragment of NBD1, that has some attributes of a kinetically trapped folding intermediate, was dramatically decreased by the ΔF508 mutation, implying F508 exerts its affects on the folding pathway. Further supporting a role for F508 in determining the folding pathway, the temperature dependencies of folding of the mutant and wild type NBD1s are significantly different. These results demonstrate that NBD1ΔF is a temperature sensitive folding mutant, and, thus, cystic fibrosis caused by the ΔF508 mutation may be due to alteration of CFTR folding kinetics rather than destabilization of the final native state. These results have implications for the development of strategies to treat the disease. (Supported by the Welch Foundation).

Su-AM-C6

LEAST ACTIVATION PATH (LAP) MODEL FOR PROTEIN FOLDING. ((T.Y.Tsong, Z.D.Su, H.M. Chen and C.J. Gross)) Hong Kong Univ of Sci & Technol, Kowloon, Hong Kong, and Univ of Minn, St. Paul, MN 55108

Stopped-flow circular dichroism of *staphylococcal* nuclease (SNase), in the time ranges 20 ms to 500 s, has detected one kinetic phase (1.77 s) for unfolding at 2 M GdmCl and three kinetic phases (31 s, 6.1 s, 430 ms) for folding at 0.34 M GdmCl. Corroborated with the quasi-two-state equilibrium unfolding and differential scanning calorimetry data, the time resolved kinetics support the sequential model for SNase folding: $U_3 \rightarrow U_2 \rightarrow U_1 \rightarrow N_0$. The three Us have similar free energies and are all populated under unfolding conditions. ΔG of transition from any of these Us to N_0 is approximately - 4.5 kcal/mol. Analysis based on the model and the observed rates reveals several characteristics of the SNase folding. 1) Although the three Us are "isoenergetic", folding follows a sequential path. In other words, the pathway of folding is not directed by the relative stabilities of the folding intermediates. Random walk, if it occurs at all, is confined to reactions faster than 2 ms (the deadtime of the stopped-flow with fluorescence detection) for the conversion of microscopic states which constitute each of the four macroscopic kinetic species. 2) Folding is a descending toward the global free energy minimum of the native state via the least activation path. Barrier avoidance leads the way and barrier height limits the rate. 3) The main folding reaction ($U_1 \rightarrow N_0$) in which the peptide chain gains its stability, and hence its structure, via van der Waals' contacts, hydrogen bonding, and electrostatic interactions, is a highly concerted process. These energy-acquiring events take place in a single kinetic phase. 4) U_1 appears to be a compact unfolded species: the rate of U_2 to U_1 reaction decreases with increasing solution viscosity. 5) The first activation barrier in folding (19.7 kcal/mol for the $U_3 \rightarrow U_2$ reaction) is mainly enthalpic while the second (18.8 kcal/mol) and the third (17.2 kcal/mol) are mainly entropic. Kinetics monitored by the Trp-140 fluorescence, and kinetics of folding of acid-denatured SNase, are also consistent with the LAP model of protein folding.

Su-AM-C7

FORCES RESPONSIBLE FOR PROTEIN FOLDING IN THE PRESENCE OF OSMOLYTES: A SWITCH IN EMPHASIS FROM SIDE CHAINS TO BACKBONE. ((Aijun Wang & D. W. Bolen)) Dept. of Human Biological Chemistry & Genetics, Univ. of Texas Medical Branch, Galveston TX 77555-1052

Sharks, rays and the coelacanth protect their cells against the osmotic pressure of the sea by concentrating solutes intracellularly. Urea is the principal solute concentrated, reaching levels of 600 mM in one species. To offset the deleterious effects urea has on structure and function of proteins, a second solute, trimethylamine -N-oxide (TMAO) is accumulated to about half that of the urea.

In order to understand how TMAO acts to protect against thermal- and urea-induced denaturation, we determined the transfer free energy of side chains and the peptide backbone from: (1) water to 1M TMAO, (2) from water to 2 M urea, and (3) from water to 1M TMAO + 2M urea. The results show it is unfavorable to expose the backbone to TMAO and that this effect is responsible for stabilization of the protein in the presence of urea. The side chains not only do not play a role in protein stabilization by TMAO, they actually promote the denatured state.

The unfavorable interaction of TMAO with the peptide backbone is a feature now shown to be common to three osmolytes, and it provides a basis for explaining the general ability of osmolytes to protect proteins against unfolding.

Su-AM-C8

EFFECTS OF PRO-117 ON THE FOLDING OF *STAPHYLOCOCCAL* NUCLEASE (SNase). ((Z.D. Su, W.Y. Ao, and T.Y. Tsong)) Dept of Biochem, Hong Kong Univ of Sci & Technol, Kowloon, Hong Kong

Cis/trans isomerization of proline occurs in the 10 s time range. In protein folding, rate processes which fall in the 10 to 100 s time ranges are often attributed to the cis/trans isomerization of one or more of the proline residues. For SNase folding, a relaxation time of 35 s has been assigned to the cis/trans isomerization of Pro-117. However, kinetics of SNase folding from GdmCl, or from acid, monitoring Trp-140 fluorescence, or peptide backbone CD, show that this 35 s rate process is remarkably sensitive to GdmCl concentration. Schmit & Baldwin (1979) reported that proline isomerization in ribonuclease A folding was not. We report a systematic study of the folding/unfolding transition of the mutant P117A by equilibrium and kinetic methods. It was found that: 1) The peptide backbone CD of P117A is nearly identical to that of the WT. The ΔH_{cal} and T_m of thermal unfolding of P117A at pH 7 are also unchanged from those of the WT. 2) For the time resolved kinetics by stopped-flow CD (20 ms to 500 s), folding of P117A at 0.34 M is tri-phasic and unfolding at 2 M GdmCl is mono-phasic, again agreeing with data for the WT. The WT and the mutant SNase both give a slow kinetic phase of ~ 35 s in folding, the amplitude of which is approximately 15% (CD at 222 nm). 3) For the WT, the time-unresolved slow CD signal (> 500 s) was 10% in both folding and unfolding directions. However, in the P117A, this slow CD signal is completely missing. It is concluded that cis/trans isomerization of Pro-117 contributed to this slow CD signal in the WT. (No such signal was detected with Trp-140 fluorescence). 4) The presence of this slow reaction in folding as well as in unfolding for the WT suggests that cis/trans isomerization of Pro-117 can take place in various stages of folding. Thus, the pathway of SNase folding is best represented by two inter-connected parallel sequences, $U_3 \Leftrightarrow U_2 \Leftrightarrow U_1 \Leftrightarrow N_0$, one of which has Pro-117 in cis, and the other in trans isomeric forms.

Su-AM-C9

DNA QUADRUPLEX ASSOCIATION OCCURS VIA CATION-LINKED DISPROPORTIONATION OF TWO [d(TG$_4$)3] TRIPLEXES: ALLOSTERIC LINKAGES. ((Charles C. Hardin[1], Matthew J. Corregan[1], Marianne E. Tioran[1], Charles A. Goss[3] and Jacqueline Hughs-Oliver[2])) Departments of [1]Biochemistry and [2]Statistics, North Carolina State University, Raleigh, NC 27695 and [3]Analytical Development Laboratories, Glaxo-Wellcome Co., Research Triangle Park, NC 27709.

Association reaction kinetics for assembly of four d(TG$_4$) strands were measured as a function of KCl, strand and buffer concentrations. The results indicate that [d(TG$_4$)$_4$ • 3 K$^+$] formation involves two resolved processes whose rates typically differ by about 10-fold. The association mechanism appears to involve allosteric activation wherein potassiums act as allosteric effectors by shifting the d(TG$_4$) strand population from 'relaxed' (R) single-strands to 'tense' (T) cation-bound [d(TG$_4$)$_m$•(K$^+$)$_n$] duplex, triplex and quadruplex [d(TG$_4$)$_m$•(K$^+$)$_n$] structures. Kinetic evidence suggests that strand delivery occurs via a recombination-like strand-passage event involving cation-driven disproportionation of two triplexes to form cation-bound quadruplex and duplex species. Donor triplex decomposition is thought to be catalyzed by solvent acid-base species, facilitating strand passage. The need to regenerate reactants during equilibration supports 'water-wheel'-like steady-state recycling of d(TG$_4$) strands driven by K$^+$, acid-base components of the solvent and Boltzmann energy. Since regenerated strands must always be present to support immediate precursor formation, quadruplex assembly does not proceed to completion under most practical conditions *in vitro* (range of apparent reaction extents: 40-90%). Solvent components support both dissociation and association of quadruplexes. In the former case, they 'chip away' at the the labile hydrogen bonds and cation-guanine linkages; in the latter, they assist these linkages to reform. By analogy- "icepicking" and "spot welding', respectively.

Su-AM-D1

MECHANISMS FOR THE FAST MOTILITY OF THE OUTER HAIR CELL. ((K.H.Iwasa)) NIDCD, NIH, Bethesda, MD 20892-0922.

Recent experimental studies have established that the fast motility of the outer hair cell is caused by a membrane motor, which directly utilizes the electric energy obtained at the plasma membrane. Such a membrane motor is based on conformational changes in the motor in which movements of a charge across the membrane is coupled with mechanical changes in the motor. These mechanical changes include the cross sectional area of the motor in the membrane. A model incorporating area changes into the membrane motor can be referred to as an 'area motor.' This model has been successful in describing the motility of the ohc [Iwasa, J. Acoust. Soc. Am. 96 (1994) 2216]. An alternative mechanism could be called 'stiffness motor,' in which mechanical changes in the motor is in the stiffness instead of in the cross sectional area. The most striking difference between the two is that whereas relatively small area changes are required to explain the magnitude of the motility in the area motor model, drastic stiffness changes are required for the stiffness motor model. In both models, the state of the motor is dependent on both the membrane potential and membrane tension, predicting a shift of the peak capacitance voltage in the depolarized direction on an increase in tension. The shift of the peak is, however, proportional to the square of tension for the stiffness motor instead of a linear dependence for the area motor. The maximum amplitude of the voltage dependence, predicted by the stiffness motor, is proportional to the internal pressure of the cell, whereas the maximum amplitude predicted by the area motor is insensitive to the pressure, provided that the cell is sufficiently inflated. The experimental data support the area motor model.

Su-AM-D2

ALTERNATE RNA WRAPPING MODES AROUND TRANSCRIPTION TERMINATION FACTOR RHO LIMIT MODELS FOR TRANSLOCATION. ((Stephen Swenson and Steven E. Seifried)) Department of Biochemistry and Biophysics, University of Hawaii, Honolulu, HI 96822.

Transcription Termination Factor rho from *E. coli* is reported to undergo a unidirectional translocation as it utilizes ATP hydrolysis to move toward the RNA polymerase, where the protein acts as a helicase to release the nascent transcript from the elongating transcription complex. Several physical mechanisms have been proposed to account for the motion of rho. A successful model must account for the observed D3 subunit organization and the ATPase functional dimer model, both previously described by this author. We present new kinetic and stoichiometric data from fluorescent polymers that clearly indicates there to be two possible wrapping modes of RNA around the rho hexamer. The first mode has the single-stranded polynucleotide cofactor wrap once around the perimeter of the protein, filling all the cofactor binding sites and activating the NTPase activity. All polynucleotide cofactor sites undergo binding and release cycles. The second mode of binding has the RNA wrapping twice around the hexamer, generating two classes of polynucleotide binding sites, one of which does not release polymer. This mode allows a tethered tracking model of translocation. Prior descriptions of the dependance of NTPase activity on the stoichiometry of added polynucleotide cofactor show that an ensemble of proteins can have a mixture of rho hexamers with one or the other of the wrapping modes.

Su-AM-D3

SINGLE MOLECULE IMAGING OF MOTION AND ATPase REACTION OF MOTOR PROTEINS

((T. Funatsu, Y. Harada, H. Higuchi, M. Tokunaga, K. Saito, R. Vale, & T. Yanagida)) *Yanagida Biomotron Project, JRDC, Mino, Osaka, Japan.*

We have refined total internal reflection fluorescence microscopy (TIRFM) to visualize single fluorescent dye molecules in aqueous solution at a full video rate (Funatsu, et al., Nature,374,555 '95). We extended this method to measurements of single molecule ATPase reaction and motion. Individual ATP turnover events by single kinesin molecules were detected by directly observing association–(hydrolysis)–dissociation of fluorescent ATP analogue, in which Cy3 is attached to ribose. Single kinesin molecules were attached to beads, of which position was controlled by optical trapping nanometry. When the kinesin molecule was in solution, apart from a microtubule on a glass surface, the ATP turnover rate was very small, ~0.2s^{-1}. While, when it was brought into contact with a microtubule, the rate was greatly enhanced to be ~10s^{-1}. Since this method enables us to control the load and measure nm–scale displacements, we will be able to measure the ATP turnovers and the unitary steps of single kinesin molecules simultaneously. This method was also used to directly observe motion of single fluorescetly–labeled kinesin molecules along microtubules.

Su-AM-D4

PROCESSIVITY OF DIMERIC KINESIN ACHIEVED BY COORDINATION OF THE ATPASE CYCLES. ((S.P. Gilbert[1,2], M.L. Moyer[1], & K.A. Johnson[1])) Biochemistry & Molecular Biology[1], Pennsylvania State University, University Park, PA 16802 and Biological Sciences[2], University of Pittsburgh, Pittsburgh, PA 15260.

Kinesin is distinctive as a mechanochemical enzyme in that a single molecule (two motor domains) will promote translocation along a microtubule for several micrometers and at maximal velocities. Previous kinetic studies have defined the mechanistic basis of this phenomenon and show that processive ATP hydrolysis is established in part by sequential release of the kinesin motor domains from the microtubule followed by immediate and very rapid rebinding of kinesin to the microtubule (Gilbert *et al.*, 1995 *Nature* 373, 671). The stopped-flow kinetic results with dimeric K401 and monomeric K341 show that rebinding of kinesin to the microtubule is also a sequential process. Furthermore, the timing of rebinding of the second head to the microtubule is dependent upon ATP binding at the active site of the first head. ATP hydrolysis is not required, and ATP binding is sufficient to induce the conformational change required for the fast rebinding of the second head. The results reveal one step in the ATPase pathway that coordinates the interactions of the kinesin heads with the microtubule lattice, leading to processive translocation. Supported by NIH GM 26726 to KAJ, U. Pittsburgh to SPG, NIH Predoctoral Fellowship to MLM.

Su-AM-D5

Load-Dependence of the Discrete Movements of Kinesin

C. M. Coppin*, J. T. Finer*, J. A. Spudich*, and R. D. Vale+*
* Dept. of Pharmacology,+ Howard Hughes Med. Inst., Univ. of California, San Francisco, CA. * Dept. of Biochem. & Develop. Biol., Beckman Ctr., Stanford Univ. School of Med., Stanford, CA

Kinesin is a molecular motor that transports organelles in one direction along microtubules. It does so by undergoing discrete movements, some of which could be resolved from the noise in positional data obtained with an optical trapping interferometer[1,2]. Kinesin has also been found capable of transporting objects against a linearly increasing load up to about 4-6 pN, at which point it appears to stall[1-4]. Two classes of models are usually considered in attempting to explain why the motor stalls under a high load. 1) The chemical ATPase cycle continues while the mechanical cycle comes to a halt (uncoupling). 2) Both the ATPase cycle and the mechanical cycle come to a halt (tight coupling with load-dependent chemical rate constants). Using an optical trap microscope with a high signal-to-noise ratio[5], we were able to directly observe numerous discrete forward and backward 5-10 nm movements of a bead attached to a single kinesin molecule traveling along a microtubule. Under a low load, a high proportion of the movements were found to go forward, but with increasing load this proportion decreased, reaching ~50% at ~5 pN. Furthermore, the load-dependence of the relative frequencies of detectable forward and backward movements could account quantitatively for the load-dependence of the mean velocity of the motor. These findings suggest that, contrary to the models above, the mechanical cycle persists under a stall-producing load, but there is a net balance between forward and backward movements. This information may provide new insights into the determinants of motor directionality.

1. K. Svoboda et al., *Nature (London)* **365**, 721 (1993).
2. K. Svoboda, S. M. Block, *Cell* **77**, 773 (1994).
3. E. Meyhöfer, J. Howard, *Proc. Natl. Acad. Sci. USA* **92**, 574 (1995).
4. S. C. Kuo, M. P. Sheetz, *Science* **260**, 232 (1993).
5. J. T. Finer et al., *Nature (London)* **368**, 113 (1994).

Su-AM-D6

A RECIPROCATING MOTILITY FUNCTION IN ELECTROFUSED ERYTHROCYTES. ((M. Baumann and A. E. Sowers)) Department of Pathology, University of Maryland at Baltimore, Baltimore, MD 21201.

We have characterized a reciprocating mechanical oscillation that can easily be found in a large fraction of electrofused erythrocytes. Under our conditions, up to about 30% of all doublet, or higher N, electrofusions show this oscillation. In fused doublets the oscillation appears as a roughly linear and slow expansion of the diameter of the "hourglass constriction" which proceeds simultaneously with a slow contraction of the pole-to-pole length. At what appears to be a threshold, the diameter shrinks simultaneously with an expansion in the pole-to-pole length. This takes place rapidly (within a few video frames). The change in length is about 10% and are easily observable by video light microscopy. The periodicity is variable from 5 - 60 sec and subsequent periods often decrease substantially in length. There is also heterogeneity in the number of cycles; some fusions produce only one, others cycle up to 10-20 times before stopping. For the range studied, the characteristics of the reciprocation do not appear to be dependent on the strength of the electric field pulse. This system is easy to reproduce and may be of interest in novel studies. To our knowledge, this phenomenon was originally discovered, but not characterized, in another laboratory (Studia Biophysica 121:37-43 |1987|). Supported by ONR grant N000-89-J-1715 and NIH grant RO3-RR07764 to AES.

Su-AM-D7

THE ROLE OF LINKER PROTEINS (PROTEIN 4.1 and ANKYRIN) IN CELL MEMBRANE FLUCTUATIONS OF HUMAN ERYTHROCYTES

(S. Tuvia, S. Levin and R. Korenstein) Department of Physiology and Pharmacology, Sackler Faculty of Medicine, Tel-Aviv University 69978 Tel-Aviv, Israel

The observation of low-frequency fluctuations of the cell membrane in erythrocytes and in several nucleated cells suggests that this phenomenon is a general property of the living cell. The study of cell membrane fluctuations (CMF) was carried out by a novel Point Dark Field Microscopy. CMF, which consist of local reversible displacements of the cell membrane in the range of 0.3-20Hz, reflect the dynamics of the cortical skeleton. The present study examines the involvement of human erythrocyte membrane-skeleton linker proteins (protein 4.1 and ankyrin) in CMF. Protein 4.1 links the skeleton to the membrane via glycophorin C and band 3. It was previously shown (Gascard et al., 1993) that decrease of intracellular levels of inositol phospholipids induce the dissociation of protein 4.1 from glycophorin C. The activation of endogenous phospholipase C (PLC) by calcium ions caused an amplitude decrease of CMF by 27%. A similar activation of inositol specific PLC in erythrocyte open ghosts, which undergo MgATP induced fluctuations, led to a 60% decrease of CMF amplitude. Therefore, it seems that the dynamic association of glycophorin C with protein 4.1 is responsible for local mechanical fluctuations of the cell membrane of human erythrocytes. Selective dissociation of ankyrin from the band 3 protein carried out by pH elevation from 7.4 to 8.7 (Low et al., 1991) led to a 40% amplitude increase of CMF. Thus, it may be suggested that the association of ankyrin to band 3 protein constrains CMF.

CARRIERS, EXCHANGERS, COTRANSPORTERS

Su-AM-E1

EXPRESSION CLONING AND CHARACTERIZATION OF THE THYROID SODIUM/IODIDE SYMPORTER. ((Ge Dai, Orlie Levy and Nancy Carrasco)) Department of Molecular Pharmacology, Albert Einstein College of Medicine, 1300 Morris Park Ave. Bronx, NY 10461.

The Na^+/I^- symporter (NIS) is a key transport membrane protein that catalyzes the active translocation of I^- into the thyroid. This protein plays a crucial role in thyroid hormogenesis and in the evaluation, diagnosis, and treatment of various thyroid pathological conditions. A cDNA clone that encodes NIS has been isolated by functional screening of a cDNA library from a rat thyroid-derived cell line (FRTL-5 cells) in *X. laevis* oocytes. Microinjection into oocytes of a cRNA transcript made *in vitro* from this single cDNA clone elicited a >700-fold increase in perchlorate-sensitive Na^+/I^- symport activity over background. The apparent K_m for I^- was 36 μM in oocytes microinjected with this transcript and the generated I^- concentration gradient in these oocytes was >30 fold, i.e. virtually identical to that observed in the thyroid gland *in vivo*. COS cells transfected with NIS cDNA clone exhibited perchlorate-sensitive Na^+/I^- symport activity. The predicted sequence of NIS comprises 619 amino acids (relative molecular mass 65,196). The hydropathic profile and secondary structure predictions of the protein suggest 12 putative transmembrane domains. Three potential N-glycosylation sites were identified. The secondary structure model predicts that both the NH_2 and COOH termini are located on the cytoplasmic side. The model also shows three charged residues located within transmembrane domains, i.e. Asp 16, Glu 79, and Arg 208 in domains I, II and VI respectively. These residues may be involved in Na^+/I^- symport activity.

Su-AM-E2

MOLECULAR CLONING OF A NOVEL Na/Ca EXCHANGER GENE PRODUCT FROM RAT BRAIN. ((J. Lytton, K.-H. Rhee, D. Bungard and S.-L. Lee)) Dept. Med. Biochem., University of Calgary, Calgary, Alberta, Canada, T2N 4N1.

Sodium-calcium exchange activity in brain neurons has been reported to have properties distinct from the exchanger of heart. We have isolated a cDNA molecule encoding a novel Na/Ca exchanger from rat cerebrum. Northern blot analysis of this clone revealed a transcript of about 10 kb in length whose expression was restricted to brain. The protein encoded by this cDNA displayed significant sequence homology to the Na/Ca-K exchanger from bovine rod outer segments. Within the hydrophobic region encompassing proposed transmembrane spans M6 to M10, there was 80% amino acid identity, and in the M1-M2 region, 60% identity At the predicted amino-terminus of our clone and in the large cytoplasmic loop, however, there was little similarity. To determine if these differences were due to alternative splicing and/or species differences of a single gene, or due to the expression of two separate genes, we used PCR to isolate a fragment of the rat eye Na/Ca-K exchanger. The eye and brain fragments had a difference of 23% scattered over the entire length of 350 nt, and were clearly the products of separate genes. Moreover, Northern blot analysis revealed that, as in cow, the rat eye Na/Ca-K exchanger was 6 kb in length and expressed only in eye. These results indicate that we have isolated a novel gene product corresponding to an isoform of the Na/Ca-K exchanger expressed in rat brain. Further analysis of this molecule is in progress.

Su-AM-E3

USE OF A CYSTEINE-CONTAINING ANALOG OF THE EXCHANGE INHIBITORY PEPTIDE TO PROBE NA-CA EXCHANGE STRUCTURE AND FUNCTION. ((C.C. Hale, S. Bliler, W.Y. Xu, and C. Gatto)) Dalton Cardiovascular Research Center and Departments of Biomedical Sciences and Physiology, University of Missouri, Columbia, MO 65202.

The exchange inhibitory peptide (XIP) is a potent inhibitor of Na-Ca exchange (NCX). A XIP analog (cysXIP) with cysteines substituted at positions 12 and 14 is nearly as potent as XIP in inhibiting NCX activity in bovine cardiac sarcolemmal vesicles (BSL). A sulfhydryl-containing heterobifunctional cross-linking agent (APDP; Pierce) labeled with ^{125}I forms a disulfide bridge with cysXIP that is readily disrupted by reducing agents. ^{125}I-APDP-cysXIP was cross-linked to BSL vesicle protein by irradiation with uv light. Vesicle proteins were subjected to reducing SDS-PAGE and autoradiography which revealed a transfer of the ^{125}I-APDP label to the 70 kDa form of the NCX protein. We have previously reported that the ability of positively charged XIP to inhibit NCX activity is a function of solution ionic strength suggesting that XIP binding may be partly electrostatic (JBC 267:17836-17841, 1992). Two negatively charged peptides IDDDIFEEDEN and GEDDDDDECGEE corresponding to regions 444-455 and 732-743 respectively of NCX cytoplasmic loop f were tested for their ability to interact with ^{125}I-APDP-cysXIP. In these experiments, ^{125}I-APDP covalently linked to IDDDIFEEDEN but not GEDDDDDECGEE. These data suggest that the 70 kDa NCX protein contains the XIP binding site and this site may include the negatively charged region of loop f at amino acid residues 444-455. Supported by the American Heart Association (CCH).

Su-AM-E4

EFFECTS OF SITE-DIRECTED MUTAGENESIS IN THE PUTATIVE TRANSMEMBRANE SEGMENTS ON CARDIAC Na^+/Ca^{++} EXCHANGER ELECTROGENICITY. ((A.E. Doering, D.A. Nicoll, J.N. Weiss, and K.D.Philipson)) UCLA Cardiovascular Research Labs, Los Angeles, CA 90024

The Na^+/Ca^{++} exchange protein transports Na^+ across the cell membrane in exchange for Ca^{++} and plays an important role in cytoplasmic Ca^{++} regulation. We have used the giant patch technique to measure Na^+/Ca^{++} exchange current in *Xenopus* oocytes expressing the cardiac Na^+/Ca^{++} exchanger. The exchanger was deregulated by exposure to cytoplasmic chymotrypsin, and outward current was activated by increasing cytoplasmic Na^+ (Na^+_i). The external medium contained 8 mM Ca^{++} and 0 Na^+. The wild type current-voltage (I-V) relation was linear with 100 mM cytoplasmic Na^+ and became steeper and more curved with 8 mM Na^+_i. This suggests that decreased Na^+_i causes some voltage-dependent reaction, presumably in the Na^+ translocation pathway, to become rate limiting. The K_D for Na^+_i increased as the membrane was hyperpolarized, as shown previously. Site-directed mutation of residue 837 (G837A), which is modeled to be at the external end of transmembrane segment 9, gave a curved I-V relationship with 100 mM Na^+_i (similar to that seen with 8 mM Na^+_i in the wild type), and the K_D for Na^+_i was no longer voltage-dependent. At 0 mV, the K_D is the same for wild type and G837A. We interpret these findings to indicate that the mutation G837A causes a voltage-dependent reaction whose rate is less dependent on Na^+_i to become rate-limiting. Potential mechanisms derived from a model of Na^+/Ca^{++} exchange rate equations will be discussed.

Su-AM-E5

KINETICS OF FORWARD AND REVERSE GLUTAMATE TRANSPORT
((N. Zerangue, E. Tanaka, and M. P. Kavanaugh)) Vollum Institute, Portland, OR 97201

Cloned human glutamate transporters were expressed in *Xenopus* oocytes and transport was measured while simultaneously recording currents under voltage clamp. In oocytes expressing the neuronal transporter EAAT3, the total concentration of endogenous substrate ($[L\text{-}Glu+L\text{-}Asp]_i$) was 4.6±0.6 mM. Following equilibration of the intracellular pool with [^{3}H]L-Glu or [^{3}H]D-Asp, elevation of $[K^+]_O$ induced a concentration-dependent release of radiolabel (EC_{50} = 11±4mM at 0 mV) and an outward current (EC_{50} =10±2mM at 0 mV), both of which were increased at more positive potentials. Efflux was blocked by external kainic acid, a non-transported competitive uptake inhibitor, with an IC_{50} of 1.3±0.2 mM. Elevation of $[K^+]_O$ induced a much larger outward current when NO_3^- was substituted for Cl^-, with no change in efflux of [^{3}H]L-Glu, indicating that reverse transport activates the same anion conductance associated with influx (Wadiche et al. Neuron 15 721 1995). A voltage jump from -80 mV to +40 mV in the presence of 30 mM $[K^+]_O$ induced an acidification in the extracellular space as measured with a pH-sensitive electrode, consistent with transport of a pH-changing species (Bouvier et al. Nature 360 471 1992). Reducing external pH to 6.5 reduced the efflux current to 56±11% of the value at pH 7.5. In the absence of external L-Glu, with $[K^+]_O$=30 mM, a pre-pulse to +80 mV to activate efflux was given followed by pulses to negative potentials. This procedure resulted in a transient inward current which appeared to reflect forward transport mediated by the fraction of transporters which had not yet unbound L-Glu during the efflux cycle. This transient current was $[Na^+]_O$-dependent (EC_{50}=33±2 mM at -120 mV), suggesting that Na^+ unbinds much more rapidly than L-Glu. The decay time constant for the inward current was 153±7 ms at -90 mV and changed e-fold/88±7 mV, similar to the voltage-dependence of [^{3}H]L-Glu uptake. The amplitude of the transient inward current exhibited an exponential dependence on the duration of the prepulse (τ=395±35 ms; prepulse to +80 mV). We suggest these values reflect time constants of partial forward and reverse transport cycles, respectively.

Su-AM-E6

DROSOPHILA AND HUMAN SEROTONIN TRANSPORTERS: EXPRESSION AND ELECTROPHYSIOLOGICAL CHARACTERIZATION. ((A. Galli, E. Barker, M. deBlaquiere, R.D. Blakely and L.J. DeFelice)) Pharmacology, Vanderbilt University, Nashville TN 37232. (Spon. by W. S. Sale) Serotonin (5HT) transporters (SERTs) are the targets for antidepressants and drugs of abuse such as cocaine. Amphetamines and psychoactive drugs such as "ecstasy" also interact with SERTs. We have microinjected cRNA encoding the *Drosophila* serotonin transporter (dSERT) into *Xenopus* oocytes to determine 5HT uptake characteristics and the ion permeation of the 5HT transporter under voltage-clamp conditions. In the absence of 5HT, substituting Na^+ with Li^+ stimulates a large, paroxetine-insensitive inward current. 5HT partially blocks this leak current. [^{3}H]5HT uptake in injected oocytes depends on membrane voltage and on extracellular Na^+ concentration. dSERT has greater than 50% amino acid similarity with human serotonin transporters (hSERT), with greatest identity in the twelve transmembrane domains and greatest diversity in the cytoplasmic tails. By addressing the effect of ion substitution and voltage on 5HT uptake and SERT-associated currents, we will examine mechanistic aspects of the transporter. hSERT expressed in *Xenopus* oocytes is also electrogenic. We are presently comparing species homologues with well-defined, differential pharmacology and have constructed dSERT/hSERT chimeras to test specific mechanistic hypotheses.

Su-AM-E7

CONSERVATIVE SER158THR REPLACEMENT INACTIVATES THE YEAST MITOCHONDRIAL PTP (PHOSPHATE TRANSPORT PROTEIN). ((A. Phelps, C. Briggs, L. Mincone, and H. Wohlrab)) Boston Biomedical Research Institute and Harvard Medical School, 20 Staniford Street, Boston, MA 02114.

The PTP from the yeast *Saccharomyces cerevisiae* has been expressed in *Escherichia coli* as inclusion bodies, purified, and reconstituted (1). The extramembrane loops of this intrinsic membrane protein have not yet been identified with catalytic function. Photolabeling studies with the ADP/ATP translocase, a membrane protein that also belongs to the mitochondrial transport protein family (triple tandem repeat, six transmembrane helices per subunit, homodimer) demonstrate that azido-atractyloside (2) and azido-ADP/ATP (3,4) react primarily with amino acids in the matrix protein loop connecting the two transmembrane helices of the second tandem repeat, the same sequence region as Ser158 in PTP. The Ser158Thr replacement cannot rescue the *Saccharomyces cerevisiae* PTP null mutant on glycerol medium. The reconstituted transport activity of this mutant PTP shows less than 2% of the wild type activity in net phosphate uptake in the presence of a pH gradient. On the other hand, replacing this Ser158 with Met or Cys results in high wild type transport activity with a wild type Km for phosphate transport. Additional studies are currently directed towards an explanation of why Met but not Thr can replace Ser158. Our present results suggest strongly that this Ser158 and its transmembrane helices-connecting loop must be located within the membrane to have a more direct role in phosphate transport. (Supported by GM33357 from the USPHS NIH). (1) *Biochemistry* (1994) **33** 9371, (2) *Biochemistry* (1983) **22** 477, (3) *Biochemistry* (1988) **27** 5141, (4) *FEBS Lett.* (1989) **244** 421.

Su-AM-E8

SIMULTANEOUS MEASUREMENTS OF PROTON AND CALCIUM CONCENTRATION PROFILES INDUCED BY A23187 IN THE IMMEDIATE MEMBRANE VICINITY ((P.Pohl, S.M.Saparov, O.N.Kovbasnjuk)) Inst. Med. Physik und Biophysik, Martin-Luther-Universität, 06097 Halle, Germany

A double barrelled microelectrode sensitive to both calcium ions and protons was used to measure concentration profiles in the immediate vicinity of a planar bilayer lipid membrane. The concentration shifts were induced by the action of the ionophore A23187. For both ions the same thickness of the unstirred layer (USL) was obtained. From theoretical considerations it was expected to be a function not only of physical properties and the velocity of the solution, but also of the diffusion coefficient of the solute. Since the size of the USL was found to be identical for different substances the conclusion was drawn that it was a constant for a given fluid motion.
Over a range of conditions the antiport ratio $2H^+:Ca^{2+}$ was found. It changed under conditions of an extremely low Ca^{2+} concentration at one side of the membrane. Channel formation and electrogenic character of the transport process were checked and found to be not responsible for this behaviour.

ANION CHANNELS

Su-AM-F1

Elimination of ClC-0 slow gating. P. Fong and T.J. Jentsch. ZMNH, University of Hamburg, Hamburg, Germany.

To elucidate the structural basis of slow gating of the *Torpedo* chloride channel, ClC-0, chimerae and deletion mutants were analyzed functionally in *Xenopus* oocytes. While substitution of the amino terminus with that of ClC-2 abolished slow gating, deletions of the native N-terminus did not change gating, suggesting that loss of gating by the former results not from a loss of native structures, but from an interaction with the introduced portion of ClC-2. This interaction differs from that responsible for ClC-2 slow gating. C-terminus substitution following transmembrane domain 12 (D12) with that region of ClC-2 also eliminated slow gating. The open channel I-V of all C-terminus chimerae studied was unchanged. When the region consisting of the conserved domain 13 and the 3' end (D13+) was replaced by its ClC-2 analog, slow gating was conserved, suggesting a dependence on structures within the interdomain stretch (IDS) between D12 and D13. Surprisingly, replacement of the native IDS with that of ClC-2 showed slow gating, albeit altered. Thus, as was the case for the N-terminus mutants, replacement of the entire C-terminus with that of ClC-2 eliminates slow gating possibly not by elimination of a native region essential for slow gating, but by interactions with the channel. Analysis of IDS substitution chimerae also reveals the presence of a novel mechanism that produces a current decrease upon very strong hyperpolarization, leading to an apparent shift in the $V_{1/2}$.

Su-AM-F2

GATING OF Ca^{2+}-DEPENDENT Cl^- CHANNELS FROM RAT PAROTID ACINAR CELLS. ((J. Arreola[1,2], J.E. Melvin[1] and T. Begenisich[2])) Depts. of Dental Research and of Physiology, Univ. of Rochester, Rochester, NY 14642.

Ca^{2+}-dependent Cl^- channels are thought to be the apical pathway for Cl^- efflux driving fluid and electrolyte secretion in exocrine glands. In these experiments the activation of macroscopic Ca^{2+}-dependent Cl^- currents ($I_{Cl,Ca}$) was studied using the whole cell configuration of the patch clamp technique in cells dialyzed with free Ca^{2+} concentrations ($[Ca^{2+}]_i$) in the range of 0 to 5 μM. $I_{Cl,Ca}$-membrane voltage (E_m) relationships had strong outward and little, if any rectification at low and high $[Ca^{2+}]_i$, respectively. $I_{Cl,Ca}$ was carried by Cl^- since the relationship between the shift of the reversal potential and external Cl^- activity had a slope of -52 mV/decade of $[Cl^-]$. The conductance-E_m relations at different $[Ca^{2+}]_i$ showed that the channel open probability increased as the E_m became positive. Furthermore, this relationship shifted toward negative E_m as the $[Ca^{2+}]_i$ increased indicating that the open probabilitly increased with increasing $[Ca^{2+}]_i$. The relationships between $[Ca^{2+}]_i$ and the relative conductance for E_m in the range of -107 to +94 mV had an E_m-dependent apparent dissociation constant which increased at negative E_m, and a Hill coefficient of 1.2-2.4. These results suggest that Ca^{2+} directly gates Cl^- channels and that more than one Ca^{2+} ion is required to activate one Cl^- channel. The results were modeled considering the channel activation as sequential transitions between 3 closed states and 1 open state ($C_1 \leftrightarrow C_2 \leftrightarrow C_3 \leftrightarrow O$). Activation starts with the sequential binding of 2 Ca^{2+} ions to 2 identical sites which moves the channel to C_3 state and then proceeds to the open state (O) with the voltage stimuli. This model reproduced the steady-state relative conductance-$[Ca^{2+}]_i$ relations, the $I_{Cl,Ca}$-E_m curves and the time course of $I_{Cl,Ca}$. It is concluded that these Cl^- channels are directly gated by Ca^{2+}, and that the Ca^{2+}-dependecy of Ca^{2+}-activated Cl^- channels is consistent with their involment *in fluid* secretion.
This research was supported by a grant from NIH DE09692.

Su-AM-F3

TRANSPOSITION OF THE CHLORIDE CHANNEL I_{CLN} FROM THE CYTOSOL INTO THE CELL MEMBRANE AFTER VOLUME STRESS

((Markus Paulmichl, Andreas Laich, Hannes Fürst, Martin Gschwentner, Ulrich O. Nagl, Anton Hittmair[§], Markus Ritter)) Department of Physiology, Fritz-Pregl-Str. 3, [§] Department of Pathology, Müller-Str. 44, University of Innsbruck, A-6020 Innsbruck, Austria, Europe.

Expression cloning revealed a 235 AA protein, which, expressed in oocytes, is similar to the swelling-dependent chloride current identified in various cell systems. Using antisense oligodeoxynucleotides identical to the (-)strand of the first 30 nucleotides of the ORF coding for I_{Cln} it was possible to abolish the endogenous chloride current provoked after swelling NIH 3T3 fibroblasts by reducing extracellular osmolarity from 290 to 240 mosM (omitting mannitol). These experiments indicate that I_{Cln} is a major constituent involved in regulatory volume decrease (RVD). Using a synthetic peptide we made a highly specific polyclonal antibody which is able to recognize I_{Cln} in the denatured as well as in the native form. These antibodies were used to identify I_{Cln} in homogenates from NIH 3T3 fibroblasts, MDCK and LLCPK1 cells. Whereas in fibroblasts and MDCK cells in the absence of osmotic stress the I_{Cln} protein is primarily identified within the cytosol with only a minute part unshroud in the membrane (≈ 5%), LLCPK1 cells show a 50/50 distribution between cytosol and membrane. A similar pattern of distribution can be recognized in the former two cell lines after reducing extracellular osmolarity pointing to the possibility that LLCPK1 cells are somehow permanently exposed to a similar stress. One source of such a constant volume challenge could be the high amount of solute/sodium cotransporter expressed in those cells. Accordingly, in the proximal tubular cells of rat kidney the I_{Cln} protein can be exclusively identified in the apical membrane of the cells.

Su-AM-F4

EFFECTS OF EXTERNAL CHLORIDE ION ON THE VOLTAGE-DEPENDENT GATING OF CLC-0 CHANNEL: A SINGLE-CHANNEL STUDY.

((T.-Y. Chen and C. Miller)) Howard Hughes Medical Institute and Department of Biochemistry, Brandeis University, Waltham, MA 02254.

The voltage-dependence of the fast gating (activation-deactivation) of *Torpedo* ClC-0 channel was recently found to be strongly affected by extracellular Cl^- concentration, prompting an idea that the movement of the permeating anion, Cl^-, across the membrane electric field accounts for all of the voltage-dependence of channel opening (Pusch et al. Nature 373: 527). To investigate this possibility, we examined the effect of external Cl^- concentration on the fast gating of single ClC-0 channels purified from the *Torpedo* electric organ. The channel was reconstituted into lipid bilayers, and the Cl^- concentration on the external side was varied from 1 mM to 600 mM with a fixed Cl^- concentration on the cytoplasmic side. Increasing external Cl^- concentration facilitates channel opening. This Cl^- effect, mainly on the opening rate of the channel, saturates at Cl^- concentrations above 300 mM. The maximal opening rate of the channel under saturated Cl^- concentration increases with membrane depolarization. The dissociation constant for Cl^- binding to the closed state channel is also weakly voltage-dependent. Thus, the voltage-dependence of channel opening comes from both the inherent voltage-dependence of the channel protein and the voltage-dependence of the Cl^- binding, with the latter playing a minor role.

Su-AM-F5

PURIFICATION AND SINGLE-CHANNEL ANALYSIS OF HETEROLOGOUSLY EXPRESSED CLC-0 CHANNELS

((R.E. Middleton and C. Miller)) HHMI, Graduate Department of Biochemistry, Brandeis University, Waltham MA 02254.

Torpedo electric organ is a rich source of a voltage-gated Cl^- channel, ClC-0, the founding member of the ClC family of Cl^- channels. This family includes the major Cl^- channel in skeletal muscle (ClC-1) and several Cl^- channels from kidney. The single-channel properties of the native *Torpedo* channel ClC-0 have been characterized extensively. However, cellular patch-clamp techniques have thus far not been useful for single-channel analysis of ClC-0 after heterologous expression. This is apparently due to channel aggregation in the plasma membrane leading to patches containing either many channels or none. We have overcome this technical limitation by purifying the ClC-0 channel after high-level expression in mammalian cells. The purified channel (5-10 μg) is dispersed in lipid-detergent micelles at a controlled density. We routinely observe single ClC-0 channels by fusing the resulting liposomes into planar lipid bilayers. The expressed channel displays the same double-barreled gating behavior observed in channels from *Torpedo* electric organs. We are analyzing ClC-0 channels with mutations at K519, a position known to affect permeation (Pusch et al., Nature 373, 527, 1995). Whereas K519R is indistinguishable from wild-type, K519Q displays ≈50% the conductance of wild-type and K519E has ≈20% the conductance of wild-type channels. This result is consistent with an electrostatic effect on Cl^- permeation. We are also using these conductance mutants in mixing experiments in order to determine the number of subunits contributing to the channel's conduction pathway.

Su-AM-F6

EXPRESSION OF HUMAN MUSCLE CHLORIDE CHANNEL DIMERS: IMPLICATIONS FOR GATING AND SUBUNIT COMPOSITION.

((Ch. Fahlke, and A.L. George)) Vanderbilt University, Nashville, TN 37232.

Substitution of a glycine for an aspartate residue in the first membrane spanning segment (D136G) of a recombinant human skeletal muscle Cl^- channel (hClC-1) causes profound changes in voltage-dependent gating. A tandem hClC-1 construct linking both wild-type (WT) and D136G sequences in a single open reading frame (WT-D136G) was examined to investigate the role of the D136 residue in voltage dependent gating and to explore subunit stoichiometry. Whole-cell patch clamp recordings of tsA201 cells transiently transfected with WT-D136G demonstrates a homogeneous population of channels with gating properties distinct from WT and D136G indicating formation of heteromultimeric channels. Subunit stoichiometry was further explored by co-expression of WT-WT and D136G-D136G homodimers. Co-expression of the two homodimers in the same population of cells results in multiple current phenotypes that resemble the addition of WT and D136G in variable proportions. These results provide evidence that the functional channel complex is composed of two hClC-1 sequences. Voltage-dependent gating in WT-D136G is qualitatively similar to WT (deactivation upon hyperpolarization, activation upon depolarization), but the fractional amplitudes of three definable kinetic states (fast deactivating, slow deactivation, non-deactivating) differ from WT in a way compatible with a 50% reduction in the number of voltage sensors. When WT-D136G channels were exposed to acidic pH (6.0) on both sides of the membrane, the channel exhibited gating properties identical with D136G, i.e. slow hyperpolarization-induced activation. We explain these findings by proposing that a charged (unprotonated) D136 functions as a voltage-sensor, and that functional hClC-1 channels are dimeric with each subunit contributing a single voltage-sensor.

Su-AM-F7

TRANSITION FROM β-SHEET TO α-HELIX IN THE F508 CONTAINING REGION OF CFTR MAY BE INVOLVED IN THE CORRECT TARGETING OF THE PROTEIN.

((Y.H. Ko, M. Bianchet, and P.L. Pedersen)) Department of Biological Chemistry, School of Medicine, Johns Hopkins University, Baltimore, MD 21205. (Spon. by P.L. Pedersen)

Cystic fibrosis is caused by mutations in the cystic fibrosis transmembrane conductance regulator (CFTR) protein, especially from a deletion of phenylalanine at position 508, a mutation that results in the retention of the protein in the endoplasmic reticulum rather than being targeted to the plasma membrane where it is found in the cells of normal healthy people. We hypothesize that the secondary structure of the region of the protein containing F508 may be involved in the folding and trafficking pathway of CFTR. A transition of this critical region from β-sheet to α-helix may direct the targeting of the protein to its correct destiny. In our study of this hypothesis the secondary structures of the wild type synthetic peptides including F508 were found to appear first in the β-sheet form, but on the addition of trifluoroethanol were transformed to peptides rich in α-helix. In addition, we found that the corresponding ΔF508 mutants of the synthetic peptides appeared first as random coils and that on the addition of trifluoroethanol they too were transformed into peptides rich in α-helix. Computer modeling of NBF1 of CFTR, based on that of the related protein F_1ATPase whose crystal structure is known, indicated that the region around F508 is indeed α-helical. The abundance of amino acid residues containing hydroxyl substituents found in the amino acid sequence of NBF1 near F508 is reminiscent of the effect of adding trifluoroethanol, a solvent that carries a highly functional hydroxyl group, to the peptides having predominantly β-sheet secondary structure.

Su-AM-F8

ARYLAMINOBENZOATE BLOCK OF THE CARDIAC CYSTIC FIBROSIS TRANSMEMBRANE CONDUCTANCE REGULATOR (CFTR) CHLORIDE CHANNEL.

((Chongmin Wang and Kenneth B. Walsh)) Department of Pharmacology, University of South Carolina, Columbia, SC 29208.

The goal of this study was to determine the relationship between the structure of arylaminobenzoates and the ability of the drugs to block the cardiac CFTR Cl^- channel. The CFTR Cl^- current (I_{Cl}) was measured using the whole-cell arrangement of the patch clamp technique in guinea pig ventricular myocytes following the application of forskolin or a membrane permeable cAMP analogue. Block of I_{Cl} by the arylaminobenzoates occurred in a voltage-dependent manner with preferential inhibition of inward currents. This voltage-dependent block was most apparent at drug concentrations below the IC_{50}. Increasing the length of the carbon chain between the benzoate and phenyl rings of the compounds resulted in a marked increase in the affinity of the drugs for the channel with IC_{50}s of 500 μM, 16 μM and 3 μM for DPC, NPEB and NPBB, respectively. Raising the external pH from 7.4 to 10 greatly weakened the block of I_{Cl} by the drugs suggesting that interaction of the arylaminobenzoates with the CFTR channel may involve a titratable positively charged site.

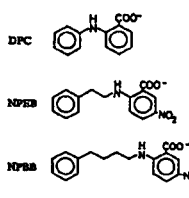

Su-AM-F9

CELLULAR MECHANISMS OF CFTR-ORCC REGULATORY INTERACTION ((Erik M. Schwiebert, *Marie E. Egan, Sandra S. Allen, Stephanie B. Fulmer, Garry R. Cutting and William B. Guggino)) Departments of Physiology and Pediatrics and Center for Medical Genetics, Johns Hopkins University School of Medicine, Baltimore, MD and *Department of Pediatrics, Yale University School of Medicine, New Haven, CT

CFTR regulates outwardly rectifying chloride channels (ORCCs) through an autocrine/paracrine signaling mechanism that requires CFTR- and cyclic AMP-dependent ATP transport out of the cell and ATP signaling through purinergic receptors expressed on the apical membrane of the airway epithelium {Schwiebert et al. *Cell* 81:1063, 1995}. In this mechanism, CFTR functions as a cAMP-regulated Cl^- channel and as a cAMP-regulated ATP channel which supplies ATP as an agonist to stimulate ORCCs. Two questions arise from these studies: (1) Which molecular domains of CFTR conduct Cl^- ions? and (2) which domains of CFTR transport ATP to stimulate ORCCs? To address these questions, we expressed a panel of mutated and truncated CFTR constructs by injecting *Xenopus* oocytes with CFTR cRNA and by lipofection of IB3-1 CF airway epithelial cells with RSV promoter-driven CFTR cDNA. Expression of two N-terminal truncated constructs, Δ259-M265, which lacks the first four predicted α-helices of CFTR, and Δ259-M265V, which lacks α-helices 1-4 with methionine 265 mutated to a valine, revealed different phenotypes. Δ259-M265 could conduct Cl^- and transport ATP to stimulate ORCCs whereas Δ259-M265V failed to conduct Cl^- but retained ATP transport function. TMD-1 CFTR, which contains only the first transmembrane domain of CFTR, functioned as a cAMP-independent Cl^- channel and failed to transport ATP. T-N-R CFTR, which contains TMD-1, NBD-1 and the R domain of CFTR, retained both functions. CFTR carrying two mild CF lung disease-causing Cl^- conduction mutations, R334W and R347P, failed to conduct Cl^- but could transport ATP, whereas A455E, a mild mutation in NBD-1, had no deleterious effect on either Cl or ATP conduction. In sharp contrast, G551D, a severe mutation in NBD-1, abolished ATP transport through CFTR. Taken together, these data suggest that TMD-1 of CFTR is required for Cl^- conduction whereas NBD-1 is essential for ATP transport through CFTR and autocrine/paracrine stimulation of ORCCs.

PHOTOSYNTHETIC REACTION CENTERS I

Su-AM-G1

STUDY OF REVERTANTS FROM THE L212GLU → GLN PHOTO-INCOMPETENT REACTION CENTER MUTANT FROM *RHODOBACTER CAPSULATUS* ((J. Miksovska*, D. K. Hanson+, M. Schiffer+ and P. Sebban*)) * CGM, Bât. 24, CNRS, 91198 Gif, France, + CMB, Argonne National Lab., Il., USA.

In bacterial reaction centers (RC), residue L212Glu in the Q_B site is involved in delivery of the second proton to Q_B^{2-}. In *Rhodobacter capsulatus* RCs, the L212Glu → Gln mutant is photo-incompetent (PS^-). To determine the function that is lost in this mutant, we selected four PS^+ revertants which all carried a different second-site substitution in addition to the original L212Gln mutation. These compensatory mutations are, in order of relative growth phenotype: L228Gly → Asp < L231Arg → Cys < M231Arg → Cys < L227Leu → Phe. The flash-induced absorbance spectroscopy measurements achieved on the reaction centers from these strains show that the rates of first and second electron transfer from Q_A (the first quinone electron acceptor) to Q_B are not much changed in either the L212Glu → Gln mutant or in the revertants, compared to the wild-type. However, the global photocycle rate measured by the rate of cytochrome photooxidation is dramatically decreased in the L212Glu → Gln mutant but restored in the revertants, although not to the wild-type level. This shows that the effect of the compensating mutations is to restore an efficient driving of the second proton to Q_B and to allow the formation of Q_BH_2 which is severely impaired in the L212Glu → Gln mutant. The electrostatic and/or structural effects of the compensating mutations is underlined by our results. Supported by U. S. Dept. of Energy, OHER Contract No. W-31-109-ENG-38 and by U. S. PHS Grant GM36598, by NATO (CRG.920725) and NSF/CNRS (DO/CB 855) grants

Su-AM-G2

THE RATE OF ELECTRON TRANSFER FROM $D^+Q_A^-Q_B$ TO $D^+Q_AQ_B^-$ IN RB. SPHAEROIDES REACTION CENTERS ((J. Li, D. Gilroy, M.R. Gunner)) Physics Dept. City College of N.Y. 138th St. and Convent Ave, N.Y., NY 10031

Electron transfer from $D^+Q_A^-Q_B$ to $D^+Q_AQ_B^-$ was monitored between 397 and 460 nm in RCs where Q_A is the native ubiquinone-10 or where Q_A is menaquinone-3. Q_B was UQ-10 in all cases. There is a larger difference between the MQ_A^- and UQ_B^- than the UQ_A^- and UQ_B^- spectra. The electron transfer rate is heterogeneous. Three rates are identified: two previously observed: at 5000/s (k_2) and 1000/s (k_3) along with a faster rate (≥15,000/s) (k_1) (pH 8, 25 C). ≈50% of the electron transfer occurs at k_1. k_1 is found at all pHs and temperatures measured. It is not present in RCs without Q_B. Its amplitude has the expected wavelength dependence for the difference between the MQ_A- and UQ_B- spectra. A fast rate is also seen in the UQ_A UQ_B RCs at 397 nm where the UQ_A- and UQ_B- spectra are different. The activation energies are <1 (k_1), 3±1 (k_2), and 8±1 kcal (k_3). There is little pH dependence in any of the rates (pH 6-9.5). The three rates suggest that there are sub-states of RCs with different Q_A to Q_B electron transfer rates. A significant fraction of the RCs are competent to transfer an electron in a process that is relatively temperature independent. In the other two states proton transfer or protein conformation changes apparently limit the electron transfer rate. Supported by N.I.H. GM-42726

Su-AM-G3

TIME-RESOLVED ELECTROCHROMISM ASSOCIATED WITH THE FORMATION OF QUINONE ANIONS IN *Rhodobacter sphaeroides* R-26 REACTION CENTERS. ((D.M. Tiede, J. Vázquez, J. Córdova and P.A. Marone)) Chemistry Division, Argonne National Laboratory, Argonne, IL 60439. (Spons. by D.M. Tiede)

Reaction center bacteriochlorophyll, Bchl, and bacteriopheophytin, Bph, cofactors provide natural probes of electrostatic fields within this protein. We have examined the electrochromic responses of these cofactors, resolved during the lifetimes of the $P^+Q_A^-Q_B$ and $P^+Q_AQ_B^-$ states, and measured as a function of temperature. These measurements provide information on the time-dependent variation in electrostatic field strength on the Bchl and Bph cofactors. Measurements in the near-infrared absorbance bands have revealed the following. First, time-dependent absorption changes of the Bchl and Bph can be kinetically decoupled. We interpret the rapid responses of the Bph band to reflect electron transfer, while the slower responses of the Bchl to reflect conformational changes in the vicinity of the Bchl site. Second, the $Q_A^-Q_B$ → $Q_AQ_B^-$ electron transfer rates are seen to be heterogeneous, attributable to a distribution of conformational states. Finally, there is no electrochromic event attributable to proton uptake into the Q_B site. This uptake must either be coupled to electron transfer, or it must not cause a quenching of the electrostatic fields associated with the Q_B anion.

Work supported by U.S. DOE, Office of Basic Energy Sci., Div. Chem. Sci., contract W-31-109-Eng-38.

Su-AM-G4

THE RATE LIMITING STEP IN THE OBSERVED REACTION, $Q_A^-Q_B \rightarrow Q_AQ_B^-$, IS NOT ELECTRON TRANSFER. ((M.S. Graige, G. Feher, M.Y. Okamura)) Dept. of Physics, University of California San Diego, 9500 Gilman Dr., La Jolla, CA 92093-0319.

The free energy dependence of the electron transfer process $k_{AB}^{(1)}$ ($Q_A^-Q_B \rightarrow Q_AQ_B^-$) was studied in reaction centers (RCs) from *Rb. sphaeroides* by substituting quinones with lower redox potentials into the Q_A site while retaining native Q_{10} in the Q_B site.[1] These substitutions increase the ***intrinsic*** electron transfer rate by changing the redox free energy (i.e. driving force) for electron transfer without affecting other processes (such as proton uptake or conformational rearrangement) which may be coupled to electron transfer. The results (see fig.) show that the ***observed*** kinetic signal monitored optically at both 750 nm and 470 nm does ***not*** depend on the redox free energy for electron transfer, even though the observed reaction has a activation barrier[2]. This suprising result shows that the observed signal is not rate limited by electron transfer. Thus, the $k_{AB}^{(1)}$ reaction must be modeled as a two (or more)-step reaction with the rate limiting step preceding electron transfer. A model in which a conformational change is required before electron transfer was previously proposed on the basis of the correlation between the rates of an electrogenic decay process and the rate of electron transfer.[3] The observations made in this work are consistent with this model, which suggests that a conformational change is the rate limiting step. (1) Labahn, A. *et.al.* (1995) *Chem. Phys.*, 197, 355. (2) Kleinfeld *et.al.* (1984) *Biochim. Biophys. Acta*, 766, 126. (3) Brzezinski *et. al* (1992) in The Photosynthetic Bacterial Reaction Center II (Breton, & Vermiglio, ed.) Plenum Press, New York, p.321. We thank J.M. Bruce for the TMNQ and TEMNQ. Supported by NIH and NSF.

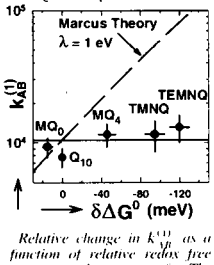

Relative change in $k_{AB}^{(1)}$ as a function of relative redox free energy for electron transfer. The dashed curve shows the prediction of Marcus theory for an electron transfer limited reaction assuming a reorganization energy of 1 eV. For quinone abbreviations see following abstract by Graige et.al.

Su-AM-G5

DETERMINATION OF THE RATE LIMITING STEP IN THE REACTION, $Q_A^-Q_B^- + H^+ \rightarrow Q_A(Q_BH)^-$. IN ASP-L213 → ASN MUTANT RCs FROM *Rb. SPHAEROIDES.** ((M.S. Graige, M.L. Paddock, G. Feher, M.Y. Okamura)) Dept. of Physics, University of California San Diego, 9500 Gilman Dr., La Jolla, CA 92093-0319.

In native RCs the proton-coupled electron transfer reaction $k_{AB}^{(2)}$ ($Q_A^-Q_B^- + H^+ \rightarrow Q_A(Q_BH)^-$) is rate limited by electron transfer.[1] In Asp-L213 → Asn [DN(L213)] mutant RCs, designed to block proton transfer to Q_B, the rate constant $k_{AB}^{(2)}$ is reduced by several orders of magnitude.[2] Thus, the question arises whether the mechanism is the same and electron transfer remains rate limiting or whether proton transfer has become rate limiting. To answer this question, $k_{AB}^{(2)}$ was measured in mutant RCs with lower potential quinones substituted into the Q_A site and native Q_B in the Q_B site. These substitutions increase the electron transfer rate by changing the redox free energy (*i.e.*, driving force) for electron transfer without affecting proton transfer. The results (see fig.) show that $k_{AB}^{(2)}$ is independent of driving force in the mutant, indicating that the mechanims has changed and that the reaction is now rate limited by proton transfer. This result is consistent with the proposed role of Asp-L213 as a component of a proton transfer pathway.[2] The quinone substitution technique can be applied to other mutant RCs to determine the mechanism of the $k_{AB}^{(2)}$ reaction. (1) Graige *et.al.* (1995) *Biophys. J.*, 68, 2, A246. (2) Paddock *et.al.* (1994) *Biochemistry* 33, 3, 734. We thank J.M. Bruce for the TMNQ and TEMNQ. Supported by NSF and NIH.

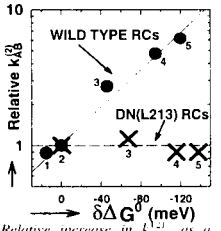

Relative increase in $k_{AB}^{(2)}$ as a function of relative redox free energy for electron transfer in wild type, ●, and DN(L213), ×, RCs. Note that the rate in wild type increases in accord with Marcus theory of electron transfer. The rate in DN(L213) RCs does not. Quinones: (1) menadione (MQ_0) (2) ubiquinone-50 (Q_{10}) (3) menatetrenone (MQ_4) (4) trimethyl naphthoquinone (TMNQ) (5) tetramethylnaphthoquinone (TEMNQ).

Su-AM-G6

THE ELECTROSTATIC EFFECTS OF GLU AND ASP AT THE L212 AND L213 SITES ON ELECTRON TRANSFERS INVOLVING Q_B IN RCs FROM *Rb. sphaeroides*.* ((M.L. Paddock, G. Feher & M.Y. Okamura)) Phys. Dept., UCSD, La Jolla, CA 92093

The bacterial reaction center (RC) plays a central role in photosynthetic energy conversion by facilitating the double reduction and protonation of a bound quinone molecule, Q_B. The two carboxylic acids Asp-L213 and Glu-L212 located near Q_B have been shown to be important for proton transfer in *Rb. sphaeroides* (1). In this work, we tested the ability of Glu to substitute for Asp at L213 and Asp to substitute for Glu at L212 by site-directed mutagenesis. Isolated RCs were characterized at pH 7.5 with respect to their charge recombination rate constant k_{BD} ($D^+Q_AQ_B^- \rightarrow DQ_AQ_B$) and proton-coupled electron transfer rate constant $k_{AB}^{(2)}$ ($DQ_AQ_B^- + H^+ \rightarrow DQ_A(Q_BH)^+$). The greater the number of Asp (fewer number of Glu) in the RC, the greater the value of k_{BD} and $k_{AB}^{(2)}$ (Table). The larger k_{BD} in RCs with Asp indicates that the electrostatic environment is more unfavorable for Q_B^- (assuming no structural changes) and suggests that Asp is predominantly ionized (low pK_a) and Glu predominantly neutral (high pK_a) at either the L212 or L213 site. $k_{AB}^{(2)}$ was also observed to increase with increasing negative electrostatic potential. This supports the proposed mechanism for $k_{AB}^{(2)}$, which involves the formation of the high energy Q_BH state (2) that is favored by the negative potential.

strain	L212 site	L213 site	k_{BD} (s^{-1})	$k_{AB}^{(2)}$ (s^{-1})
ED(L212)	Asp	Asp	8	~8,000
native	**Glu**	**Asp**	**0.7**	**1,200**
ED(L212)/DE(L213)	Asp	Glu	0.7	130
DE(L213)	Glu	Glu	0.02	18

*Supported by NIH & NSF. (1) Paddock et al. (1989) PNAS 86, 6602; Takahashi & Wraight (1992) Biochem. 31, 855; Paddock et al. (1994) Biochem. 33, 734. (2) Graige et al., preceding abstract.

Su-AM-G7

USING STIGMATELLIN TO PROBE THE ELECTROSTATIC ENVIRONMENT OF THE Q_B SITE IN BACTERIAL RCs. ((M.S. Graige, M.L. Paddock, G. Feher, M.Y. Okamura)) Dept. of Physics, University of California San Diego, 9500 Gilman Dr., La Jolla, CA 92093-0319.

The protonated semiquinone, Q_BH, has been proposed to play an important role in the proton-coupled electron transfer reaction ($Q_A^-Q_B^- + H^+ \rightarrow Q_A(Q_BH)^-$).[1] To investigate the factors that might affect the protonation of Q_B^-, we used stigmatellin, a phenolic inhibitor which binds to the Q_B site[2], as an analogue for the protonated semiquinone (see figure). The ionization of stigmatellin was studied spectroscopically as a function of pH by monitoring a peak in the ionized minus protonated difference spectrum at 272 nm. In solution the hydroxyl group of stigmatellin titrates with a pK ~ 9.3 (see figure). When bound in the Q_B site, the pK in native RCs is shifted to > 11 and in Asp-L213 → Asn mutant RCs the pK is ~ 9.9. These results indicate that 1.) in the absence of Asp-L213, the environment near Q_B is similar to that of aqueous solution and 2.) the presence of ionized Asp-L213 creates a negative potential which can shift the pKs of titratable groups. We suggest that ionized Asp-L213, through electrostatic interactions, influences the rate of the proton-activated electron transfer reaction ($Q_A^-Q_B^- + H^+ \rightleftarrows Q_A^-(Q_BH) \rightarrow Q_A(Q_BH)^-$) by increasing the fraction of protonated intermediate, Q_BH. (1) Graige *et.al.* (1995) *Biophys. J.*, 68, 2, A246. (2) Lancaster et.al. (1995) in Reaction Centers of Photosynthetic Bacteria. Structure and Dynamics. (Michel-Beyerle, M.E. ed.) Springer-Verlag, Berlin, in press. Supported by NIH and NSF.

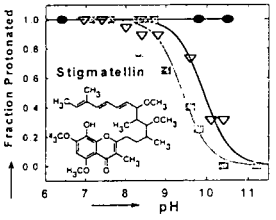

pH titration curves for stigmatellin in buffer ■, native RCs ●, and Asp-L213 → Asn mutant RCs ▽. The structure of stigmatellin is shown. Conditions: 2.3μM RC, 1.5μM stigmatellin.

Su-AM-G8

EPR AND ESEEM OF Q_A^- AND TRANSIENT EPR OF $P_{960}^+Q_A^-$ IN ZN SUBSTITUTED REACTION CENTRES FROM *RPS. VIRIDIS*. ((A.T. Gardiner, H. Käß, S.G. Zech, R. Bittl,. F. MacMillan, F. Lendzian, W. Lubitz)) Max-Volmer-Institut, TU Berlin, Straße des 17. Juni 135, 10623 Berlin, Germany.

In RCs of *Rps. viridis* the high spin Fe^{2+} has been partially replaced by diamagnetic Zn^{2+} by either biosynthetic (1) or chemical methods (2). The radical anion of the primary quinone was generated by dithionite reduction and its *g*-tensor values measured by Q-band EPR (2.0059, 2.0050, 2.0021) were close to those obtained for the menaquinone radical anion. Stimulated echo ESEEM at 20K revealed interactions with two nitrogen nuclei with different quadropole coupling parameters K and η (see Fig.). One of them (◊) is assigned to δN of a histidine ligand, the second (+) one could belong to a nitrogen from the backbone. Transient EPR spectra of the light-induced radical pair $P_{960}^+Q_A^-$ recorded at X-band shows an EAE polarisation pattern. The spectral width is smaller than that found for $P_{865}^+Q_A^-$ in RCs from *Rb. sphaeroides*. This is consistent with the smaller *g*-anisotropy of Q_A^- in *Rps. viridis*. (1) K.F. Ferris (1987) Ph.D. Thesis, Princeton University. (2) R.J. Debus, G. Feher & M.Y. Okamura (1986) *Biochemistry* 25:2276-2287. Supported by DFG (Sfb 312) and AvH-Stiftung.

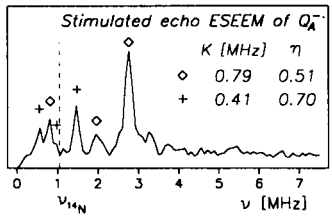

NUCLEIC ACID RECOGNITION

Su-AM-SymII-1

HAIRPIN AND CYCLIC POLYAMIDES FOR RECOGNITION IN THE MINOR GROOVE OF DNA. ((Peter B. Dervan)) Division of Chemistry and Chemical Engineering, California Institute of Technology, Pasadena, CA 91125.

Small molecules that specifically bind with high affinity to any designated DNA sequence in the human genome would be useful tools in molecular biology and potentially in human medicine. Simple rules have been developed to rationally alter the sequence specificity of minor groove-binding polyamides containing *N*-methylimidazole and *N*-methylpyrrole amino acids. Crescent-shaped polyamides bind as antiparallel dimers with each polyamide making specific contacts with each strand on the floor of the minor groove. The DNA sequence specificity of these small molecules can be controlled by the linear sequence of pyrrole and imidazole amino acids. An imidazole ring on one ligand complemented by a pyrrolecarboxamide ring on the neighboring ligand recognizes a G•C base pair, whereas a pyrrolecarboxamide/imidazole combination targets ad C•G base pair. A pyrrole/pyrrole pair is degenerate for A•T or T•A base pairs. Hairpin and cyclic polyamides have been synthesized that bind designated DNA sequences at subnanomolar concentrations.

Su-AM-SymII-2

THE GEOMETRY OF RECOGNITION OF DNA BY PROTEINS. ((R. Dickerson)) UCLA.

Su-AM-SymII-3

THE ROLE OF BENDS AND BENDABILITY IN NUCLEIC ACID RECOGNITION. (D. M. Crothers) Department of Chemistry, Yale University , New Haven, CT 06511.

The free energy required to distort nucleic acid structure can be a function of base sequence. As a consequence, the binding free energy for proteins that bend DNA can be modulated by a sequence-dependent free energy of deformation, as is observed for both histones and gene regulatory proteins. Another example is the interaction of a protein with a bent helix resulting from the interaction of two RNA loops, for which the helix formation free energy is highly dependent on sequence. Recognition of DNA can also be modulated by an outside source of energy that provides for the necessary distortion. This case is illustrated by the alteration of binding constant for DNA-bending proteins by pre-bending the DNA. A possible consequence of this mechanism is indirect interaction between DNA binding proteins, which can bind in a cooperative fashion without necessarily touching each other.

Su-AM-SymII-4

THERMODYNAMICS AND KINETICS OF THE INTERACTION OF REGULATORY COMPLEXES WITH SPECIFIC SITES ON THE DNA GENOME. P. H. von Hippel, W.A. Rees, K. Rippe, and K.S. Wilson. Institute of Molecular Biology and Department of Chemistry, University of Oregon, Eugene, OR 97403.

In this lecture we analysis and illustrate the principles that underlie the specificity mechanisms that control the initiation, elongation, and termination phases of transcription. Thermodynamic mechanisms dominate in the first steps of initiation, where promoters at various levels of activation can be considered to be in equilibrium competition for a limiting supply of core RNA polymerase. In later stages of initiation, as well as in elongation and termination, the regulatory mechanisms that control specificity are largely kinetic, involving rate competition between branching reaction pathways. The stability of the transcription elongation complex drops abruptly within terminator sites along the DNA template, and here the regulatory outcome can be easily switched from one competing pathway to another by minor changes in the relative rates of elongation and termination (RNA release). *Cis* effectors, defined as sites at which regulatory proteins bind to upstream activation loci on either the DNA or the nascent RNA, play important roles in both initiation and elongation-termination control. Examples that illustrate the flexibility and additivity of simple regulatory components in multiple determinant control mechanisms in transcription will be presented, and the generality of these regulatory principles will be stressed.

K CHANNELS: STRUCTURE-FUNCTION

Su-AM-H1

DETECTION, ORIENTATION AND TOPOLOGICAL ARRANGEMENT OF α-HELICES IN VOLTAGE-DEPENDENT K^+ CHANNELS FROM FOURIER ANALYSIS OF SEQUENCE VARIABILITY. ((Perozo, E. and Rosales, R.)) Centro de Biofisica y Bioquimica. Instituto Venezolano de Investigaciones Cientificas. Caracas, Venezuela.

A systematic analysis of sequence variability was performed on sequence alignments of the putative transmembrane (TM) segments of voltage-dependent K^+ channels. Alignments were made from sequences having more than 30 % identity, and a variability profile was constructed for all putative TM segments. Fourier analysis of the variability profile was used to detect the periodicity of sequence variability within each TM segment. The power spectra derived from these calculations show a large peak at around 100 degrees (periodicity of 3.6 residues) for putative segments S1, S2, S5 and S6. This result is taken as evidence for the α-helical nature of these regions. The same analysis was performed for these segments using other physical properties like hydrophobicity, or membrane propensity. When all these properties were considered, it was found that all segments (S1-S6) have periodicities consistent with an α-helical structure, but segments S3 and S4 are probably not accessible to membrane lipid. Interestingly, power spectra of the variability profile in the P region showed a peak around 180 degrees, suggesting the presence of a β structure. A variability moment per TM segment was calculated for all helical segments on the basis of the individual variabilities at each position in the alignment. We interpreted this vectorial quantity to be proportional to the direction of highest solvent accessibility in an α-helix. A model for TM segment packing in K^+ channels is proposed. This model is consistent with known experimental results, and identifies transmembrane segments S1 and S2 as the most accessible to membrane lipids while segment S4 appears buried from interactions with other transmembrane segments. (Supported by CONICIT grant S1-2657)

Su-AM-H2

IDENTIFICATION OF SHORT-RANGE STRUCTURAL INTERACTIONS BETWEEN TRANSMEMBRANE CHARGED RESIDUES IN SHAKER K^+ CHANNELS. ((S. K. Tiwari-Woodruff, W. R. Silverman, A. F. Mock and D. M. Papazian)). Department of Physiology, UCLA School of Medicine, Los Angeles, CA 90095-1751.

We are using a strategy related to intragenic suppression to identify electrostatic structural interactions between conserved transmembrane charged residues in Shaker K^+ channels (*Neuron* **14**, 1293, 1995). In our approach, a primary mutation that disrupts proper folding is specifically rescued by a complementary second site mutation. Charge-neutralizing and charge-reversing mutations that disrupt protein maturation and eliminate functional activity were expressed in *Xenopus* oocytes, singly or in double and triple mutant combinations. Specific suppressers of the primary mutation were identified by the restoration of maturation; the fraction of protein in the mature vs. immature forms was quantified by densitometry. Many of the rescued constructs expressed functional channels, some with novel phenotypes. Previous results had suggested that K374 (in S4), E293 (in S2) and D316 (in S3) form a cluster of interacting residues. We have now identified short range interactions between a second cluster including E283 (in S2), R368 (in S4) and R371 (in S4). In addition, we have obtained evidence that R377 (in S4) interacts with E293 (in S2) and D310 (in S3), but these residues may not be as close as the clustered residues mentioned above. These results have been used to generate a model for the packing of transmembrane segments S2, S3 and S4 in Shaker K^+ channels (Silverman et al., this volume). We are now testing predictions of this model using intragenic suppression strategy.
Supported by the Pew Charitable Trust (DMP) and the NIH (STW, and WRS).

Su-AM-H3

A MODEL FOR THE PACKING OF TRANSMEMBRANE SEGMENTS S2, S3, AND S4 IN SHAKER K+ CHANNELS. ((W.R. Silverman, S.K. Tiwari-Woodruff, F. Bezanilla, and D.M. Papazian)) Department of Physiology, UCLA School of Medicine, Los Angeles, CA 90095-1751.

Using a strategy of directed intragenic suppression, we have identified likely short-range structural interactions between charged residues in transmembrane segments S2, S3, and S4 in Shaker K+ channels (*Neuron* **14**, 1293, 1995; Tiwari-Woodruff et al., this volume). We used the graphical computer program Insight II (Biosim) to determine whether a packing model that satisfies the suppression data could be generated. We assumed that 1) S2, S3, and S4 are in right-handed α-helices, 2) the interactions between charged residues stabilize the tertiary structure of the channel, 3) the side chains are fully extended, and 4) standard ϕ and ψ angles apply. The apparent short-range interactions between E293 (in S2), D316 (in S3), and K374 (in S4); and E283 (in S2), R368 (in S4) and R371 (in S4); and the somewhat longer-range interactions between E293 (in S2), D310 (in S3), and R377 (in S4) can be accomodated by tilting the helices relative to each other. Both S2 and S4 are tilted relative to S3; S2 is tilted further. This preliminary packing model makes predictions that can be easily tested by an extension of the suppression strategy or other biochemical approaches. Several cycles of testing and refining the model should result in a reasonable, low resolution picture of the packing of transmembrane segments in Shaker K+ channels. Supported by the Pew Charitable Trust (DMP) and the NIH (WRS, STW, FB).

Su-AM-H4

EXPRESSION OF hKv1.7, AN ATYPICAL INTRON-CONTAINING *SHAKER* K^+ CHANNEL. ((R. Shehee, J. Sanchez, M. McIntyre, M. Lancaster, K. Kalman, G. Chandy, I. Dukes & J. Worley)) Glaxo Wellcome, RTP, NC and University of California, Irvine, Irvine CA.

Kv1.7 is a putative member of the *Shaker* family of voltage-dependent K^+ channels. Previous studies have demonstrated expression in pancreatic Islets of Langerhans (Betsholtz et al. FEBS Lett 263:121).The genomic sequence of Kv1.7 appears to contain three coding exons and two introns making it a unique member of the *Shaker* family. A Human genomic restriction fragment containing these exons was cloned into a vector with a CMV promoter, IRES sequence and a Neomycin resistance gene. Stably transformed CHO cells were selected with G418. Cells positive for Kv1.7 expression by Northern analysis demonstrated characteristic delayed rectifier-type current measured using the whole cell patch configuration. Membrane currents were selective for K^+ over Na^+ & Cl and demonstrated voltage-dependent activation. Kv1.7 currents were activated at potentials >-40mV and peak currents at 60mV varied from 200-800pA. Moreover, time-dependent inactivation was observed. As predicted from the amino acid sequence, external TEA (10mM) did not produce inhibition of Kv1.7 currents, while complete block was observed by 500μM 4-AP. We have expressed a unique Human *Shaker* K^+ channel with properties similar to a delayed rectifier current observed in pancreatic β-cells.

Su-AM-H5

RNA EDITING GENERATES DIVERSE TRANSCRIPTS ENCODING SQUID Kv2 K^+ CHANNELS. ((D.E. Patton and F. Bezanilla)) UCLA, Departments of Physiology and Anesthesiology, Los Angeles, CA 90095.

The possibility of RNA editing occurring on transcripts encoding squid Kv2 K^+ channels was explored by comparing cDNA and genomic DNA sequences derived from the same animal. mRNA was isolated from the optic lobe of a single *Loligo pealei*, reverse transcribed and subjected to PCR using primer pairs specific for the squid Kv2 K^+ channel. Genomic DNA isolated from the mantle of the same animal was also amplified by PCR. Products were subcloned and recombinants were sequenced in the region encoding S4 through S6. DNA sequences from a total of 10 genomic clones derived from 2 independent PCR amplifications were nearly identical to one another with the exception of 5 bases in a total of 6,700 bases sequenced. 39 cDNA clones derived from 5 independent PCR amplifications were sequenced. Differences from the genomic sequence that showed up in more than 1 PCR amplification were considered to be due to RNA editing. A total of 13 sites in the region encoding S4 through S6 were found by this criterion to be edited. Only 2 of these edits were silent. All of the editing sites contained adenine in the genomic DNA and guanine in the edited cDNA sequence. The various sites appear to be edited at different efficiencies ranging from 100% to 5%. Many of the editing sites are in regions previously shown to be important for K^+ channel function. There are 4 amino acid substitutions in the S4 segment, 1 in the S4-S5 linker, 2 in S5, 1 in the P region (Y/C at the position equivalent to 449 in *Shaker*) and 2 in S6. Preliminary electrophysiological analysis of several of the editing variants suggests that the changes have subtle effects on gating. Supported by NIH grant GM 30376

Su-AM-H6

EVIDENCE FOR AN EVOLUTIONARILY CONSERVED SERINE PROTEASE-LIKE DOMAIN IN MAXI K(CA) CHANNELS. ((G.W.J. Moss*, J. Marshallt, J. Howe* and E.G. Moczydlowski*)) *Dept. of Pharmacology, Yale Univ. School of Medicine, New Haven, CT 06520. †Dept. of Mol. Pharmacology, Brown University, Providence, RI 02912

Bovine pancreatic trypsin inhibitor (BPTI) is a 58 residue protein that belongs to the Kunitz family of serine protease inhibitors. Previously we found that BPTI binds to an intracellular site on large-conductance Ca-activated K-channels (maxi K(Ca)) and induces the appearance of discrete substate events. We screened other classes of serine protease inhibitors for inhibition of a cloned bovine maxi K(Ca) channel (Bslo α-subunit) expressed in HEK 293 cells and found that chicken ovoinhibitor (OI), a 7-headed protease inhibitor of the Kazal family, is also effective. The sequences and core structures of Kunitz and Kazal inhibitors are completely different, but both contain a loop of ~6 amino acids that is complementary to a contact surface at the active site of many serine proteases. In crystal structures the peptide backbone of this loop region in Kunitz and Kazal proteins is superimposable. Inhibition of Bslo currents by both BPTI and OI suggests that their protease binding regions may be important for K(Ca) channel interactions. We also tested inhibitor activity on Dslo channels (from Drosophila). Dslo shares 60% sequence identity with Bslo yet both BPTI and OI dramatically reduced macroscopic currents through Dslo channels, suggesting that the channel's protease inhibitor binding site has been conserved through evolution. Furthermore, the BPTI-trypsin complex is inactive on Dslo channels, as also found for the mammalian maxi K(Ca) channels. A crystal structure of the BPTI-trypsin complex shows that most of the inhibitor's surface is exposed to water, except in the BPTI inhibitory loop region. Inactivity of this complex in the channel assay suggests that the channel and trypsin bind to overlapping regions of the BPTI molecule. The kinetics of Bslo and Dslo interactions with BPTI are also different: for Dslo, the mean substate dwell-time is ~24 minutes, whereas for Bslo the mean dwell-time is ~3 seconds. We hypothesize that Bslo and Dslo channel α-subunits contain a domain that is structurally homologous to a serine protease. A sequence alignment of seven serine proteases with Bslo and Dslo suggests that the C-terminal region of the maxi K(Ca) channel is the most likely location of the protease inhibitor binding site. (Supported by the Donaghue Foundation, AHA and NIH.)

Su-AM-H7

CHIMERIC APPROACH TO MAP THE FUNCTIONAL DETERMINANTS OF MAXIK CHANNELS RESPONSIBLE FOR β SUBUNIT REGULATION. ((P. Meera, M. Wallner, and L. Toro)) Dept. of Anesthesiology, University of California, Los Angeles, California - 90095.

Coexpression of β subunit cloned from human uterine smooth muscle with its α subunit (hSlo) dramatically increased the apparent Ca^{2+} sensitivity upon heterologous expression in *Xenopus* oocytes whereas the *Drosophila* homologue (dSlo, variant-A1C2EIG310) was unmodulated by this mammalian β subunit. We employed this functional difference and generated chimeras between the hSlo and dSlo channels to map the domains responsible for the functional effect of the β subunit. To obtain optimal expression levels for macro currents in oocytes we modified untranslated regions in both clones. Twelve out of fourteen chimeric constructs studied so far yielded functional channels upon cRNA injection in oocytes. Exchange of the unique C-terminal tail regions (S9-S10) between hSlo and dSlo yielded similar results as reported earlier (Wei et al, Neuron 1994). However, many other chimeric constructs deviated from wild type channels in their apparent Ca^{2+} sensitivity in spite of the similar Ca^{2+} sensitivity of the wild type channels. These results stress the importance of the whole protein in determining the apparent Ca^{2+} sensitivity rather than the highly conserved negatively charged tail region alone. For example, the chimeric construct, hd11 consisting of S7 and S8 of dSlo and the rest (S1 to S6, S9 and S10) contributed by hSlo channels has a lower apparent Ca^{2+} sensitivity. The half activation potential at 10 μM Ca^{2+} is ~80 mV for hd11, and ~20 mV for the wild type channels (dSlo or hSlo). Therefore, to evaluate the functional coupling of the β subunit with the chimeric constructs we compared the apparent Ca^{2+} sensitivities as relative shifts of the voltage-activation curves at 10 μM Ca^{2+}. Using this strategy, we found that a stretch of ~ 50 amino-acids of the hSlo core region makes dSlo susceptible for β subunit regulation. (Supported by NIH HL54970)

Su-AM-H8

NEW ASPECTS IN THE MEMBRANE TOPOLOGY OF VOLTAGE GATED AND Ca^{2+} MODULATED MAXIK CHANNELS. ((M. Wallner, P. Meera and L. Toro)) Department of Anesthesiology, UCLA, California 90095.

Voltage gated K^+ channels, single domains of voltage dependent Na^+ and Ca^{2+} channels and MaxiK channels were aligned with the GCG program pileup. A striking feature of the alignments is the existence of highly conserved charged residues in the region from the beginning of transmembrane segment S2 to the end of S4. Some of these charged residues have been shown to play important roles for voltage dependent gating. The homology of MaxiK channels to voltage gated channels in the region from S2 to S4 together with our studies of gating and ionic currents suggest that they are gated by voltage and modulated by Ca^{2+} binding and the association with its β subunit. Surprisingly, most of the suggested models of the transmembrane topology from S1 to S3 of MaxiK channels are inconsistent with these sequence alignments. Based on this observation we propose a modification of the transmembrane topology. Assuming that the region in MaxiK channels homologous to S1 to S3 have the same orientation as their counterparts in voltage gated channels, this model suggests that the region previously thought to form a large extracellular loop between transmembrane segment S1 and S2 would be intracellular. The previous transmembrane region S1 would be left as an additional hydrophobic region at the N-terminus unique for MaxiK channels. This hydrophobic region may traverse the membrane thereby directing the N-terminus of MaxiK channels to the extracellular space as found for other membrane proteins: e.g. most members of the superfamily of G-protein coupled seven helix receptors have an extracellular N-terminus in the absence of a signal sequence. Experiments adding a signal sequence for translocation (across the endoplasmic reticulum) from the rat sodium channel β1 subunit to the N-terminus of MaxiK channels suggest that this may be actually the case as this modification did not lead to obvious changes in channel function. (Supported by NIH HL 54970).

Su-AM-H9

EVIDENCE OF HETEROMULTIMERIC K^+ CHANNELS FROM CO-EXPRESSION OF *DROSOPHILA EAG* AND *SHAKER* cRNAs IN *XENOPUS* OOCYTES. ((M.L.Chen, T. Hoshi* and C.-F. Wu)) Department of Biological Sciences, * Department of Physiology and Biophysics, University of Iowa, Iowa City, IA 52242.

K^+ channels play crucial roles in many physiological functions. Co-assembly of different K^+ channel subunits could greatly enhance the diversity of K^+ channels. *In vivo* studies of *Shaker* (*Sh*) and *eag* mutants in *Drosophila* have indicated interaction of their gene products in different K^+ channels (Zhong and Wu, *J.Neurosci.* 13:4669). We examined whether *eag* and *Shaker* subunits can form functional heteromultimeric K^+ channels in *Xenopus* oocytes by co-injecting *eag* and *Sh*B cRNAs. A delayed rectifier-like current was obtained from oocytes injected with *eag* cRNA and a transient A-type current from oocytes injected with *Sh*B cRNA. An early transient current followed by a sustained current component was recorded from oocytes co-injected with both cRNAs. The time course of the transient current produced by co-injection of *eag* and *Sh*B was faster than the current produced by *Sh*B alone. Co-injection of *eag* and *Sh*B also slowed the recovery from twin-pulse inactivation. The resulting currents (a) could not be well-fit by a weighted linear summation of *eag*- and *Sh*B-mediated currents (b). These results are consistent with a combinatorial hypothesis of *eag* and *Shaker* subunit assembly, suggested previously, based on mutational analysis in *Drosophila*.

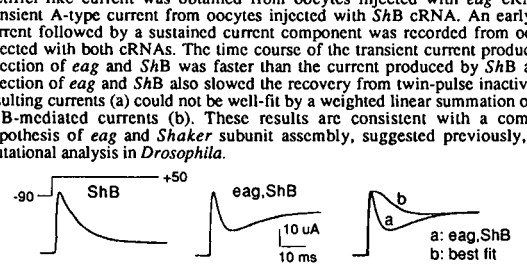

Su-AM-H10

ASSEMBLY AND SUPPRESSION OF ENDOGENOUS Kv1.3 CHANNELS IN HUMAN T LYMPHOCYTES. ((G.Panyi and C. Deutsch)). Dept. of Physiology, University of Pennsylvania, Phila., PA 19104-6085.

The predominant K^+ channel in human T lymphocytes is Kv1.3, which inactivates by a C-type mechanism. To study assembly of these tetrameric channels in Jurkat, a human T-lymphocyte cell line, we have characterized the formation of heteromultimeric channels between endogenous wild-type (WT) Kv1.3 subunits and heterologously expressed mutant (A413V) Kv1.3 subunits. We use a kinetic analysis of C-type inactivation of currents produced by homomultimeric channels (τ = 150 ms and 4 ms for WT and A413V, respectively) and heteromultimeric channels to determine the distribution of channels with different subunit stoichiometries. The distributions are well-described by either a binomial distribution or a binomial distribution plus a fraction of WT homotetramers. This indicates that subunit assembly is a random process occurring prior to expression at the plasma membrane and that tetramers expressed in the plasma membrane do not dissociate and reassemble. Additionally, endogenous Kv1.3 current is suppressed by a heterologously expressed truncated Kv1.3 consisting of the amino-terminus and the first two transmembrane segments. Suppression, which is maximal at 48 hours after transfection, overlaps with the time course of heteromultimer formation between heterologously expressed A413V and endogenous WT channels. Our findings suggest that diversity of K^+ channel subtypes in a cell is regulated not by spatial segregation of monomeric pools, but rather by the degree of temporal overlap and the kinetics of subunit expression. (Supp. GM 41476, 52302, and FO5 TWO 5079).

Su-AM-I1

3-D STRUCTURE OF THE ACROSOMAL BUNDLE OF LIMULUS SPERM BY 400 KV ELECTRON CRYO-MICROSCOPY: HELICAL AND 3-D TILT SERIES RECONSTRUCTIONS ((Michael F. Schmid, Misha Sherman, Joanita Jakana, Paul Matsudaira* and Wah Chiu)) Verna and Marrs McLean Dept of Biochem and W.M. Keck Ctr. for Computational Biol., Baylor Coll. of Med., Houston, TX ; *Whitehead Inst. MIT, Cambridge, MA

EM has a central role in integrating structural information from x-ray and NMR methods in macromolecular assemblies, which are difficult to studyby the other methods. We are using cryoelectron microscopy to study the structure of the acrosomal bundle from *Limulus*, made up of scruin and actin, and the interactions within and among the actin:scruin filaments that make up the bundle.

The bundle can be considered as a 3-dimensional crystal, with 28 actin subunits and scruin molecules per unit cell. We have been able to image the bundle to better than 7 Å resolution.

Our approach is in two stages. First, we used helical symmetry to determine the structure of isolated acrosomal filaments from the bundle at 13Å resolution. Scruin was shown to have two domains, which contact two different actin subunits in the same actin filament. Holmes' x-ray actin filament model was fit to the reconstruction. Scruin contacts helix-loop-beta motifs in subdomain 3 of one actin subunit and in the structurally similar subdomain 1 of the next actin subunit along the helix. Thus scruin, a tandemly repeated molecule, binds structurally homologous subdomains of two consecutive actin subunits.

We are now analyzing three-dimensional tilt series of the bundle to reveal the interfilament interactions in the bundle. Preliminary analysis shows complex crosslinks with scruin, and deviation from the classical helical model of F-actin.

This work is supported by NIH Center for Research Resources, NSF, the W.M. Keck Foundation, and the Office of Research , Baylor Coll. of Medicine.

Su-AM-I2

THE STRUCTURE OF HORSE PLASMA GELSOLIN TO 2.5 Å, ((L.D. Burtnick*, R.C. Robinson+ and E.K. Koepf*)) *Chemistry Dept., UBC, Vancouver, Canada V6T 1Y6, and +LMB, Oxford University, Oxford, U.K., OX1 3QU.

We collected native and isomorphous derivative x-ray diffraction data sets from crystalline whole gelsolin purified from horse plasma. An electron density map calculated to 2.5 Å resolution shows gelsolin to contain six similarly folded domains. The two halves, S1-3 and S4-6, are connected with a 20 residue linker and pack together into a globular shape. The internal packing of S1 and S3, mimicked by S4 and S6, has the central β-sheets abutting to form a continuous sheet. This results in kinks near the ends of helices in S3 and S6 to avoid collision with corresponding helices of S1 and S4. We can generate models of F-actin that contain an actin-human gelsolin S1 (coordinates from P. McLaughlin, U. of Edinburgh) and overlay our structure so the S1s occupy the same volume. A clear picture emerges of how gelsolin caps the fast growing end of a filament. Our structure is devoid of Ca, yet the backbone of horse S1 lies almost exactly on that of Ca-containing human S1, showing that Ca binding doesn't cause restructuring within S1. Ca-induced hydrodynamic and spectral changes in gelsolin likely reflect shifts in the relative positions of the six domains to permit tight interaction with actin.

Su-AM-I3

DISTANCE BETWEEN MYOSIN HEADS IN RIGOR COMPLEX MEASURED BY FLUORESCENCE RESONANCE ENERGY TRANSFER. ((S.Ishiwata[1], M.Miki[2], I.Shin[1], T.Funatsu[1], K.Yasuda[3], and C.G.dos Remedios[4])) Department of Physics, School of Science and Engineering, Waseda University, 3-4-1 Okubo, Shinjuku-ku, Tokyo 169, Japan[1], Department of Applied Chemistry and Biotechnology, Fukui University, Fukui-shi 910, Japan[2], Advanced Research Laboratory, Hitachi Ltd., Hatoyama, Saitama 350-03, Japan[3] and Muscle Research Unit, Department of Anatomy, The University of Sydney, Sydney 2006, Australia[4].

Fluorescence resonance energy transfer (FRET) spectroscopy has been used to measure the distance between heads of myosin (heavy meromyosin (HMM) or subfragment-1 (S1)) which are attached to F-actin under rigor conditions (0.1M KCl, 1mM $MgCl_2$, pH 8.0, 20 ℃). For this purpose, the sulfhydryl group (SH1; Cys707) on myosin heads was specifically labeled with either (N-(iodoacetyl)-N'-(1-sulfo-5-naphthyl)-ethylenediamine (IAEDANS) employed as a fluorescent energy donor or with 5-(iodoacetamido)fluorescein (IAF) as an energy acceptor of fluorescence. Thus, intra- and inter-molecular distances between the heads of HMM and S1 or within an HMM molecule in the rigor complex were estimated based on a model calculation in which we assumed that FRET occurs between adjacent heads on F-actin and the binding constant of S1 (HMM) and F-actin is $10^7(5x10^7)/M$. The inter-molecular distances between S1 molecules, between HMM molecules and between S1 and HMM molecules thus estimated were about 6.0 nm, being equal to each other within the experimental error. On the other hand, intra-molecular inter-head distance within an HMM molecule, of which heads were heterogeneously labeled with IAEDANS and IAF, was estimated to be appreciably longer than that mentioned above, i.e., about 7.8 nm. There will be at least the following two ways to interpret this result: (1) the intra-molecular distance is in fact longer than the inter-molecular distances because of the distortion of the structure of the rigor complex, and (2) this is only apparent and the binding constant between HMM and F-actin was lowered when the heads are heterogeneously labeled with two different probes. These results should be compared with the structure of the rigor complex inferred from the crystallographic data.

Su-AM-I4

EFFECTS OF SMOOTH MUSCLE CALPONIN ON ACTIN ASSEMBLY ((J.X. Tang, P.T. Szymanski*, P.A. Janmey, and T. Tao*)) Brigham and Women's Hospital, 221 Longwood Ave., LMRC301, Boston, MA 02115, and *Boston Biomedical Res., Inst., 20 Staniford St., Boston, MA 02114.

The effects of unphosphorylated recombinant chicken gizzard calponin (CaP) on the kinetics of actin polymerization and the bundling of the resultant filaments were studied by a combination of fluorescence, light scattering, co-sedimentation and electron microscopic techniques. Sub-stoichiometric amounts of CaP accelerated actin polymerization at low ionic strengths, but this effect was diminished at [KCl]>150 mM. Quenching of the pyrene fluorescence was determined to be caused by the binding of CaP to F-actin, under conditions when no actin bundles were formed. At low ionic strengths, micromolar concentrations of CaP induced the formation of large bundles of actin filaments as revealed by light scattering, low speed sedimentation, and electron microscopy. At a higher ionic strength and at a fixed concentration of actin, a higher concentration of CaP was required to induce the formation of lateral aggregates. The average diameter of the actin bundles decreased with the increase of ionic strength. Actin bundles assembled at below 100 mM KCl were dispersed by raising the concentration of KCl to above 200 mM. Millimolar concentrations of ATP, ITP or GTP also dispersed such bundles to single filaments or smaller aggregates, even though a significant fraction of CaP remained bound to the filaments. We propose that the strong basic property of gizzard CaP induces the formation of F-actin bundles simply by reducing the electrostatic repulsion between the negatively charged actin filaments. (Supported by AR38910 to PAJ and P01-AR41637 to TT).

Su-AM-I5

MOLECULAR MOTIONS OF SINGLE ACTIN FIELDS IN DILUTE, SEMIDILUTE AND LIQUID CRYSTALLINE SOLUTIONS ((J. Käs†, H. Strey‡, J.X. Tang†, D. Finger†, R. Ezzell*, E. Sackmann‡ and P.A. Janmey†)) †Div. of Experimental Medicine, Brigham and Women's Hospital, Harvard Medical School, Boston, MA 02115, USA ‡Technische Universität München, Physik Department, Biophysics Group, 85748 Garching, FRG * Surgery Research Laboratory, Massachusetts General Hospital, Dept. of Surgery, Harvard Medical School, Charlestown, MA 02129, USA

Single semiflexible actin filaments were analyzed in solutions ranging from dilute (0.2 mg/ml) where filaments interact only with solvent to concentrations (4.0 mg/ml) at which F-actin forms a nematic phase. In dilute solutions the filaments exhibit thermal bending undulations in addition to diffusive motion. At higher semidilute concentrations (1.4 mg/ml) three-dimensional reconstructions of confocal images of fluorescently labeled filaments in a matrix of unlabeled F-actin reveal steric interactions between filaments which account for the viscoelastic behavior of these solutions. The restricted undulations of these labeled chains reveal the tube formed around a filament by the surrounding actin. The diffusion of filaments in semidilute solutions (c = (0.1 - 2.0) mg/ml) is dominated by diffusion along the filament contour (reptation), and constraint release by remodeling of the surrounding filaments is rare. The self-diffusion coefficient $D_{||}$ along the tube decreases linearly with the chain length for semidilute solutions. For concentrations > 2.5 mg/ml a transition occurs from an isotropic entangled phase to a coexistence between isotropic and nematic domains. Analysis of the molecular motions of filaments suggests that the filaments in the aligned domains are in thermal equilibrium and that the diffusion coefficient parallel to the director $D_{||}$ is nearly independent of filament length. We also report the novel direct observation of u-shaped defects , called hairpins, in the nematic domains.

Su-AM-I6

IDENTIFICATION OF A NOVEL NEBULIN-LIKE PROTEIN IN CARDIAC MUSCLE. ((Carole L. Moncman and Kuan Wang)) Dept. of Chemistry and Biochemistry. University of Texas. Austin, TX 78712

The large actin binding protein, nebulin, is believed to be found exclusively in skeletal muscle. We have identified a novel 107 kD cardiac myofibrillar protein that is nebulin-like based on immunological crossreactivity and sequence similarity. Immunoprecipitation and immunoblot assays with certain anti-nebulin mAbs detect a 107 kD protein in chicken, mouse and rabbit cardiac extracts. Immunofluorescence localization with the anti-nebulin mAbs in embryonic chicken cardiac myofibrils indicates that the crossreacting protein is a component of the I-Z-I complex and that this protein is not extractable with 500 mM KCl or KI. Human and chicken cDNAs corresponding to the nebulin-like protein have been isolated by immunological screening of cardiac cDNA libraries. Both cDNAs recognize an approx. 8 kb transcript in cardiac RNAs by northern analysis. Thus far, 1.2 kb of the chicken cDNA and 4 kb of the human cDNA have been sequenced. Both cDNAs encode open reading frames composed entirely of nebulin-like 35 residue modules marked by the highly conserved sequence motifs: SXXXYK and TPD. These open reading frames exhibit the strongest homology with nebulin modules located near the carboxyl terminus of human skeletal muscle nebulin. The presence of the nebulin modules suggest that this cardiac protein is a nebulin-like protein. The distribution of this protein relative to actin, α-actinin, myosin, and titin has been analyzed in spreading cardiomyocytes by immunofluorescence microscopy. Our results suggest that the cardiac nebulin-like protein becomes aligned with the nascent myofibrils early during cardiac myofibrillogenesis. To distinguish this smaller nebulin-like protein from the 700-900 kD skeletal muscle nebulin, we have named it nebulette. (Supported by grants from the USDA and NIH)

Su-AM-I7

NEBULIN-RELATED PROTEINS IN MOUSE MUSCLE: SEQUENCE ANALYSIS AND LOCALIZATION. ((Gang Luo, Jian Q. Zhang, Amy H. Herrera and Robert Horowits)) NIAMS, NIH, Bethesda, MD 20892.

We previously described a novel muscle specific mRNA of approximately 6 kb that contains sequence homologous to nebulin. We have now cloned and sequenced the full length cDNA for this message from mouse skeletal muscle. The full length cDNA contains an open reading frame of 3525 base pairs which is predicted to encode a protein of 133 kDa. A 587 amino acid region near the C-terminus is 45% identical to human nebulin, containing more than two complete 245 residue nebulin super repeats. The homology with nebulin suggests that this region may be an actin binding domain. The N-terminus contains the consensus sequence of a cysteine rich LIM domain, which may function in mediating protein-protein interactions. These data suggest that the encoded protein may link actin filaments to some other proteins or structure. Therefore, we propose to call the encoded protein nebulin-related anchoring protein (N-RAP). We expressed 56 kDa of the nebulin-like region of N-RAP in E. coli. Using an antibody raised against a 20 amino acid peptide from the nebulin-like region of N-RAP, we detected the fragment of N-RAP expressed in E. coli as well as a number of proteins in both skeletal muscle and heart. Proteins detected in skeletal muscle include nebulin as well as a 110 kDa protein, which is the band most likely to correspond to the cloned N-RAP protein. Immunofluorescent staining of mouse skeletal muscle with this antibody showed specific staining at the myotendonous junction and in cardiac muscle at the intercalated disc. We propose that N-RAP anchors the terminal actin filaments in the myofibril to the membrane and may be important in transmitting tension from the myofibrils to the extracellular matrix.

Su-AM-I8

TROPOMYOSIN MOVEMENT IN THIN FILAMENTS FOLLOWING Ca^{2+}-ACTIVATION ((W. Lehman[1], R. Craig[2], P. Uman[2] and P. Vibert[3])) [1]Dept. Physiology, Boston Univ. Sch. Med., Boston MA 02118; [2]Dept. Cell Biology, Univ. Mass. Med. Sch., Worcester MA 01655; [3]Rosenstiel Ctr., Brandeis Univ., Waltham MA 02254.

Native thin filaments from troponin-regulated *Limulus* and frog muscles were isolated under relaxing conditions and examined by negative-staining. 3-D reconstructions of the filaments showed continuous strands of density attributable to tropomyosin running along the surface of successive actin monomers. Consistent with the "steric-blocking model" of muscle regulation, the position occupied by tropomyosin in the "off-state" coincides with myosin-binding sites on actin (Lehman *et al., Nature* **368**:65, 1994; *J. Mol. Biol.* **251**:191, 1995). Reconstructions of *Limulus* filaments examined in the "on-state" following addition of Ca^{2+} revealed a ~25° azimuthal movement of tropomyosin about the actin helix, uncovering myosin binding sites (Lehman *et al.*, 1994); however, related X-ray diffraction studies by Poole *et al.* (*Biophys. J.* **68**:348s, 1995) suggested that this movement does not expose myosin binding sites entirely. S-1 decorated *Limulus* thin filaments, examined under rigor conditions in the absence of ATP, indeed showed a further ~10° shift in tropomyosin strand position, thereby exposing the entire myosin-binding domain, implying that a third state of the filament is produced during the myosin-binding process *per se*. Here, tropomyosin lies immediately adjacent to but not in direct contact with the tip of each bound S-1. Ca^{2+}-binding alone therefore may not be sufficient for full-activation of filaments. This may occur only after an initial docking of sufficient numbers of myosin-crossbridges switching-on thin filaments. This process of activation may explain the cooperative nature of crossbridge docking and cycling.

Su-AM-I9

TOWARDS AN ATOMIC MODEL FOR REGULATION BY TROPOMYOSIN/TROPONIN ((P. Vibert[1], R. Craig[2], P. Uman[2] & W. Lehman[3])). [1]Rosenstiel Ctr., Brandeis Univ., Waltham MA 02254; [2]Dept. Cell Biology, Univ. Mass. Med. Ctr., Worcester MA 01655; [3]Dept. Physiology, Boston Univ. Sch. Med., Boston MA 02118.

To define more precisely the contacts of actin and tropomyosin in regulated filaments in the *"off"* and *"on"* states, we fitted our 3D-EM density maps of thin filaments in EGTA, Ca^{2+} and S1-decorated states with the atomic model of F-actin of Lorenz et al. (1993). The fit establishes the locations of the actin subdomains and reveals that the cleft between subdomains-2 and -4 is resolved in our maps. In EGTA (Lehman et al., *J. Mol. Biol.* **251**:191, 1995), tropomyosin closely contacts subdomain-1 near its junction with subdomain-3, but bridges over subdomain-2 to the next actin monomer without making further contact. Among actin residues thought to interact with myosin, one group of mostly charged residues (including 1-4 and 93-95 in subdomain-1) appears still to be accessible in the *"off"* state. A larger, more hydrophobic group (including 24-28 and 340-346 in subdomain-1, and 144-148 and 332-336 at the junction of subdomain-1 and -3) appears to be occluded by the tropomyosin strand. Strong myosin association with actin would therefore be inhibited, halting crossbridge cycling, but weak and transient actin-myosin interactions could still occur without producing force, as indicated by biochemical and mechanical data. In the presence of Ca^{2+}, most of the myosin-binding residues on actin, especially on subdomain-1, are exposed by tropomyosin's 25° rotation from the *"off"* state. However some residues (including 332-336) appear still to be blocked. Fitting the actin model into S1-decorated filaments shows that when myosin is tightly bound, these residues are not covered by tropomyosin but become part of the extensive actin-myosin interface. There seems to be no interaction of the rigor S-1 with the "weak-binding" actin residues 1-4 and 93-95, but to confirm this conclusion we will need to do further fitting using atomic models of S1 as well as of F-actin.

PROTEIN STRUCTURES

Su-AM-J1

X-RAY STRUCTURE OF MITOCHONDRIAL CREATINE KINASE ((Karin Fritzwolf and Wolfgang Kabsch))
Max-Planck Institut, Jahnstrasse 29, D-69028 Heidelberg, Germany
((Thomas Schnyder and Theo Wallimann*))
Institute for Cell Biology, ETH-Hönggerberg, CH-8093 Zürich, Switzerland

The first crystal structure of octameric mitochondrial creatine kinase (Mi_b-CK, with a M_r of 345'560) from chicken cardiac muscle has been determined at 3 Å resolution. The two structures of Mi_b-CK obtained with or without ATP are very similar. Each Mi_b-CK monomer contains its separate active site which is not shared between two monomers of the enzymatically acitve Mi_b-CK dimer.The monomer consists of a small, purely alpha-helical domain (residues 1-112) and a large domain (residues 113-380), which contains an eight-stranded antiparallel beta-pleated sheet flanked by seven alpha-helixes. The conserved amino acid residues in the class of guanidino kinases, to which Mi_b-CK belongs, form a compact three dimensional cluster covering the cleft between the domains and the bound nucleotide. Several amino acid residues, implicated by biochemical studies to be involved in catalysis and/or substrate binding, could be identified in the X-ray structure. The octamer possesses approximate 422 point group symmetry and has the overall appearance of a unique cube-like structure with a side length of 93 Å and with a 20Å wide channel extending through the entire octamer along the fourfold axis, as well as a smaller opening on each side. The overall appearance of the Mi_b-CK octamer is consistent with its proposed function as a mitochondrial "energy channelling molecule". The exposed surface clusters at the fourfold top and bottom faces of positively charged C-terminal amino acids (Lys360-Lys380) can explain the observed mediation by Mi_b-CK of intermembrane adhesions between inner and outer mitochondrial membranes due to interaction with negatively charged head groups of phospholipids.

Supported by DFG, NSF, Horten-Found., Swiss Muscle Found., Careal Hold. ZH

Su-AM-J2

STRUCTURE OF σσ HUMAN ALCOHOL DEHYDROGENASE COMPLEXED WITH NAD^+ AT 3Å RESOLUTION. ((Peiguang Xie & Thomas D. Hurley)) Department of Biochemistry and Molecular Biology, Indiana University School of Medicine, Indianapolis, IN 46202

The three-dimensional structure of σσ human alcohol dehydrogenase (ADH) complexed with NAD^+ has been determined to 3Å resolution by X-ray crystallography. The structure has been refined to an R-factor of 21.7% and an R_{free} of 30% using XPLOR. The structural difference between σ-ADH and β_1-ADH is consistent with their different kinetic behaviors. There are two significant conformational changes: one at substitutions of Asn for Gly at residues 260 and 261, and the other at residue 117, which is deleted in σ-ADH. Substitutions of Phe for Leu309 and Cys for Ala317 in σ-ADH result in a twist in the NAD^+ nicotinamide ring. Residues 48 and 93 are also shifted relative to β_1-ADH and create a larger binding site around the zinc. These changes could account for the high K_M for ethanol oxidized by σ-ADH. The changes in the substrate binding site caused by deletion at residue 117 and the substitutions at residues 141 and 309 may explain the K_M dependence on the substrate hydrophobicity. The substitutions of His for Arg271 and Leu for Ile224 may affect the dissociation of the NAD(H) adenine moiety. Additional NAD(H) strain imposed by substitutions of Phe309 and Cys317 may also be expected to accelerate coenzyme dissociation and could account for σ-ADH's high V_{max}.
(This work was supported by PHS-K21-AA00150.)

Su-AM-J3

SNAPSHOTS THROUGH AN ENZYME MECHANISM: THYMIDYLATE SYNTHASE. ((R.M. Stroud, J.S. Finer-Moore, T.J Stout, and E.E. Rutenber,)) Dept. of Biochemistry & Biophysics, UCSF, San Francisco, CA 94143-0448.

Structures of the enzyme thymidylate synthase have been trapped at various stages through the reaction mechanism. The combination of mutations which impair certain stages of the reaction and unusual inhibitors have been used to determine high resolution atomic structures for the unliganded enzyme, the enzyme bound to substrate, the enzyme bound to cofactor, a catalyzed alteration in the cofactor that leads to ring opening, a covalent addition of the substrate to the enzyme, the covalent addition of cofactor substrate and enzyme, and the enzyme product complex. From these structural snapshots through the reaction mechanism, a mechanism of chaperoning the substrates into the binding site and into the correct orientation for catalysis emerges. Mutational analysis is used to determine the critical elements in orienting the substrate. Two critical water molecules involved in the reaction chemistry are positioned during the orientation and set up for reaction. Calculations based on the transition state in the reaction versus bound substrates lead to an understanding of transition state stabilization. Mutations of several residues in the active site define the roles of key residues in the enzyme mechanism. The result is a detailed picture of the stereochemistry and dynamics of catalysis in four dimensions.

Su-AM-J4

NMR STRUCTURE OF A RECEPTOR BOUND G PROTEIN PEPTIDE: STRUCTURE REFINEMENT AND UPDATE. ((E.A.Dratz, D.Gizachew, S.C.Busse, S. Rens-Domiano#, and H.E.Hamm#, Dept. Chem. and Biochem., MT State Univ. Bozeman, MT 59717 and #Dept. of Physiol. and Biophys. Univ. of IL College of Medicine, Chicago, IL. 60680

We previously reported Transferred-NOESY NMR studies of the 3D structure of a G protein peptide bound to rhodopsin and to light excited rhodopsin, MII (Dratz, et al, Nature, 363: 276-80, 1993). The peptide investigated is the C-terminus of the Gα subunit (Ac-340-350 K341R) which is able to bind to rhodopsin and MII, to block the coupling of rhodopsin to the G protein, and to stabilize MII (the form of light excited rhodopsin that couples to the G protein). The initial bound structure reported were based on the isolated two spin approximation (ISPA). When we attempted to refine the bound structure, with backcalculation, we found a resonance misassignment (initially pointed out to us by Rizo and Gierasch, personal communication) which made the reported structure less clearly favored. More seriously, several regions of the bound structure could not be refined satisfactorily. Zheng and Post (JMR Ser. B,101:262-270, 1993) showed that lack of agreement between the backcalculated and the experimental Tr-NOESYs of bound ligands with known structures could be due to nonuniform spin diffusion between different ligand protons and the receptor. We used a spin echo method, which allowed the receptor spins to dephase during a delay and refocused the ligand spins, so that the receptor spin magnetization did not modulate the Tr-NOESY cross peaks. The differences in cross peak intensities with and without the spin echo provide a map of the ligand protons which are in most intimate contact with the receptor. The spin echo filtered NOESY cross peak intensities also provide interproton distances that are corrected for spin diffusion when analyzed with complete ligand relaxation matrix methods (Mardigras and Irma). The refined receptor bound G protein peptide structures will be presented and discussed. (Supported by NIH EY06913 and NSF OSR-9350546).

Su-AM-J5

THE CRYSTAL STRUCTURE OF HUMAN ENDOTHELIN AND ITS ROLE IN G-PROTEIN COUPLED RECEPTOR BINDING ((B.A. Wallace and R.W. Janes)) Dept. of Crystallography, Birkbeck College, University of London, London, England

The recently solved (Nature Struct. Biol. 1:311-319) crystal structure of human endothelin-1, the most potent naturally-occurring vasoconstrictor, has revealed structural features of the polypeptide that differ considerably from those found in the reported structures of endothelin as determined by NMR spectroscopy (Prot. Sci. 4:75-83). The most significant differences are in those regions important for receptor binding and specificity, namely the central loop and the C-terminal helix. Comparisons of the crystal structure with the structures of chemically-unrelated but very potent antagonists (Peishoff et al, submitted) show a strong correspondence in their 3-dimensional structures and correlations with binding and activity data for a large number of naturally-occurring and synthetic mutants strongly support the crystal structure as being biologically relevant with respect to binding to their G-protein coupled receptors.

(Supported by the British Heart Foundation)

Su-AM-J6

THE SOLUTION STRUCTURE OF A NOVEL RIBONUCLEASE POSSESSING LECTIN ACTIVITY ISOLATED FROM THE OOCYTES OF A BULLFROG (*R. CATESBEIANA*). ((C. Chen, K. Hom, R.F. Huang, P. J. Chou, Y.D. Liao and T.H. Huang)) Institute of Biomedical Sciences, Academia Sinica, Taipei 11529, Taiwan, R.O.C. (Spon. T.H. Huang)

RC-RNase is a 111 amino acid, pyrimidine-guanine sequence specific ribonuclease purified form the oocytes of *Rana catesbeiana*. It is also a sialic acid binding lectin and exhibits receptor mediated cytotoxicity. We have assigned nearly all proton NMR resonances of this protein using a large set of multidimensional NMR spectra. The structure of RC-RNase was determined by restrained molecular dynamics and simulated annealing techniques, based on a large set of NMR constraints. The structure was found to consists of two triple-stranded anti-parallel β-sheets and three short N-terminal α-helices folded into a bowl shape, similar to that of P-30. However, we detected the existence of multiple conformation in certain region of the structure. Substrate analoques were found to interact with residues located in the cleft region. The pK_as of the active site histidines were also determined. The structure-functional relationship of RC-RNase and its relatrion to other pyrimidine specific ribonucleases will be discussed.

Su-AM-J7

PEPTITERGENTS: A NEW APPROACH TO SOLUBILIZING MEMBRANE PROTEINS. ((R.M. Stroud & C.E. Schafmeister)) Dept. of Biochemistry & Biophysics, UCSF, San Francisco, CA 94143-0448.

Peptides designed to form α-helices approximately 40 Å in length are capable of solubilizing membrane proteins when the peptides form strongly amphipathic helices. Several such peptides have been synthesized and characterized for their properties and the variation in properties correlated with change in sequence of the amphipathic peptides. These peptides are shown to solubilize bacteriorhodopsin and rhodopsin and are thus capable of coating the outside of a transbilayer membrane protein in a manner reminiscent of that of a soluble protein. The goal is to crystallize the peptitergent solubilized proteins taking advantage of the more orderly exterior. The properties of these peptides in bilayers are also discussed. They are capable of forming transbilayer ion-conducting channels in which a polar center leads to the ion-conducting region and the hydrophobic outsides interface with the lipid. This is the opposite of the action on membrane proteins where the hydrophobic surface interfaces with the transbilayer region and the polar exterior with solvent.

Su-AM-J8

INFRARED CRYSTALLOGRAPHY: STRUCTURAL REFINEMENT THROUGH SPECTROSCOPY

((J.T. Sage, W. Jee)) Northeastern University

Polarized IR measurements on single crystals yield the orientation of vibrational transition dipoles. In favorable cases, this determines the orientation of bonds assigned to well-resolved, vibrationally isolated stretching modes with greater precision than the macromolecular structure refined from diffraction data. We will present detailed measurements of the orientation of small ligands bound at the heme sites of myoglobin (Mb) crystals, including CO, CN^-, and N_3^-. As reported previously, we find that in MbCO crystals CO is displaced less than 10° from the heme normal (Ivanov et al., JACS 116, 4139 (1994)), probably 7° in a direction between pyrroles C and D. This result contradicts X-ray and neutron structures of $P2_1$ MbCO crystals, which show CO displaced in various directions by more than 30°. Recent picosecond photoselection measurements (Lim et al., Science 269, 962 (1995)) have confirmed that the CO lies within 7° of the heme normal in solution, but do not reveal the direction of tilt. Unlike X-ray diffraction, which leads to a time averaged electron density map, IR crystallography can independently characterize spectrally resolved bands. This allows us to observe the effect of changes in distal pocket structure and iron spin on ligand binding geometry.

Su-AM-J9

NEUTRON RESONANCE SCATTERING FROM $^{240}Pu^{3+}$ BOUND TO THE Ca^{2+}-BINDING SITES IN CALMODULIN: A NEW STRUCTURAL PROBE. ((P. A. Seeger, S. E. Rokop, P. D. Palmer, S. J. Henderson, D. E. Hobart, and J. Trewhella)) Los Alamos National Laboratory, Los Alamos, NM 87545.

^{240}Pu has a strong nuclear resonance at 0.278 Å. At this wavelength the coherent scattering from ^{240}Pu is ~1000 times that of any other nucleus present in a protein. Pu^{3+} has the same ionic radius as Ca^{2+}, and we demonstrated that we could substitute $^{240}Pu^{3+}$ for Ca^{2+} in calmodulin. We further showed that the $4^{240}Pu^{3+}$•calmodulin complex activates myosin light chain kinase. We then collected neutron scattering data from solutions of $4^{240}Pu^{3+}$•calmodulin and $4Ca^{2+}$•calmodulin in order to extract the resonance scattering arising from the ^{240}Pu. This resonance scattering contains periodic terms that are directly related to the distances between the Pu^{3+}/Ca^{2+}-binding sites in the protein. Any flexibility in the protein, and hence variation in these distances, will result in some dampening of these periodic terms. Using a Monte Carlo simulation of the neutron source target /moderator system we have recently determined the instrument resolution function that is needed in order to extract correctly the resonance scattering terms. We will present the results of this analysis, and of modeling calculations used to interpret the resonance scattering in terms of ^{240}Pu-^{240}Pu distances. This experiment is the first demonstration of the use of neutron resonance scattering as a structural probe in a protein, and it is also the first use ^{240}Pu resonance scattering in any system.

CONTRACTILITY, LOCOMOTION, MOTILITY: CONTRACTION

Su-AM-K1

STEPWISE SHORTENING IN SINGLE SARCOMERES OF SINGLE MYOFIBRILS. ((Tsukasa Tameyasu, Arun Ramakrishnan, and Gerald H. Pollack)) Center for Bioengineering, Box 35-7962, Univ. of Washington, Seattle WA 98195.

Previous reports of stepwise sarcomere shortening remain controversial. Despite the array of methods with which the steps have been observed, including several from other laboratories, concern about instrument artifact lingers (*cf.* Burton and A. F. Huxley, Biophys J. 168: 2429-2443, 1995). In the present study we report preliminary results obtained using single isolated honeybee myofibrils. The striation pattern was projected onto a 512-element photodiode array. Each scan produced a trace of intensity distribution along the myofibril axis. By computing the position of the center of mass of each A-band along the myofibril, the length of each sarcomere could be obtained, automatically. The myofibril was ramp-released using a motor attached to one end, and the striation pattern was recorded. R.M.S. noise level was typically 2 - 5 nm per sarcomere. Of 32 myofibrils examined to date, virtually all showed some evidence of steps. In most records, detectable steps were interposed with regions of either smooth shortening or of shortening with noise too high to allow determination. Other records showed clear cascades of steps. To test for artifact associated with the photodiode array we carried out two tests. First, we shifted the array to a new position along the myofibril axis; within the limits of noise and repeatability, the stepwise pattern of the particular sarcomere remained the same. Second, we substituted two alternative arrays of different size; both gave similar stepwise patterns. We are developing an algorithm to measure step size accurately. By eye, occasional steps on the order of 0.1 μm can be seen. The preponderance of steps, however, appear to be in the range 20 - 25 nm per sarcomere.

Su-AM-K2

SPATIAL POSITION OF LYS-553 OF S1 RELATIVE TO THE THIN FILAMENT AXIS IS DEPENDENT ON FILAMENT SATURATION
((Andrzej A. Kasprzak, Raoul Bertrand, and Ridha Kassab)) *CRBM-CNRS, INSERM-U.249, 34033 Montpellier, France*

Lys-553 of myosin subfragment 1 (S1) is located in the immediate vicinity of the acto-S1 interface. We have tried to locate this residue in space relative to the actin filament by performing distance measurements by FRET. Lys-553 was modified by 6-(fluorescein-5-(and 6)-carboxamido)hexanoic acid succinimidyl ester (FHS) to produce FH-S1. Three loci on actin were labeled: 1,5-IAEDANS or monobromobimane were conjugated to Cys-374, Gln-41 was modified with EDANS using transglutaminase, and the actin's nucleotide was replaced by εATP. When binary G-acto-FH-S1 complexes were formed, FRET was generally low (*ca.* 8-12%), but increased to > 50% in the F-acto-rigor complex. The efficiency of FRET was dependent on the filament saturation: when actin filament was 40% saturated with FH-S1, a relatively large FRET was seen; however, for the same filament, when the saturation was brought to 85% with *unlabeled* S1, FRET was reduced to the level comparable to G-acto-FH-S1, although, as demonstrated by cosedimentation, negligible amount of S1 dissociated from the filament. ADP (~ 1 mM) had no effect on FRET in the F-actin filament, however its presence excluded the possibility that the changes in FRET efficiency are due to the bundling of actin by S1. The results show that the saturation-depending differences in the structure of the acto-S1 complex involve also the interface region.

Su-AM-K3

TILTING MOTIONS OF RHODAMINE PROBES AT FIVE DIFFERENT SITES ON THE MYOSIN REGULATORY LIGHT CHAIN (RLC) FOLLOWING LENGTH STEPS IN CONTRACTING MUSCLE FIBERS ((Seth C. Hopkins[A], Cibele Sabido-David[B], Lakshmi D. Saraswat[C], Yale E. Goldman[A], Malcolm Irving[B], and Susan Lowey[C])) [A]Pennsylvania Muscle Inst., Univ. of PA; [B]Randall Inst., King's Coll. London; [C]Rosensteil Center, Brandeis Univ. (Spon. by V.T. Nachmias)

To examine tilting of the light-chain region of the myosin head, we measured polarized fluorescence from the 5 and 6 isomers of acetamidotetramethyl rhodamine (ATR) covalently bound to cysteine 2, 73, 94, 126, or 155 engineered into chicken skeletal RLC. Labeled RLC was exchanged for native RLC in rabbit psoas muscle fibers. A gaussian distribution (peak angle θ_o, half-width σ) of probe dipoles with limited sub-nanosecond mobility was fit to three independent fluorescence polarization ratios to obtain time courses of θ_o and σ (see Fig.). For all 10 probes, the angle change between active contraction (Act) and rigor is toward or across the equatorial plane. Releases of 5 nm / half sarcomere (h.s.) in Act tilt all 10 probes in the direction of the rigor orientation, suggesting that the RLC tilts during the working stroke toward the rigor orientation. For all probes, the angle change from Act to rigor is larger than the angle change (<5°) for a release of 5 nm/h.s., consistent with the idea that only a fraction of the cross-bridges respond to the length change. Supported by NIH grant AR26846, AR17350, the MDA, and the Wellcome Trust, UK.

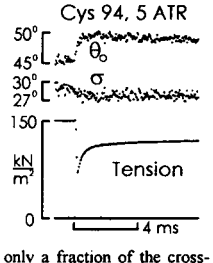

Su-AM-K4

Effects of temperature and ionic strength on myosin head orientation in relaxed demembranated fibers from rabbit psoas muscle, studied with a birefringence-interference microscope. ((Duncan E. Folkes, Neil C. Millar & Malcolm Irving)) Randall Institute, King's College London, 26 Drury Lane, London WC2B 5RL, UK.

Changes in muscle birefringence, the difference in refractive index between light polarized parallel and perpendicular to the muscle fiber axis, are associated with changes in myosin cross-bridge orientation (Peckham, M. & Irving, M. (1989). *J. Mol. Biol.* **210**, 113-126). Birefringence is measured by dividing the birefringence retardation Γ (the phase lag between the parallel and perpendicular components of the light passing through the fiber) by **d**, the optical path length through the fiber. Birefringence, however, is affected by changes in fiber volume, so we also measured the interference retardation Δ (the phase lag between light passing through and bypassing the fiber). Dividing Γ by Δ gives the anisotropy index α, a measure of myosin cross-bridge orientation that is independent of changes in **d** and fiber volume. In relaxed fibers α increased by 2.9 ± 0.4% (n=8, mean ± SEM, ionic strength (IS) = 0.17M) when temperature was raised from 12 to 17°C, but did not change significantly between 5 and 12°C, or between 17 and 30°C. The increase in α between 12 and 17°C suggests that the long axes of the myosin heads become more parallel with the thick filament axis, consistent with changes in the x-ray diffraction pattern in this temperature range (Lowy, J. *et al.*, (1991). *Biophys. J.* **60**, 812-824). At 5°C α also increased with increasing IS. In 0.02M IS relaxing solution the value of α was close to that in rigor, but raising IS to 0.2M increased α by 4.9 ± 0.9% (n=7). In contrast no significant change in α was seen when IS was varied between 0.06 and 0.2M at 20°C. Supported by Wellcome Trust and BBSRC, UK.

Su-AM-K5

LOAD-DEPENDENT EFFICIENCY IN SINGLE GLYCERINATED MUSCLE FIBERS ACTIVATED BY LASER FLASH PHOTOLYSIS OF CAGED CALCIUM IN THE PRESENCE OF A LIMITED AMOUNT OF ATP.
(H. Sugi, H. Iwamoto and H. Ushitani) Dept. of Physiol., Sch. Med., Teikyo Univ. Tokyo 173, Japan

To study the load-dependent efficiency of muscle contraction in simplified conditions, we activated single glycerinated rabbit psoas muscle fibers containing 200 μM ATP under various auxotonic loads by laser flash photolysis of caged calcium. The fiber was exposed in air immediately before the laser flash irradiation, so that the number of ATP molecules in the fiber was equal to the number of myosin heads. In such a condition, all myosin heads are believed to be in the form of M-ADP-Pi before activation. The flash-induced auxotonic shortening was interrupted at various times after the onset of shortening, and the magnitude of the subsequent isometric force development was taken as a measure of M-ADP-Pi remaining in the fiber. As the initial sarcomere length was 2.4 μm, all myosin heads could interact with actin filaments. Rather unexpectedly, the time versus length, force and power output traces under a wide range of auxotonic load were all superimposed each other if normalized with respect to their maximum values, suggesting that the fiber senses the amount of auxotonic load at the beginning of shortening to determine its subsequent mechanical behavior. Further analysis of the results obtained indicated that the efficiency of chemo-mechanical energy conversion in each myosin head may differ greatly in a load-dependent manner.

Su-AM-K6

DISTRIBUTED FILAMENT COMPLIANCE IN THE SARCOMERE: A SIMPLE MODEL. ((JN Peterson)) UVM College of Medicine, Burlington, VT 05405.

Mechanical studies using muscle stiffness to estimate the fraction of attached cross-bridges (n_{XBr}) assume that thin and thick filaments are non-compliant, such that stiffness is directly proportional to n_{XBr}. Recent data (e.g., Higuchi *et al*, Biophys J 69: 1000, 1995) show that the filaments *are* compliant, so muscle stiffness may not be a suitable index of n_{XBr}. I have developed a model of distributed filament compliance (top figure), in which muscle stiffness is a non-linear function of n_{XBr}. One important implication of this model is that each XBr along the thick filament endures different strains and forces, as shown in the bottom figure (18 XBr's are attached). Strain dependent rate constants, coupled with different strains on each XBr, will thus lead to an ensemble of XBr's cycling at different rates. A simple lumped parameter version of this model is derived at http://salus.med.uvm.edu /~peterson/amstiff.html.

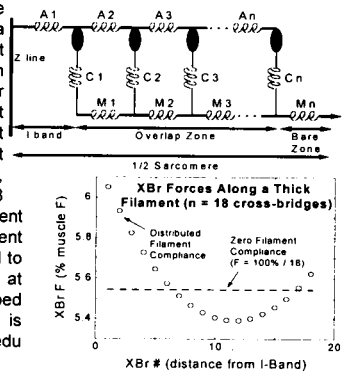

ION MOTIVE ATPases I

Su-AM-L1

ENZYME ACTIVATION LEVEL DETERMINES ELECTROMAGNETIC (EM) SIGNAL TRANSDUCTION IN Na,K-ATPase. M Blank and L Soo. Department of Physiology and Cellular Biophysics, Columbia University, New York, NY 10032

Changes in Na,K-ATPase activity in electric and magnetic fields depend only upon the level of enzyme activation. Below .05-.1μmolesP/min/mgprotein, both fields increase enzyme function. Above this activation, electric fields inhibit, magnetic fields stimulate. If we assume that **enzyme activation increases with mobile charge concentration,** we can account for the effects of both fields. **Magnetic fields** affect mobile charges throughout the protein, and the effect is smaller as the charges increase with activation. **Electric fields** change charge distribution at interfaces, penetrating into the interior at low activation (when all mobile charges are needed to polarize the interface), and polarizing the interface without penetrating to the interior at high activation. Mobile charges unaffected by the electric field are not coordinated and interfere with charge conduction in the enzyme. The number of charges in the enzyme at the critical activation can be estimated (1-2) from electric double layer theory. Linkage of signal transduction with intra-molecular conductance suggests that gene activation by magnetic fields may be due to interaction with conducting elements within DNA. The threshold for magnetic field effects on Na,K-ATPase, .2-.3μT, is in the range reported to stimulate transcription (.8μT), and is at the threshold in epidemiological studies linking magnetic field exposure to human diseases.
(We thank EPRI and the Heineman Foundation for their support.)

Su-AM-L2

COMPARISON OF TRANSIENT Na/K-ATPase CURRENTS IN EXCISED PATCHES FROM GUINEA PIG HEART CELLS INDUCED BY AN ATP CONCENTRATION JUMP OR A VOLTAGE PULSE. ((T. Friedrich & G. Nagel))
Max-Planck-Institut für Biophysik, D-60596 Frankfurt, F.R.G.

Previously we have shown that in a giant excised patch a transient outward current, followed by a decay to a stationary pump current, can be observed after photolysis of caged ATP with a laser flash of 308 nm wavelength. This signal is Na and ATP dependent and can be abolished by ortho-vanadate. Whereas the rate of the decay of the signal is related to ATP and caged ATP binding and dissociation, the rate constant of about 200 s^{-1} of the rising phase reflects a transport step of the Na,K-ATPase (presumably the E_1P-E_2P conformational change), which compares well with experiments using purified Na,K-ATPase on lipid bilayer membranes (Fendler et al., 1987, *FEBS Letters* 224:83-88).

By subtraction of voltage pulse induced currents in the absence of ATP from the ones with ATP present, it is also possible to obtain Na,K-ATPase current transients with a monoexponential decay, with a rate constant which is the sum of the forward and backward rates of the voltage dependent equilibrium (Hilgemann, 1994, *Science* 263:1429-1432, see also Nakao & Gadsby, 1986, *Nature* 323:628-630). We obtained these voltage induced Na,K-ATPase current transients additionally from the same patch and the transferred charges and voltage dependent rate constants were compared with data from caged ATP experiments. Again we find a rate constant of about 200 s^{-1} at 24°C and 0 mV for the electrogenic forward step. We conclude from these extended measurements that the electrogenic Na^+ translocation step has a rate constant of 200 s^{-1} at 24°C and 0 mV or is limited by a preceding electroneutral step (E_1P-E_2P transition) with this rate constant.

(Supported by the Deutsche Forschungsgemeinschaft.)

Su-AM-L3

VOLTAGE-DEPENDENCE OF NA/K PUMP IN ISOLATED FROG SKELETAL MUSCLE MEMBRANES. ((W. Chen, and Y. Han)) Department of Surgery, The University of Chicago, Chicago, IL 60637

So far, direct measurement of pump current in skeletal muscle fiber has not been reported. Recently, we succeed in detection of Na/K pump current using an improved double Vaseline-gap voltage clamp technique on cell membrane of frog skeletal twitch muscle fibers.
The Na/K pump current was identified by the ouabain-sensitive current as a difference between traces of pre- and post-application of ouabain. However, any changes in leakage currents and residual channel currents may induce errors in pump current measurement. According to the previous studies, two assumptions have been made to identify the pump currents: 1) The steady-state Na/K pump currents is very small and negligible at the membrane potential below -150 mV. 2) The leakage current underneath the Vaseline seals is linear voltage-dependence responding to potentials around -150 mV. To accurately identify the ouabain-sensitive current, The I-V curves both pre- and post-ouabain-application were first corrected by subtracting straight lines fitting data points at membrane potentials below -130 mV. The remaining will, then, be resubtracted, result of which will be defined as I-V curve for the Na/K pump currents.
The membrane holding potential was at -40 mV. Outward K currents were reduced by lowering K concentration in the internal solution to 10 mM and by adding 65 mM TEA in the external solution for blocking K channels. To minimize inward currents in Ca and K channel, external solutions were nominally Ca-free and included small amounts of Cd, Ba and Cs. The resulting low membrane conductance facilitate the control of membrane potential over an extensive range and enhanced the signal-to-noise ratio for detection of Na/K pump current.
Steady-state current-voltage relationship and transient charge movement of the Na/K pump were obtained. The results showed a similarity to those obtained from cardiac muscle and a difference in the pump density. When removing intracellular Na or extracellular K ions, transient pump charge movement currents were also obtained. The steady-state charge movement I-V curve showed a Boltzmann distribution.
This study is partially supported by NIH grant GM-50785.

Su-AM-L4

TRANSIENT CHARGE MOVEMENT DURING K^+-TRANSLOCATING STEPS BY THE Na PUMP. ((R.D. Peluffo and J.R. Berlin)) Bockus Research Institute, Graduate Hospital, Philadelphia, PA 19146.

Electrogenic events associated with K:K-exchange by the Na pump were studied in enzymatically isolated rat ventricular myocytes superfused with a nominally Na^+-, K^+- and Ca^{2+}-free Tyrode's solution containing (mM) 0.025-0.1 Tl^+, 2.3 Ba^{2+}, 2 Mg^{2+}, 0.2 Cd^{2+}, and 145 TMA. Cells were voltage-clamped at 11°C to 21°C with single patch electrodes containing (mM) 155 K^+, 20 TEA, 0.7 ATP, 10 Mg^{2+}, 9 HEDTA, 30 phosphate. Ouabain-sensitive charge (see figure), measured over the range -160 to +100 mV by applying voltage steps from a holding potential of -40 mV, was found to be saturable and [Tl^+]-dependent. The total amount of charge moved with 100 μM Tl^+ (11.2 ± 0.9 fC/pF, n = 4) was the same for the *on* and *off* processes. The apparent rate constant for relaxation of the transient charge movement (k_{on}) was voltage independent at positive potentials but increased with hyperpolarization. Fitting k_{on} as a function of the voltage yielded, at 100 μM Tl^+ and 14°C, a pseudo-first order forward rate constant at 0 mV equal to 28.8 ± 11.2 s^{-1}, a reverse rate constant at 0 mV of 504.8 ± 20.1 s^{-1}, a symmetry factor of 1.00 ± 0.01, and an apparent valence of 0.47 ± 0.08. The temperature coefficient (Q_{10}) for k_{off} was found to be 1.5 ± 0.1. Thus, K^+ binding to, but not release from, extracellular sites is electrogenic and may become rate-limiting for steady state ion transport by the Na pump under appropriate conditions.

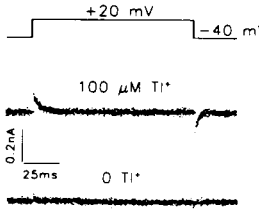

Su-AM-L5

Na/K-PUMP-MEDIATED CHARGE MOVEMENTS AS AN ASSAY OF Na' TRANSLOCATION AND OCCLUSION/DEOCCLUSION RATES

((J. Wagg, M. Holmgren, D.C. Gadsby, F. Bezanilla, R.F. Rakowski and P. De Weer))
Marine Biological Laboratory, Woods Hole, MA 02543, USA.

At least two steps during translocation of 3 Na' by the Na/K-pump are believed electrogenic: (i) deocclusion and/or release of the first Na' into the extracellular compartment, and (ii) deocclusion and/or release of the last 2 Na'. The kinetics of the charge movement associated with these reactions were characterized in squid (Loligo pealei) giant axons superfused and internally dialyzed with K'- and Cl'-free solutions to prevent cycling. Transient pump current, assayed by subtracting currents (filtered at 5 or 80 kHz and digitized at 20 or 250 kHz) elicited by voltage steps from 0 mV to -110 to +50 mV in the presence of 100 μM dihydrodigitoxigenin from those obtained in its absence, comprised 3 distinct components: ultrafast ($\tau_e < 10$ μs), fast ($\tau_e \leq 100$ μs), and slow ($\tau_e \sim 1$ ms). The relaxation rate of the slow component showed marked dependence on temperature, extracellular Na' concentration, and membrane potential, while that of the fast component depended only weakly on those parameters. Ultrafast kinetics were not resolved. These findings are consistent with a kinetic model in which the sole electrogenic events are movements of Na' within access channels that connect the extracellular compartment with the Na' binding sites. Transient currents are interpreted as reflecting these Na' movements: an initial ultrafast redistribution of Na' within the channels subsequently drives reactions across either fast [$E_1P2Na <-> E_1P(Na_2)$] or slow [$E_1P(Na_2)Na <-> E_1P(Na_2)$] Na' occlusion/deocclusion steps (assumed electroneutral) that rate-limit accompanying further electrogenic movement of Na' within, respectively, either low-field, or high-field access channels.

(Supported by HHMI and NIH grants HL36783, GM30376, NS22979 and NS11223)

Su-AM-L6

CONSEQUENCES OF FUNCTIONAL EXPRESSION OF THE PLASMA MEMBRANE Ca^{2+} PUMP ISOFORM 1a IN ENDOTHELIAL CELLS.

((S. Muallem, B. Liu, X. Xu, R. Fridman, and T. Kuo)) Univ of TX SW Med Ctr, Dallas, TX 75235 and Wayne State Univ Sch of Med, Detroit, Michigan.

The plasma membrane Ca^{2+} pump is an integral component of the Ca^{2+} signaling system. To understand the physiological function of the pump, isoform 1a (PMCA 1a) was stably over expressed. The cell lines selected expressed 3-4 fold increased functional pump protein which was correctly targeted to the plasma membrane. In isolated vesicles the over expressed pump displayed typical dependence on Ca^{2+} and calmodulin. Measurement of $[Ca^{2+}]_i$ showed that expression of PMCA1a had profound effect on different aspects of the Ca^{2+} signal. The peak increase in $[Ca^{2+}]_i$ evoked by ATP and/or Tg was lower but the plateau phase was similar in the PMCA1a expressing cells. Accordingly, titration with ionomycin of Ca^{2+} content of internal stores, Ca^{2+} uptake into the Tg-sensitive pool (ER), analysis of SERCA mRNA and protein, showed that expression and activity of the SERCA pump was down regulated in cells expressing PMCA1a pump. Expression of PMCA1a also down-regulated expression of the IP_3-activated Ca^{2+} channel and the rate of IP_3-mediated Ca^{2+} release. On the other hand the rate of Ca^{2+} and Mn^{2+} influx into PMCA1a expressing cells was increased by about 2.6 fold. Measurement of $[Ca^{2+}]_{out}$ showed that the rate of Ca^{2+} efflux in cells expressing PMCA1a was about 1.45 fold higher than Neo controls, despite the 4 fold increase in the amount of functional pump protein. The overall study points to the flexibility, interdependence and adaptability of the different components of the Ca^{2+} signaling systems to regulate the expression and activity of each component and maintain a nearly constant Ca^{2+} signal.

Su-AM-L7

FABRICATION OF VECTORIALLY ORIENTED MONOLAYERS OF DETERGENT-SOLUBILIZED Ca^{2+}-ATPase FROM SARCOPLASMIC RETICULUM.

((L.A. Prokop, R.M. Strongin, A.B. Smith, III, and J.K. Blasie)) Department of Chemistry, University of Pennsylvania, Philadelphia, PA 19104 . ((L.J. Peticolas and J.C. Bean)) AT&T Bell Laboratories, Murray Hill, NJ 07974.

The general approach established by Chupa, et al. (*Biophys. J., 67*, 1995, 336-348) for tethering detergent-solubilized integral membrane proteins to solid surfaces has been utilized to form vectorially oriented monolayers of the energy-dependent Ca^{2+} pump protein, Ca^{2+}-ATPase, from the sarcoplasmic reticulum (SR). Bifunctional alkylsiloxane self-assembled monolayers (SAMs) possessing "headgroup" binding specificity for the substrate and "endgroup" binding specificity for the enzyme are utilized to tether the enzyme to the substrate. Specifically, an amine-terminated SAM was found to bind the enzyme electrostatically. Fluorescent labeling of the Ca^{2+}-ATPase in conjunction with the formation of these monolayers on quartz substrates allowed the determination of the nature of protein binding via fluorescence spectroscopy. Formation of the monolayers on Ge/Si multilayer substrates fabricated by molecular beam epitaxy (MBE) allowed the determination of the profile structure for the system by X-ray interferometry, and proof of the correctness of these so-derived profile structures by X-ray holography, to a spatial resolution of ~7 Å. Such vectorially oriented monolayers of detergent-solubilized Ca^{2+}-ATPase from SR allow for a wide variety of correlative structure/function studies to be performed that would serve to elucidate the mechanism of Ca^{2+} transport by this enzyme.

Su-AM-L8

NEW SUBUNITS OF V-ATPase; POSSIBLE INVOLVEMENT IN ENERGY COUPLING.

(N. Nelson, F. Supek, L. Supekova and H. Nelson) Department of Biochemistry, Tel Aviv University, Tel Aviv, ISRAEL and Roche Institute of Molecular Biology, Nutley, NJ 07110. (Spon. by N. Nelson)

Eukaryotic cells contain numerous acidic compartments composed of elements of the vacuolar system. V-ATPase is responsible for acidifying the interior of these organelles and providing the energy for numerous transport processes across their membranes. V-ATPase is related in its structure and mechanism of action to F-ATPase, which is present in chloroplasts, mitochondria, and eubacteria. They not only share a common structure and mechanism of action but also have a common evolutionary ancestry. We have recently cloned a bovine cDNA and a yeast gene-*VMA8* encoding subunits D of the respective V-ATPases. Although no significant sequence homology was found between subunit D and the γ subunit of F-ATPases, structural analysis indicated similar motifs in the two proteins. We concluded that subunit D is analogous to the γ subunit in its structure and function. The subunit structure of V-ATPase membrane sector is not entirely known. The proteolipid is the only subunit that was implicated in the mechanism of energy transfer in the enzyme. We identified a protein (M16) that copurifies with the V-ATPase complexes from yeast and bovine chromaffin granules. Amino acid sequence analysis revealed that M16 exhibits a significant homology to subunit *b* of F-ATPases. M16 is smaller than subunit *b* and contains no apparent transmembrane segment in its N-terminus. The remainder of subunit b is related to M16 not only by its amino acid sequence but also in its predicted structure of helix-turn-helix. The structural, mechanistic, and evolutionary implications of this finding are discussed.

Su-AM-L9

CHARACTERIZATION OF A SMALL EXCHANGEABLE INHIBITOR BOUND TO A LARGE MEMBRANE PROTEIN USING HIGH RESOLUTION SOLID STATE NMR SPECTROSCOPY

((#D.A. Middleton, R. Robins, #D.G. Reid and A. Watts)) Biochemistry Dept., University of Oxford, South Parks Road, Oxford, OX1 3 QU, UK and SmithKline Beecham Pharmaceuticals, The Frythe, Welwyn, Herts, AL6 9AR, UK. (Spon. by P. Spooner)

The conformation of a carbon-13 labelled, reversible inhibitor at the high affinity binding site of gastric H/K-ATPase in membranes is being investigated using magic angle spinning (MAS) NMR. Before detailed and reliable structural information can be gained, however, it is essential to ascertain that the NMR spectrum represents exclusively the ligand at its specific binding site. For this purpose, a sequential spectroscopic approach was used to characterize exchangeable ligands bound to membrane protein, namely: a). Inhibitor was titrated into the membrane and spectra were acquired under non-freezing conditions to maintain the *in vivo* protein environment and to permit free exchange of the inhibitor between free and bound regimes; (b). cross polarization (CP) MAS was employed as a filter to select signal exclusively from the bound ligand and to report on its exchange dynamics, with the natural abundance background signal being eliminated by difference spectroscopy; (c). ligand binding specificity was investigated by observing the response of the spectrum to the presence of known antagonists with non-specific interactions being detected using a dipolar dephasing CP-MAS experiment. By combining CP-MAS NMR and changes in physical conditions, it has been possible to obtain spectra directly from the inhibitor bound to the high affinity site of H/K-ATPase. This approach is being exploited further to measure distances in the bound inhibitor from rotational resonance magnetization exchange curves.

Su-AM-M1

ROLE OF P450 MONOOXYGENASES IN REGULATION OF CALCIUM RELEASE ACTIVATED CHANNEL IN HEPATOMAS.
((J. Duszynski, B.A. Stanley, and K.F. LaNoue))
Pennsylvania State University College of Medicine, Hershey, PA 17033

Intracellular generation of inositol trisphosphate (IP_3) mobilizes Ca^{2+} from intracellular stores and after a short delay (in some cell types) non-voltage dependent Ca^{2+} channels open. Permeation through these channels has been found not to depend on IP_3 but rather on the extent of depletion of Ca^{2+} stores. The nature of the signal from Ca^{2+} stores to the plasma membrane has not been determined but a number of studies show that reagents which block cytochrome P450's also block the Ca^{2+} release activated channels (I_{CRAC}). In order to determine the specificity of the P450 blockers additional procedures were used to block cytochrome P450 activity. In one set of experiments 1.0 mM hydroxymalonate and 100 μM dehydroepiandrosterone were used to block generation of NADPH via malic enzyme and glucose-6-phosphate dehydrogenase. After 20 min preincubation these inhibitors had no effect on Ca^{2+} release from stores (as measured by Fura-2 fluorescence in H4IIE hepatoma cells) but they effectively (>85%) blocked Ca^{2+} entry from the media. In order to lower basal levels of P450 monooxygenases in these hepatoma cells, cultured hepatoma cells were treated with antisense oligonucleotides corresponding to the conserved heme binding site of cytochrome P450, and in separate studies a conserved region specific for cytochrome P450 family IA. Both blocked the channel 90% (following Ca^{2+} release from stores) after three days of antisense treatment. Controls utilizing a randomized oligonucleotide corresponding to the IA family specific oligonucleotide and a second nucleotide corresponding to creatine phosphokinase had no effect on Ca^{2+} entry. The data suggest that a product of cytochrome P450 IA which has fatty acid monooxygenase activity may regulate I_{CRAC}.

Su-AM-M2

ROLES OF ENDOPLASMIC RETICULUM AND CAPACITATIVE CURRENT IN BURSTING PANCREATIC β-CELLS. ((T.R. Chay)) Department of Biological Sciences, University of Pittsburgh, Pittsburgh, PA 15260.

Recent experiments indicate that a calcium store (e.g., endoplasmic reticulum) and a capacitative current are involved in electrical bursting and $[Ca^{2+}]_i$ oscillation in pancreatic β-cells. I update my earlier models [1] by incorporating a voltage-independent inward current I_{in}, which is activated by depletion of luminal Ca^{2+} of the endoplasmic reticulum. In this model, the luminal calcium concentration, $[Ca^{2+}]_{ER}$, oscillates slowly (see the dashes on the left frame), and this slow dynamic in turn gives rise to electrical bursting (the left) and $[Ca^{2+}]_i$ oscillation (the right) by activating the I_{in} channel.

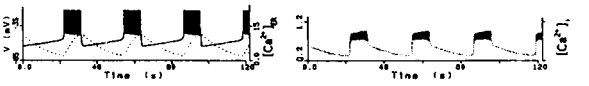

This model is capable of providing answers to some puzzling phenomena (which other models could not), e.g., why do single pancreatic β-cells burst with a low frequency (the left frame) while the cells in an islet burst with a much high frequency (the right frame)?

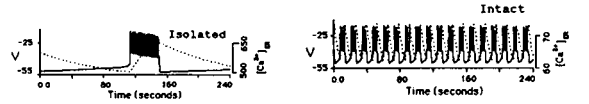

[1] T.R. Chay, **J. Phys. Chem. 1983**. 87: 2935-2940; **Physica. 1985**. 6D. 233-242; **Cell Biophys. 1987**. 11, 77-90; **J. Theor. Biol. 1990**. 142: 305-315; **Am. J. Physiol. 1990**. 258 (Cell Physiol. 27): C55-C965; **Adv. Biophys. 1993**. 29: 75-103.

Su-AM-M3

ROLE OF cAMP-DEPENDENT PHOSPHORYLATION IN HIPPOCAMPAL CALCIUM CHANNEL POTENTIATION. ((M.R. Plummer and E.T. Kavalali)) Dept. of Biological Sciences, Rutgers University, Piscataway, NJ 08855-1059

There is considerable evidence that dihydropyridine-sensitive, voltage-gated calcium channels can show enhanced activity following conditioning depolarizations. In some cases, it has been suggested that this enhancement results from voltage-dependent phosphorylation of the calcium channel by cAMP-dependent protein kinase or a novel kinase. We have examined this issue with regard to voltage-dependent enhancement of Lp calcium channel activity in hippocampal neurons by using the inhibitors H-89 and H-7 as well as 8-CPT-cAMP, a membrane-permeable cAMP analog. As shown below (**D**), 100 μM H-7 did not prevent prepulse-induced increases (**B, C**) in Lp channel activity. However, it totally blocked 8-CPT-cAMP-mediated increases in Lp channel opening (not shown). These data suggest that although cAMP-dependent phosphorylation can increase Lp channel availability with a consequent increase in potentiation, it is not required for Lp channel potentiation. Supported by NIH (NS-34061) and the American Heart Association (93-G-53).

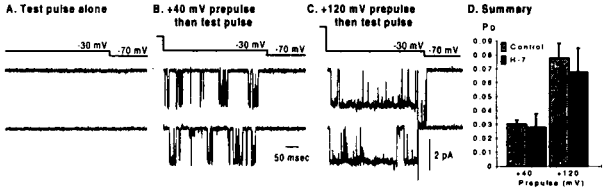

Su-AM-M4

VITAMIN D_3 ANALOGUES REGULATE L-TYPE CALCIUM CHANNELS IN RAT OSTEOSARCOMA CELLS. K. Tacheuchi, S.Yukihiro and S.E. Guggino, Department of Medicine, Johns Hopkins University, Baltimore, MD 21205.

L-type calcium channels are found in ROS 17/2.8 osteosarcoma cells where they stimulate bone matrix (osteocalcin) production (PNAS USA:2957-2960, 1989). We and others (J. Biol. Chem. 264: 20265-20274, 1989) have found that 1,25 dihydroxyvitamin D_3 rapidly (sec) potentiates the opening of L type calcium channels by causing a left shift in the threshold activation of currents to more physiological plasma membrane potentials. Activation is highly potent ($K_{½}$ 1.25 D_3 is 1 nM), saturable and occurs for naturally occurring analogues at physiological (serum) concentrations. But the mechanism of activation of calcium channels is unclear. To determine whether the opening of calcium channels is mediated by the classical genomic vitamin D_3 receptor, multiple naturally occurring and synthetic analogues of 1,25 D_3 were tested on calcium channel activation. Using the perforated whole-cell version, of the patch clamp technique we found a pharmacological profile for activation of calcium channels which is not consistent with stimulation via the classical nuclear vitamin D_3 receptor. We speculate that L-type calcium channels are regulated by a separate signal transduction pathway involving a unique vitamin D_3 binding protein which may reside in the plasma membrane.

Su-AM-M5

CALCIUM IS AN ESSENTIAL COFACTOR FOR THE ACTIVATION OF CAPACITATIVE CALCIUM ENTRY CHANNELS BY STORE DEPLETION. ((Adam Zweifach and Richard S. Lewis)). Dept Mol. Cell. Physiol., Stanford U. Sch. Med., Stanford, CA 94305.

Ca^{2+} influx through Ca^{2+} release-activated Ca^{2+} (CRAC) channels is triggered by Ca^{2+} store depletion in many cell types. We find that complete store depletion is insufficient to activate CRAC channels maximally in whole-cell patch clamp recordings from Jurkat cells. Extracellular Ca^{2+} (Ca^{2+}_o) is a potent cofactor. Rapid application of extracellular Ca^{2+} or hyperpolarizing voltage steps enhances the activity of CRAC channels in store-depleted cells by triggering a slow increase in current amplitude (τ = 5 s). The increase (maximum extent ~4-fold) is absolutely dependent on the presence of Ca^{2+}_o, but its magnitude is both Ca^{2+}_o- and voltage-dependent, increasing with hyperpolarization. We call this phenomenon Ca^{2+}-dependent potentiation (CDP). We determined that CDP results from a change in channel gating rather than an increase in single-channel current. The binding site for CDP is not intracellular, because 1) CDP is unaffected by pipette-applied Ca^{2+} buffers and 2) Ni^{2+}, a channel blocker, can substitute for Ca^{2+}. CDP can be explained economically by a model in which Ca^{2+} binding to a site located within the pore of open channels allows triggers a transition to a high P_o mode. CDP makes a large contribution to macroscopic ion selectivity, as Ba^{2+}, which can transiently permeate CRAC channels, cannot substitute for Ca^{2+} in promoting CDP. CDP confers a modest voltage dependence on whole-cell I_{CRAC}. Importantly, if a slow transition from low P_o to high P_o modes is responsible for CDP, then this transition may be a rate-limiting step in the activation of channels by depletion.

Su-AM-M6

FUNCTIONAL ASSOCIATION BETWEEN FYN KINASE AND THE INOSITOL 1,4,5-TRISPHOSPHATE RECEPTOR ((K. Ondrias, T. Jayaraman, and A. R. Marks)) Mount Sinai School of Medicine, N.Y., N.Y. 10029

Non-receptor tyrosine kinases indirectly elevate cytoplasmic calcium by activating phospholipases that generate inositol 1,4,5-trisphosphate (IP3) and diacylglycerol. IP3 directly activates the IP3 receptor (IP3R)/intracellular calcium release channel on the endoplasmic reticulum. We have cloned and sequenced the human type 1 IP3R (IP3R1) which contains two putative tyrosine phosphorylation sites. We now show that IP3R1 is tyrosine phosphorylated in brain and T lymphocytes (Jurkat). Antigen-specific stimulation of the T cell receptor (TCR) complex triggers a physical association between fyn kinase and IP3R1 and rapidly induces tyrosine phosphorylation of IP3R1. Tyrosine phosphorylation by fyn kinase (3 units), activates the IP3-gated calcium channel in planar lipid bilayers, increasing the open probability by 350% (n=4), without altering the amplitude of conductance for calcium or sensitivity to heparin which blocks the channel. These results indicate for the first time that IP3R1 is physically associated with fyn, a non-receptor protein tyrosine kinase, after T cell activation and that tyrosine phosphorylation can activate the IP3-gated calcium channel (IP3R1) *in cerebellum and in* human T lymphocytes.

Su-AM-M7

CALCIUM BUFFERING AND ENCODING OF ACTION POTENTIAL FREQUENCY IN DENDRITES OF PYRAMIDAL NEURONS. ((F. Helmchen, K. Imoto*, B. Sakmann)) Abt. Zellphysiologie, Max-Planck-Institut für med. Forschung, D-69120 Heidelberg; and *Dept. of Information Physiology, Nat. Inst. for Physiol. Sciences, Okazaki 444, Japan.

The effect of Fura-2 on Ca^{2+} dynamics was studied in proximal apical dendrites of neocortical layer V pyramidal neurons in rat brain slices using somatic whole-cell recording and a CCD camera. A single action potential evoked a transient increase in the intradendritic calcium concentration ($[Ca^{2+}]_i$) that was reduced in size and prolonged when the Fura-2 concentration was increased from 20-250 μM. Extrapolation to zero Fura-2 concentration suggests that 'physiological' transients at 37 °C have large amplitudes (150-300 nM) and fast decays (time constant <100 ms). Assuming a homogeneous compartment model for the dendrite, 0.5-1% of the total Ca^{2+} entering during an action potential was estimated to remain free. Wash-out of cytoplasmic Ca^{2+} buffers was not detectable, suggesting that they are relatively immobile. During trains of action potentials, $[Ca^{2+}]_i$ increased and rapidly reached a steady-state (time constant <200 ms), fluctuating around a plateau level which depended linearly on the action potential frequency. Thus, the mean dendritic $[Ca^{2+}]_i$ encodes the action potential frequency during physiological patterns of electrical activity and may regulate Ca^{2+}-dependent dendritic functions in an activity-dependent way.

Su-AM-M8

CELLULAR MECHANISMS FOR TYROSINE KINASE INHIBITOR-INDUCED ATTENUATION OF MYOPLASMIC CALCIUM RESPONSE TO ENDOTHELIN ((C. Y. Liu and M.Sturek)) Dalton Cardiovascular Research Center and Dept. of Physiology, School of Medicine, Univ. of Missouri, Columbia, MO 65211

We have previously shown that the tyrosine kinase inhibitor, genistein (GEN), inhibits the myoplasmic Ca ($[Ca]_m$) response to endothelin (ET) in smooth muscle cells from porcine coronary arteries. This study was designed to elucidate the cellular mechanisms for the actions of tyrosine kinase inhibitors on the $[Ca]_m$ response. The $[Ca]_m$ in dispersed cells was measured with fura-2. Both GEN and methyl 2,5-dihydroxycinnamate (MDHC) inhibited the initial transient phase of the $[Ca]_m$ response to 10 nM ET by 54% and 81%, respectively, in the presence of extracellular Ca. GEN also caused a delay of the $[Ca]_m$ response with the latent period being increased 2.5-fold. In the absence of extracellular Ca, the ET-induced $[Ca]_m$ response was also decreased 92% by GEN. However, the $[Ca]_m$ response to inositol trisphosphate (IP_3) applied intracellularly via a patch clamp pipette was not affected by GEN. Both GEN and MDHC also abolished the sustained phase of the $[Ca]_m$ response to ET, when added after a sustained phase had been established. However, the $[Ca]_m$ response to depolarization with 80 mM K was not affected by MDHC and only inhibited 22% by GEN. These results suggest that 1) activation of tyrosine kinases is an important regulatory mechanism for ET-induced $[Ca]_m$ response in vascular smooth muscle and 2) an upstream signaling event that leads to IP_3 production is regulated by tyrosine kinases. (Support: NIH grants, HL41033, RCDA HL02872 and AHA grant, 93011900 and an AHA-Missouri Affiliate postdoctoral fellowship)

HEME PROTEINS I

Su-AM-N1

MODULATION OF CARBON MONOXIDE BINDING TO MYOGLOBIN BY INTRODUCTION OF EXOGENOUS PROXIMAL LIGANDS INTO CAVITY MUTANT H93G. ((S.M. Decatur†*, G.D. DePillis*, and S.G. Boxer*)) *Department of Chemistry, Stanford University, Stanford, CA 94305-5080; †Department of Chemistry, Mount Holyoke College, South Hadley, MA 01075.

In the sperm whale myoglobin mutant H93G, the proximal histidine (histidine 93) has been converted to glycine, creating a cavity in the proximal heme pocket; when this protein is expressed and purified in the presence of imidazole, an imidazole molecule occupies this cavity and serves as ligand to the heme iron (Barrick, 1994). Previously, we have demonstrated that this imidazole can be replaced by other exogenous molecules which also serve as proximal ligands to the heme iron (DePillis et al., 1994; Decatur et al., 1995). By using this technique, we expand our repertoire of potential proximal ligands beyond the twenty naturally-occurring amino acids, and therefore we can systematically explore the role of the proximal ligand in modulating myoglobin function in detail not possible using conventional site-directed mutagenesis.

In this work, we report the carbon monoxide binding properties of H93G containing a series of substituted imidazoles and pyridines. When the substitution on the imidazole or pyridine ligands is varied, we observe changes in the on and off rates for CO binding to myoglobin as well as the infrared spectrum. These changes can be correlated with factors such as proximal ligand pKa and proximal ligand-protein interactions.

Barrick, D. (1994) *Biochemistry 33*, 6546-6554.
DePillis, G.D., Decatur, S.M., Barrick, D. and Boxer, S.G. (1994) *J. Am. Chem. Soc. 116*, 6981-6982.
Decatur, S.M. and Boxer, S.G. (1995) *Biochemistry 34*, 2122-2129.

Su-AM-N2

OXYGEN BINDING STUDIES OF FEII/COII HYBRID HEMOGLOBINS. ((A.L. Klinger and G.K. Ackers)) *Department of Biochemistry and Molecular Biophysics, Washington University School of Medicine, St. Louis MO 63110.*

O_2 binding studies on mixed metal hybrid hemoglobins[1] were of the first to address the energetics of ligation microstates. Here we present work on 1:1 mixtures of normal and Co^{II} substituted hemoglobin that form a hybrid having Fe^{II} in the hemes of one dimer and Co^{II} in the hemes of the other. From a global fit to the resulting concentration dependent isotherms that constrains the association free energy for the deoxy hybrid in combination with those from independent resolution of the parent linkage schemes[2], we determined the overall binding free energies of several hybrid intermediate ligation species. Of particular interest are the parameters for the species in which both Fe-heme sites of one dimer are bound while both Co-heme sites of the opposite dimer are vacant. The binding free energy of a species having ligands only on one dimer, has not previously been measured with O_2. Much evidence has shown, however, that this species is fundamentally different from the other doubly ligated species and that it has not undergone the T to R quaternary switch[3]. The cooperative free energy determined in this work for this species is consistent with this evidence, and with the value calculated for the analogous species with CO bound[4]. We present these results and the methodology that has been developed in this laboratory that will allow for direct determination for all the O_2 microstate cooperative free energies.

[1] Imai *et al.* (1980) *J. Mol. Biol. 138*:635-648
[2] Doyle *et al.* (1991) *Biochem. 30*:7263-7271 and Chu *et al.* (1984) *Biochem. 23*:604-617.
[3] Ackers *et al.* (1992) *Science, 255*:54-63.
[4] Huang & Ackers (1995) *submitted to Biochemistry*

Su-AM-N3

Contributions from the Surface Histidyl Residues to the Bohr Effect of Hb A ((D. Philip Sun, Ming Zou, Nancy T. Ho and Chien Ho)) Department of Biological Sciences, Carnegie Mellon University, Pittsburgh, PA 15213

The Bohr Effect of human normal adult hemoglobin (Hb A) is part of the allosteric mechanism of a Hb molecule that enables it to respond to changes in the electrostatic environment such as variations in pH and anion concentration. In this presentation, we shall summarize our current knowledge on the microscopic contributions from individual histidyl residues to the macroscopic Bohr Effect. We have constructed recombinant mutant Hbs using site-specific mutagenesis and our *E. coli* Hb expression system. In each of these mutant Hbs, one surface histidyl residue is replaced by a non-titratable glutaminyl residue. In some cases, combination of mutations are constructed to compensate structural perturbations caused by the replacement of a histidyl residue. By comparing the ^{1}H-NMR resonances of the recombinant Hbs to those of human Hb A, we have asigned all the C-2 proton resonances of the surface histidyl residues in both the deoxy and oxy spectra of Hb A. Using existing pK values of these resonances in the literature, we have calculated the contribution of the individual histidyl residues to the Bohr Effect under various buffer conditions. These results also provide new insights into the effects of other heterotropic effectors such as Cl^- and inorganic phosphate on Hb. [Supported by a grant from NIH (HL-24525) and in part by a grant from American Heart Association, PA. Affiliate to D. P. S.]

Su-AM-N4

LIGAND LINKED ASSEMBLY OF *SCAPHARCA* DIMERIC HEMOGLOBIN ((W. E. Royer, Jr., R. A. Fox, F. R. Smith, D. Zhu and E. Braswell)) University of Massachusetts Medical Center, Worcester, MA 01605 and University of Connecticut, Storrs, CT 06269

The intracellular homodimeric hemoglobin of the blood clam *Scapharca inaequivalvis* shows cooperative oxygen binding with a Hill coefficient of 1.5. High-resolution crystal structures of liganded and unliganded *Scapharca* dimeric hemoglobin show a novel assembly of "myoglobin-like" subunits and strongly suggest that cooperativity relies on tertiary structural transitions involving the heme groups and a small number of residues. The dimeric interface is highly hydrated with a more extensive ordered water structure in the deoxy than in liganded structures. We have investigated the stability of the dimeric interface in the liganded state by analytical gel chromatography, and in both liganded and unliganded states by sedimentation equilibrium. These measurements indicate that the CO-liganded dimer dissociates into monomers with a dissociation constant between 10^{-7} and 10^{-8}M, while the deoxygenated dimer shows no measurable dissociation. These results demonstrate that, despite a more extensive water structure in the subunit interface, the deoxygenated form is assembled significantly more tightly than is the liganded form. (Supported by NIH, NSF and AHA)

Su-AM-N5

EXTRACELLULAR HEMOGLOBIN OF GLOSSOSCOLEX PAULISTUS: EQUILIBRIUM OF DIFFERENT SPECIES IN THE MET FORM.

((Sylvana C.M. Agustinho, Maria H. Tinto, Janice R. Perussi, Marcel Tabak and Hidetake Imasato)), Instituto de Quimica de São Carlos-USP, C.P.780, 13560-970, São Carlos, S.P., Brasil.

Chromatography in Sephadex G-200 of giant whorm extracellular hemoglobin of G.paulistus in the met form evidentiates an unique band at pH 7.0 and two low molecular weight bands at pH 9.0. In the oxidized state (met form) the alkaline dissociation into low molecular weight subunits is complete. The unique band obtained at pH 7.0 corresponds to the whole protein. The two bands at pH 9.0 are assigned to the trimer not completely resolved from the linker chains and the monomer. The molecular weights are very similar to the ones described previously for the oxy form (Biophys. J. 64, A49, 1993). Optical absorption spectra for the whole protein, fraction I, the trimer, fraction II, and the monomer, fraction III, were analyzed as a function of pH. The analysis was carried out using the convex constraint analysis (CCA) programm developed by Fasman et al to study protein secondary structure from C.D. spectra. For the whole protein two pKs of 7.7 and 9.5 were observed corresponding to an irreversible transition from aquomet form to a hemichrome I and an reversible transition from the hemichrome I to hemichrome II. For trimer and monomer fractions only the second reversible transition was observed suggesting the irreversible hemichrome formation. Our results indicate that the hemoglobin of G.paulistus in the met form is quite unstable both regarding the alkaline dissociation and the hemichrome formation. C.D. measurements also suggest a sharp decrease of the Soret band signal upon hemichrome formation implying a weaker heme-globin interaction.

Support : CNP_q, CAPES and FINEP.

Su-AM-N6

DEFINING THE ALLOSTERIC PATHWAY IN HEMOGLOBIN: TIME-RESOLVED UV AND VISIBLE RESONANCE RAMAN SPECTROSCOPY OF KINETIC INTERMEDIATES.

((V. Jayaraman[a], K. R. Rodgers[b], I. Mukerji[c] and T. G. Spiro[a])) [a]Dept. of Chemistry, Princeton University, Princeton, NJ 08544, [b]Department of Chemistry North Dakota State University, Fargo, ND-58105 and [c]Department of Biochemistry and Molecular Biology, Wesleyan University, CT 06457.

Time-resolved resonance Raman spectra were obtained for hemoglobin [Hb] in the nanosecond to microsecond interval following HbCO photolysis. Excitation at 230 nm provides enhancement of tyrosine and tryptophan vibrational modes, which probe different regions of the protein, and complementary experiments with 436 nm excitation provide enhancement of heme vibrational modes, which monitor relaxation of the porphyrin ring and of the Fe-histidine bond, as well as the time course of CO recombination. Spectra of the intermediates are extracted from the transient data. Structural interpretation of these spectra enable the construction of a model for the allosteric transition in Hb, which contains the following features: photolysis of HbCO [A] produces a geminate state [B], in which the CO is trapped in the heme pocket and strain is generated in the heme-F helix linkage. This strain relaxes with a 20 ns time constant, producing intermediate R, in which half the hemes are religated and the E helix is displaced towards the heme in the other half. In turn this displacement relaxes with a time constant of 0.5 μs, producing intermediate S, in which the subunits have rearranged and T-like quaternary contacts have started to form, but the Fe-His bond stays relaxed. Intermediate T is produced with a 17 μs time constant in which the Fe-His bond is strained, as in deoxyHb, and the quaternary contacts are locked in place. However, the H-bond contacts across the $\alpha_1\beta_2$ are weaker than in deoxyHb, and hence it is proposed that the $\alpha_1\beta_2$ interface is deformed as a result of two ligands binding to the same dimer within the tetramer.

Su-AM-N7

STRUCTURAL HETEROGENEITY OF NI(II)-OCTAETHYLPORPHYRIN IN ORGANIC LIQUIDS AND GLASSES.

((M. Leone[1], E. Unger[2], W. Jentzen[3], A. Cupane[1], L. Cordone[1], H. Gilch[2], W. Dreybrodt[2] and R. Schweitzer-Stenner[3])) [1]Insituto di Fisica, University of Palermo, 90123 Palermo, Italy; [2] Institut für Experimentelle Physik, Universität Bremen, 28359 Bremen, Germany; [3] Fuel Science Department, Sandia National Laboratories, Albuquerque, NM 87185, USA.

We have measured the absorption spectrum of Ni(II)-octaethylporphyrin (NiOEP) in CH_2Cl_2 and in a 50% v/v isopentane/ethyl ether mixture as a function of temperature between 150 and 300 K and 40 and 300 K, respectively. The Soret band can be decomposed into two subbands whose frequencies differ by 220 cm^{-1}. By analogy with resonance excitation profiles of conformational sensitive Raman bands (i.e. ν_{10}, ν_{19}) we attribute the low frequency subband to a conformer with a non-planar macrocycle, whereas the high frequency subband is assigned to one or even two planar conformers. The subbands' intensity ratio exhibit a solvent dependent van't Hoff behavior between 300 and 160 K. Crystallization of CH_2Cl_2 prevents measurements at lower temperatures. For NiOEP in the glass forming isopentane/ethyl ether mixture the intensity ratio bends over in a region between 150 K and 100 K and remains constant below. These data can be fitted by a modified van't Hoff expression, which accounts for the freezing into a non equilibrium distribution of the conformers below a distinct temperature T_f. The fit yields a freezing temperature of $T_f \approx 121$ K and a transition region of 52 K. In accordance with Raman data we found that the non-planar conformer has the lowest free energy. Moreover the Soret band's width exhibits a temperature dependent Gaussian contribution. It results from low frequency modes to which the electronic B-state transition is vibronically coupled. This comprises out-of-plane modes of the porphyrin involving the central metal atom, and molecular motions within the liquid environment. At temperatures above the solvent's glass transition the amplitudes of these motions increase above the values predicted by a purely harmonic model. This indicates to non-nharmonic contributions to their potential energy and parallels findings on porphyrins embedded into a protein environment.

Su-AM-N8

POSSIBLE FUNCTIONAL ROLES OF NON-PLANAR CONFORMERS OF TETRAPYRROLES IN PROTEINS.

((J. A. Shelnutt[1,2])) [1]*Fuel Science Department, Sandia National Laboratories, Albuquerque, NM 87185-0710.* [2]*Department of Chemistry, University of New Mexico, Albuquerque, NM 87131.*

Tetrapyrroles in proteins undergo remarkable nonplanar distortions that alter the chemical and photochemical properties of these important cofactors. These non-planar macrocycle conformations are seen in the X-ray crystal structures of many hemoproteins and photosynthetic proteins and are best depicted in the X-ray crystal structures of photosynthetic reaction centers and cytochromes. Recently, it has come to light that a variety of metastable nonplanar conformers may be energetically accessible at physiological temperatures and that these non-equilibrium conformers may be involved in biological function. Both the porphyrin ground-state conformation and these higher energy conformers can influence such properties as reduction potentials, electron-transfer and other reaction rates. Moreover, the protein environment can alter the relative energies of these low energy conformers as a way of regulating the biological properties of the porphyrin cofactor. Antithetically, changes in the metalloporphyrin that occur during its function, such as a change in oxidation state or ligation state of the metal, influence the relative energies of the low energy conformers and their interaction with the protein, allowing the porphyrin to alter the apoprotein moiety. We have devised a quantitative means of classifying these non-planar conformers based on symmetric distortions along only the five lowest-frequency normal mode coordinates of A_{2u} (*doming*), B_{1u} (*ruffling*), B_{2u} (*saddling*), and E_g (*waving*) symmetries of the nominally D_{4h} planar porphyrin. For symmetrically substituted model porphyrins, conformers exhibiting pure distortions with these symmetry properties are often observed. In proteins and non-symmetrically substituted porphyrins, observed distortions are typically composed of linear combinations of distortions alone these five normal coordinates. The possible role of higher energy porphyrin conformers in their biological function will be considered.

(Supported by U.S. DOE Contract DE-AC04-94AL85000.)

SOCIETY AWARD WINNERS SYMPOSIUM

Awards-Sym-1

STRINGS AND MOTORS: BIOPHYSICAL APPROACHES TO SENSORY TRANSDUCTION BY VERTEBRATE HAIR CELLS.

((D.P. Corey)) Mass. Gen. Hospital and Howard Hughes Medical Institute, Boston, MA 02114.

In the current model for transduction and adaptation by hair cells, deflection of the hair bundle towards the tallest stereocilia stretches fine filaments ("tip links") that extend between adjacent stereocilia. These pull on mechanically-sensitive ion channels at the tips of the stereocilia. We tested this model by cutting the tip links (observed by electron microscopy) and found that the mechanical sensitivity is concurrently and irreversibly lost. With Winfried Denk, we used calcium imaging to locate the transduction channels. As in reports, channels are at the tips of stereocilia. They can be at either end, probably both ends, of the tip links. During a maintained deflection, channels adapt towards the resting open probability of about 15%. Howard and Hudspeth speculated that the upper attachment of each tip link can move along the side of the stereocilia, drawn upwards by a myosin-based motor or slipping under excess tension. We measured calcium-dependent rates of adaptation and constructed a mechanical model for adaptation, which successfully predicts a small (~100 nm) voltage-dependent movement of an unrestrained bundle. The incompleteness of adaptation suggests an additional linkage between the motor complex and the actin cores of stereocilia. Cutting the tip links allows the attachment to climb, as observed with TEM. To search for the adaptation myosin, we used degenerate PCR and found ten myosin genes expressed in the sensory epithelium. With Tama Hasson, we found that at least three are expressed in hair cells: myosins VI and VIIa (which cause deafness when defective), and myosin Iβ. As Gillespie and Hudspeth had shown, myosin Iβ is in the tips of stereocilia, making it a candidate for the adaptation motor.

Awards-Sym-3

FRAMESHIFTS, RETROVIRUSES AND PSEUDOKNOTS

(I. Tinoco, Jr., X. Chen, J. V. Hines, H. Kang, L. X. Shen) Department of Chemistry, University of California and Structural Biology Division, Lawrence National Berkeley Laboratory, Berkeley, CA 94720.

Retroviruses synthesize essential viral enzymes—including protease, reverse transcriptase, and integrase—as part of polypeptides produced by minus-one frameshifts as the viral RNA is translated. These programmed frameshifts occur in response to signals composed of a sequence of seven nucleotides at the shift site and a nearby pseudoknot downstream of the shift site. The mechanism of frameshifting is not known, although a pseudoknot might slow or transiently arrest the ribosome at the shift site, and thus promote slippage into the minus-one reading frame. We previously showed that the nucleotide sequence at the junction of the stems of a pseudoknot was important for efficient frameshifting, apparently because it determines a characteristic bent conformation. We have now determined the structures of two pseudoknots with very poor frameshifting ability. One is linear, the other is bent, but in the opposite direction from the efficient frameshifter. The requirement for a precise conformation for efficient frameshifting indicates that a specific interaction occurs between the viral RNA pseudoknot and the host protein-synthesizing machinery.